

A Consistent Reduced Network for HCN Chemistry in Early Earth and Titan Atmospheres: Quantum Calculations of Reaction Rate Coefficients

Ben K. D. Pearce,^{1,*} Paul W. Ayers,² and Ralph E. Pudritz¹

¹*Origins Institute and Department of Physics and Astronomy, McMaster University, ABB 241, 1280 Main St, Hamilton, ON, L8S 4M1, Canada*

²*Origins Institute and Department of Chemistry and Chemical Biology, McMaster University, ABB 156, 1280 Main St, Hamilton, ON, L8S 4M1, Canada*

Abstract: HCN is a key ingredient for synthesizing biomolecules such as nucleobases and amino acids. We calculate 42 reaction rate coefficients directly involved with or in competition with the production of HCN in the early Earth or Titan atmospheres. These reactions are driven by methane and nitrogen radicals produced via UV photodissociation or lightning. For every reaction in this network, we calculate rate coefficients at 298 K using canonical variational transition state theory (CVT) paired with computational quantum chemistry simulations at the BHandHLYP/aug-cc-pVDZ level of theory. We also calculate the temperature dependence of the rate coefficients for the reactions that have barriers from 50–400 K. We present 15 new reaction rate coefficients with no previous known value. 93% of our calculated coefficients are within an order of magnitude of the nearest experimental or recommended values. Above 320 K, the rate coefficient for the new reaction $\text{H}_2\text{CN} \longrightarrow \text{HCN} + \text{H}$ dominates. Contrary to experiments, we find the HCN reaction pathway, $\text{N} + \text{CH}_3 \longrightarrow \text{HCN} + \text{H}_2$, to be inefficient, and suggest the experimental rate coefficient actually corresponds to an indirect pathway, through the H_2CN intermediate. We present CVT using energies computed with density functional theory as a feasible and accurate method for calculating a large network of rate coefficients of small-molecule reactions.

INTRODUCTION

HCN is a precursor to the building blocks of life. For example, HCN reacts to produce nucleobases, the building blocks of RNA/DNA, as well as amino acids, the building blocks of proteins, in aqueous environments^{1–5}. For adenine synthesis, HCN first condenses in water to form oligomers, which then forms adenine upon hydrolysis⁶. HCN may have formed in the atmosphere of the prebiotic Earth through the reaction of photochemically driven and/or lightning-induced methane and nitrogen radicals^{7,8}. HCN is similarly produced in Titan's present-day atmosphere⁹.

Given the significance HCN as a precursor to biomolecules, it is of interest to discern how much was produced in the early Earth atmosphere in order to understand whether it potentially played a role in the emergence of life in warm little ponds¹⁰. Titan provides a good test environment for atmospheric HCN production, given that one can compare abundances from chemical simulations to the measured HCN profile from the Cassini mission^{11,12}.

Chemical networks including a variety of species and reactions have been employed to simulate the atmospheric HCN composition of early Earth^{13,14} and Titan^{9,15–18}. The reaction rate coefficients in these networks are generally a combination of a) theoretical, b) experimental, and c) suggested values typically estimated using thermodynamics, similar reactions and/or experimental results at much higher temperatures. Each of

these sources has errors associated with it, and there are often a range of experimental and theoretical values to choose from for a single reaction. As a result, atmospheric HCN compositions can vary by orders of magnitude from one simulation to the next. Therefore, it is perhaps unsurprising that, as of yet, no simulation has matched the HCN profile of Titan completely.

There are also several reactions without past experimental, theoretical, or suggested values that are missing in these networks that may play important roles in HCN formation (e.g. $^1\text{CH}_2 + ^2\text{N} \longrightarrow \text{H}_2\text{CN}$ and $\text{H}_2\text{CN} \longrightarrow \text{HCN} + \text{H}$).

The focus of this work is to create a theoretical reduced HCN chemical network, where all the rate coefficients are consistently calculated with the same theoretical and computational method. Using this strategy, all reactions can be theoretically validated before being employed in a chemical network, and key reaction pathways with previously unknown rate coefficients can be included. Furthermore, by constructing a model chemistry^{19,20} the errors for consistently calculated rate coefficients are expected to be similar, thus employing such a network has a chance to improve accuracy.

The limitation of calculating a consistent theoretical network is that one cannot feasibly include a large number of molecular species. For every additional species, there is a potential additional reaction with all the existing species in the network. Therefore in this work, we focus only on the small set of reactions involved in the production of HCN from methane and nitrogen dissociation radicals, as well as the direct competing reactions. This totals 42 reactions between 11 species. We are the first to calculate a completely consistent theoretical reac-

* Corresponding author:pearcbe@mcmaster.ca

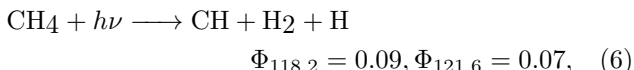
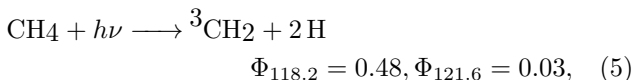
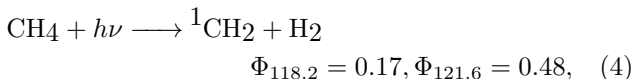
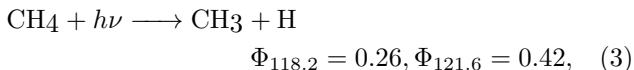
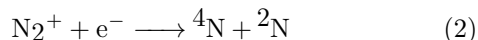
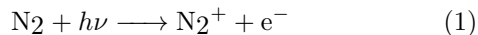
tion network of this size for atmospheric chemistry simulations.

In the Background section of this paper, we motivate and describe the reactions in our chemical network. Then in the Methods section, we detail the theoretical and computational methods used to calculate the reaction rate coefficients in our network. In the Results section, we present the results of our calculations, including their conformance to experimental values, and the effects of spin configuration on these values. The reader who is just interested in the calculated rate coefficients can skip ahead to Tables 3 and 4, where we present the calculated reaction rate coefficients at 298 K, and the Arrhenius coefficients for temperature dependences, respectively. Finally, in the Conclusions section we summarize the main results of the paper.

The supporting information (SI) contains a wealth of technical data and calculation details including: 1) a summary of the experimentally measured and previously theoretically calculated rate coefficients in this network, 2) an example rate coefficient calculation using the CVT method and a computational methods comparison, 3) a breakdown of the calculations of specific reactions, and 4) reaction path symmetry number calculations.

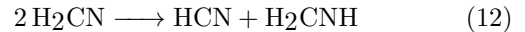
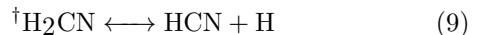
BACKGROUND

The abiotic production of biomolecules such as nucleobases and amino acids requires a reactive source of nitrogen, typically HCN or NH_3 ^{5,8,21–23}. HCN can be produced in early Earth and Titan atmospheres through reactions involving N_2 and CH_4 dissociation products. Such dissociation products are produced when N_2 and CH_4 interact with UV photons⁷, cosmic rays²⁴, or lightning²⁵. N_2 and CH_4 photodissociation can be broken down into the following pathways



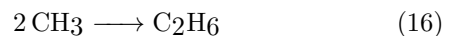
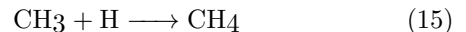
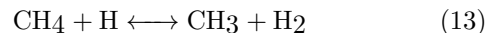
where the leading superscripts signify the singlet, doublet, and quartet spin states, $h\nu$ signifies an ultraviolet photon and $\Phi_{118.2}$ and $\Phi_{121.6}$ signify the branching ratios measured from lab experiments at 118.2 and 121.6 nm, respectively^{7,26,27}.

Multiple possible pathways to produce HCN from the above radicals (at or near 298 K) have been reported from experiments or suggested in the literature. Note that molecular spin states are not included in this list and that each of these reactions represents 1–5 reaction spin configurations; each with a unique reaction rate coefficient.



Three experimentally reported or suggested reaction pathways have not been included in this list as our theoretical work shows they more likely proceed through two steps involving combinations of the above equations. These reactions are $\text{CH}_3 + \text{N} \longrightarrow \text{HCN} + \text{H}_2$ ²⁸, $\text{CH}_3 + \text{N} \longrightarrow \text{HCN} + 2\text{H}$ ²⁸, and $\text{CH}_2 + \text{N} \longrightarrow \text{HCN} + \text{H}^7$ (see theoretical case studies in SI for complete analysis).

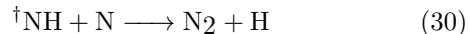
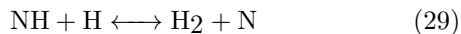
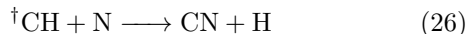
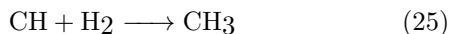
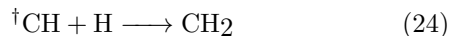
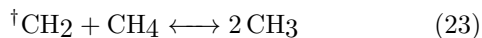
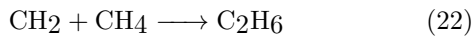
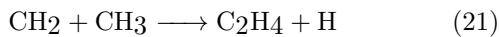
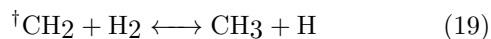
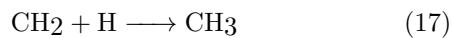
There are also multiple competing reaction pathways to the above reactions at or near 298 K. In this network, we only include competing pathways involving the radicals produced from N_2 and CH_4 dissociation in the atmosphere. One exception is that we also include the reactions of ${}^3\text{NH}$ with H and N as recombination pathways to H_2 and N_2 . See Table 1 for list of primary molecular species.



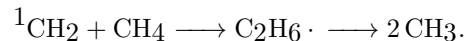
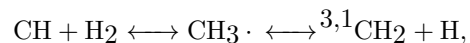
[†]Reactions without experimental or suggested values for at least one spin configuration in this network.

TABLE 1. List of primary molecular species involved in this study and their spin states.

Species	Spin state	Ground/Excited state
HCN	singlet	ground
H ₂ CN	doublet	ground
N ₂	singlet	ground
² N	doublet	excited
⁴ N	quartet	ground
CH ₄	singlet	ground
CH ₃	doublet	ground
¹ CH ₂	singlet	excited
³ CH ₂	triplet	ground
CH	doublet	ground
H ₂	singlet	ground
H	doublet	ground
³ NH	triplet	ground



Four experimentally reported^{29–38} two-step reaction pathways have been reduced to their first steps in this list. These reactions are



Our theoretical work shows the first steps are the rate-limiting steps, and the intermediates are reactants with other available reaction pathways in our chemical network (see theoretical case studies in SI for complete details).

One other experimentally reported³⁹ reaction has not been included in this list. This reaction is



Experiments suggest that ¹H₃CNH decays into CH₃ + ³NH with a branching ratio of 0.3 ± 0.1, and that the majority of ¹H₃CNH decays into ¹H₂CNH + H (Φ = 0.8 ± 0.2). Our theoretical work also suggests ¹H₃CNH preferentially decays into ¹H₂CNH + H, however we alternatively find the decay into CH₃ + ³NH to be very inefficient (k ~ 10⁻²⁹ cm³ s⁻¹); therefore we do not consider this decay pathway in this network.

The focus of this work is to calculate the rate coefficients for an atmospheric HCN reaction network which can be applied to both Titan and early Earth atmospheres. For each reaction, a detailed analysis of spin state configurations and an series of computational quantum chemistry simulations are performed at temperatures between 50–400 K.

In Table 2 we summarize the molecules and spin states involved in this reaction network. We define reactions with rate coefficients greater than 10⁻²¹ s⁻¹ for unimolecular reactions or greater than 10⁻²¹ cm³s⁻¹ for bimolecular reactions as “fast,” and exclude the “slow” reactions with smaller rate coefficients from this network.

TABLE 2. Detailed list of reactions considered in this study, including the accessible potential energy surfaces, and spin-state configurations. The focus of this network is reactions involved in the production of HCN from nitrogen and methane dissociation radicals. Direct competing reactions are also included. We define a fast reaction rate coefficient to be $>10^{-21} \text{ s}^{-1}$ for unimolecular reactions and $>10^{-21} \text{ cm}^3 \text{ s}^{-1}$ for bimolecular reactions.

Reaction equation	PES	Spin Configuration	Fast $k_f(298)?$	Fast $k_r(298)?$
$\text{H}_2\text{CN} \longleftrightarrow \text{HCN} + \text{H}$	doublet	$\text{H}_2\text{CN} \longleftrightarrow \text{HCN} + \text{H}$	Y	Y
$\text{H}_2\text{CN} + \text{H} \longleftrightarrow \text{HCN} + \text{H}_2$	singlet	$\text{H}_2\text{CN} + \text{H} \longleftrightarrow \text{HCN} + \text{H}_2$	Y	N
$\text{H}_2\text{CN} + \text{N} \longleftrightarrow \text{HCN} + \text{NH}$	singlet	$\text{H}_2\text{CN} + {}^2\text{N} \longleftrightarrow \text{HCN} + {}^1\text{NH}$	N	N
	triplet	$\text{H}_2\text{CN} + {}^4\text{N} \longleftrightarrow \text{HCN} + {}^3\text{NH}$	Y	N
		$\text{H}_2\text{CN} + {}^2\text{N} \longleftrightarrow \text{HCN} + {}^3\text{NH}$	N	N
$2\text{H}_2\text{CN} \longleftrightarrow \text{HCN} + \text{H}_2\text{CNH}$	singlet	$2\text{H}_2\text{CN} \longleftrightarrow \text{HCN} + \text{H}_2\text{CNH}$	Y	N
$\text{CH}_4 + \text{H} \longleftrightarrow \text{CH}_3 + \text{H}_2$	doublet	$\text{CH}_4 + \text{H} \longleftrightarrow \text{CH}_3 + \text{H}_2$	Y	Y
$\text{CH}_4 + \text{N} \longleftrightarrow \text{H}_3\text{CNH} \cdot \longleftrightarrow \text{H}_2\text{CNH} + \text{H}$	doublet	$\text{CH}_4 + {}^2\text{N} \longleftrightarrow \text{H}_3\text{CNH} \cdot \longleftrightarrow \text{H}_2\text{CNH} + \text{H}$	Y	N
$\text{CH}_4 + \text{N} \longleftrightarrow \text{H}_3\text{CNH} \cdot \longleftrightarrow \text{CH}_3 + \text{NH}$	doublet	$\text{CH}_4 + {}^2\text{N} \longleftrightarrow \text{H}_3\text{CNH} \cdot \longleftrightarrow \text{CH}_3 + {}^3\text{NH}$	N	N
$\text{CH}_3 + \text{H} \longleftrightarrow \text{CH}_4$	singlet	$\text{CH}_3 + \text{H} \longleftrightarrow \text{CH}_4$	Y	N
$\text{CH}_3 + \text{N} \longleftrightarrow \text{H}_3\text{CN} \cdot \longleftrightarrow \text{HCN} + \text{H}_2$	singlet	$\text{CH}_3 + {}^2\text{N} \longleftrightarrow {}^1\text{H}_3\text{CN} \cdot \longleftrightarrow \text{HCN} + \text{H}_2$	N	N
$\text{CH}_3 + \text{N} \longleftrightarrow \text{H}_3\text{CN} \cdot \longleftrightarrow \text{H}_2\text{CN} + \text{H}$	singlet	$\text{CH}_3 + {}^2\text{N} \longleftrightarrow {}^1\text{H}_3\text{CN} \cdot \longleftrightarrow \text{H}_2\text{CN} + \text{H}$	Y	N
	triplet	$\text{CH}_3 + {}^4\text{N} \longleftrightarrow {}^3\text{H}_3\text{CN} \cdot \longleftrightarrow \text{H}_2\text{CN} + \text{H}$	Y	N
		$\text{CH}_3 + {}^2\text{N} \longleftrightarrow {}^3\text{H}_3\text{CN} \cdot \longleftrightarrow \text{H}_2\text{CN} + \text{H}$	Y	N
$2\text{CH}_3 \longleftrightarrow \text{C}_2\text{H}_6$	singlet	$2\text{CH}_3 \longleftrightarrow \text{C}_2\text{H}_6$	Y	N
$\text{CH}_2 + \text{H} \longleftrightarrow \text{CH}_3$	doublet	${}^3\text{CH}_2 + \text{H} \longleftrightarrow \text{CH}_3$	Y	N
		${}^1\text{CH}_2 + \text{H} \longleftrightarrow \text{CH}_3$	Y	N
$\text{CH}_2 + \text{H}_2 \longleftrightarrow \text{CH}_4$	singlet	${}^1\text{CH}_2 + \text{H}_2 \longleftrightarrow \text{CH}_4$	Y	N
$\text{CH}_2 + \text{H}_2 \longleftrightarrow \text{CH}_3 + \text{H}$	triplet	${}^3\text{CH}_2 + \text{H}_2 \longleftrightarrow \text{CH}_3 + \text{H}$	Y	Y
$\text{CH}_2 + \text{N} \longleftrightarrow \text{H}_2\text{CN}$	doublet	${}^3\text{CH}_2 + {}^4\text{N} \longleftrightarrow {}^2\text{H}_2\text{CN}$	Y	N
		${}^3\text{CH}_2 + {}^2\text{N} \longleftrightarrow {}^2\text{H}_2\text{CN}$	Y	N
		${}^1\text{CH}_2 + {}^2\text{N} \longleftrightarrow {}^2\text{H}_2\text{CN}$	Y	N
	quartet	${}^1\text{CH}_2 + {}^4\text{N} \longleftrightarrow {}^4\text{H}_2\text{CN}$	Y	N
		${}^3\text{CH}_2 + {}^2\text{N} \longleftrightarrow {}^4\text{H}_2\text{CN}$	Y	N
$2\text{CH}_2 \longleftrightarrow \text{C}_2\text{H}_4$	singlet	${}^3\text{CH}_2 + {}^3\text{CH}_2 \longleftrightarrow {}^1\text{C}_2\text{H}_4$	Y	N
		${}^1\text{CH}_2 + {}^1\text{CH}_2 \longleftrightarrow {}^1\text{C}_2\text{H}_4$	Y	N
	triplet	${}^3\text{CH}_2 + {}^1\text{CH}_2 \longleftrightarrow {}^3\text{C}_2\text{H}_4$	Y	N
$\text{CH}_2 + \text{CH}_3 \longleftrightarrow \text{C}_2\text{H}_5 \cdot \longleftrightarrow \text{C}_2\text{H}_4 + \text{H}$	doublet	${}^3\text{CH}_2 + \text{CH}_3 \longleftrightarrow \text{C}_2\text{H}_5 \cdot \longleftrightarrow {}^1\text{C}_2\text{H}_4 + \text{H}$	Y	N
		${}^1\text{CH}_2 + \text{CH}_3 \longleftrightarrow \text{C}_2\text{H}_5 \cdot \longleftrightarrow {}^1\text{C}_2\text{H}_4 + \text{H}$	Y	N
	quartet	${}^3\text{CH}_2 + \text{CH}_3 \longleftrightarrow {}^4\text{C}_2\text{H}_5 \cdot \longleftrightarrow {}^3\text{C}_2\text{H}_4 + \text{H}$	N	N/A
$\text{CH}_2 + \text{CH}_4 \longleftrightarrow \text{C}_2\text{H}_6$	singlet	${}^1\text{CH}_2 + \text{CH}_4 \longleftrightarrow \text{C}_2\text{H}_6$	Y	N
$\text{CH}_2 + \text{CH}_4 \longleftrightarrow 2\text{CH}_3$	triplet	${}^3\text{CH}_2 + \text{CH}_4 \longleftrightarrow 2\text{CH}_3$	Y	Y
$\text{CH} + \text{H} \longleftrightarrow \text{CH}_2$	singlet	$\text{CH} + \text{H} \longleftrightarrow {}^1\text{CH}_2$	Y	N
	triplet	$\text{CH} + \text{H} \longleftrightarrow {}^3\text{CH}_2$	Y	N
$\text{CH} + \text{H}_2 \longleftrightarrow \text{CH}_3$	doublet	$\text{CH} + \text{H}_2 \longleftrightarrow \text{CH}_3$	Y	N
$\text{CH} + \text{N} \longleftrightarrow \text{HCN} \longleftrightarrow \text{CN} + \text{H}$	triplet	$\text{CH} + {}^4\text{N} \longleftrightarrow {}^3\text{HCN} \longleftrightarrow \text{CN} + \text{H}$	Y	N
		$\text{CH} + {}^2\text{N} \longleftrightarrow {}^3\text{HCN} \longleftrightarrow \text{CN} + \text{H}$	Y	N
$2\text{CH} \longleftrightarrow \text{C}_2\text{H}_2$	singlet	$\text{CH} + \text{CH} \longleftrightarrow \text{C}_2\text{H}_2$	Y	N
$\text{CH} + \text{CH}_4 \longleftrightarrow \text{C}_2\text{H}_5 \cdot \longleftrightarrow \text{C}_2\text{H}_4 + \text{H}$	doublet	$\text{CH} + \text{CH}_4 \longleftrightarrow \text{C}_2\text{H}_5 \cdot \longleftrightarrow \text{C}_2\text{H}_4 + \text{H}$	Y	N
$\text{NH} + \text{H} \longleftrightarrow \text{H}_2 + \text{N}$	doublet	${}^1\text{NH} + \text{H} \longleftrightarrow \text{H}_2 + {}^2\text{N}$	N/A	N
		${}^3\text{NH} + \text{H} \longleftrightarrow \text{NH}_2 \cdot \longleftrightarrow \text{H}_2 + {}^2\text{N}$	N	Y
	quartet	${}^3\text{NH} + \text{H} \longleftrightarrow \text{H}_2 + {}^4\text{N}$	Y	N
$\text{NH} + \text{N} \longleftrightarrow \text{N}_2\text{H} \cdot \longleftrightarrow \text{N}_2 + \text{H}$	doublet	${}^3\text{NH} + {}^4\text{N} \longleftrightarrow \text{N}_2\text{H} \cdot \longleftrightarrow \text{N}_2 + \text{H}$	Y	N
		${}^1\text{NH} + {}^2\text{N} \longleftrightarrow \text{N}_2\text{H} \cdot \longleftrightarrow \text{N}_2 + \text{H}$	N/A	N
		${}^3\text{NH} + {}^2\text{N} \longleftrightarrow \text{N}_2\text{H} \cdot \longleftrightarrow \text{N}_2 + \text{H}$	Y	N

Reactions are N/A if they require species that are not efficiently produced in this network.

METHODS

ceeds along a coordinate (e.g. the distance between two

Variational Transition State Theory

Reactions can be visualized in one dimension using potential energy diagrams (see Figure 1). A reaction pro-

atoms), from the reactant geometry, to the product geometry. In some cases, the minimum energy path (MEP) from reactants to products requires proceeding through a geometry of higher potential energy than the reactant and product geometries. This increase in potential energy along a reaction coordinate is known as the energy barrier. The peak of the energy barrier describes the conventional transition state.

In reality, reactions have more than one dimension (e.g. bond distances, angles between bonds, dihedral angles), thus the energy barrier is more appropriately described as a saddle point, and the MEP is the path of steepest descent from saddle point to the reactant and product minima. The rate of a reaction can be described as how frequently molecules travel the entire MEP, and is quantified by the reaction rate coefficient, k .

We calculate gas phase chemical reaction rate coefficients using canonical variational transition state theory (CVT). The basis for this method is to vary the reaction coordinate (e.g. the carbon-hydrogen bond distance) along the MEP in order to find the minimum rate constant. Unlike conventional transition state theory, CVT allows us to calculate reaction rate coefficients for both barrierless and non-barrierless reactions, while minimizing the error due to trajectories that recross the transition state rather than descend into products⁴⁰. This can be visualized as finding a location past the saddle point of the MEP, that recrossing reactants tend not to reach (see Figure 1). This location is determined as the location where the generalized transition state (GT) rate coefficient is at its smallest value, therefore providing best dynamical bottleneck⁴⁰.

The CVT reaction rate coefficient is expressed as^{41–43}

$$k_{CVT}(T, s) = \min_s \{k_{GT}(T, s)\}. \quad (31)$$

Neglecting the tunneling effect, the generalized transition state theory (GT) reaction rate coefficient can be approximated via the Eyring Equation^{41–49}. The Eyring equation uses a statistical mechanics approach to calculate the rate coefficient by dividing the density of forward-crossing states per unit time by the density of reactant states.

$$k_{GT}(T, s) = \sigma \frac{k_B T}{h} \frac{Q^\ddagger(T, s)}{\prod_{i=1}^N Q_i^{n_i}(T)} e^{-E_0(s)/RT} \quad (32)$$

where σ is the reaction path symmetry number or reaction path multiplicity (i.e. the number of equivalent reaction paths from reactants to products), k_B is the Boltzmann constant (1.38×10^{-23} J K⁻¹), T is temperature (K), h is the Planck constant (6.63×10^{-34} J·s), Q^\ddagger is the partition function of the transition state per unit volume (cm⁻³), with its zero of energy at the saddle point, Q_i is the partition function of species i per unit volume, with its zero of energy at the equilibrium position of species i

(i.e. as if it is infinitely separated from any other reactant), n_i is the stoichiometric coefficient of species i , N is the number of reactant species, E_0 is the energy barrier (the difference in zero-point energies between the generalized transition state and the reactants) (kJ mol⁻¹), and R is the gas constant (8.314×10^{-3} kJ K⁻¹ mol⁻¹).

Because classical partition functions involve integrating over the Boltzmann factor ($e^{-E/RT}$), an additional exponential factor appears naturally in the Eyring equation due to the difference in zeros of energy between the transition state and reactant states.

To find the location along the MEP where the GT rate coefficient is at its smallest value, we use the maximum Gibbs free energy criterion, which gives a compromise of energetic and entropic effects^{41,50}. To obtain a similar accuracy for all calculations, we use a reaction coordinate precision of 0.01 Å. Looking at the quasithermodynamic representation of transition-state theory, we see that the maximum value for $\Delta G_{GT}(T, s)$ corresponds to a minimum value for $k_{GT}(T, s)$

$$k_{GT}(T, s) = \frac{k_B T}{h} K^0 e^{-\Delta G_{GT}(T, s)/RT}, \quad (33)$$

where K^0 is the reaction quotient under standard state conditions (i.e. 1 for unimolecular reactions, and 1 cm³ for bimolecular reactions), and $\Delta G_{GT}(T, s)$ is the difference in the Gibbs free energy between transition state and reactants (kJ mol⁻¹).

The conventional transition state, energy barrier, and variational transition state are illustrated with a potential energy diagram in Figure 1.

The zero-point energies and partition functions for the reactants and transition states are calculated using the Gaussian 09 software package⁵¹. A brief summary of the theory behind these calculations is detailed below. We refer the reader to Ochterski⁵² for further details.

The partition functions per unit volume are expanded into their 4 components

$$Q = \frac{q_t}{V} q_e q_v q_r. \quad (34)$$

where q_t is the translational component, V is the volume (cm⁻³), q_e is the electronic component, q_v is the vibrational component, q_r is the rotational component not including the rotational symmetry number (this is included in the reaction path multiplicity).

From classical statistical mechanics, the translational partition function per unit volume is⁵²

$$\frac{q_t}{V} = \left(\frac{2\pi m k_B T}{h^2} \right)^{3/2}, \quad (35)$$

where m is the mass of the species (kg).

The electronic partition function is estimated as the degeneracy of the first energy level, i.e. the spin multiplicity⁵²

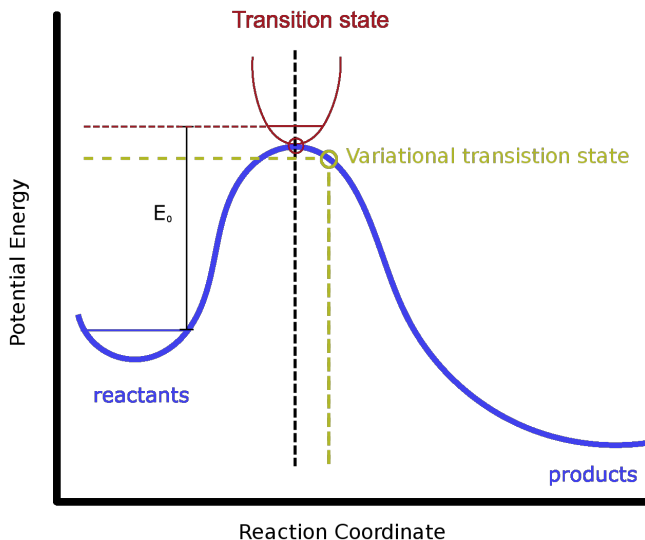


FIG. 1. A schematic representation of a reaction: proceeding from the reactants, over the potential energy barrier, E_0 , through the transition state (red circle), and onto the products. The variational transition state (gold circle) is a location beyond the conventional transition state, where reactants that recross the barrier tend not to reach. The variational transition state is located where the reaction rate coefficient is at a minimum, thus providing the best dynamical bottleneck.

$$q_e = 2S + 1, \quad (36)$$

where S is the total spin due to unpaired electrons. For example, a hydrogen atom has 1 unpaired electron of spin $1/2$, and thus its $q_e = 2(1/2) + 1 = 2$.

Gaussian calculates the vibrational partition function as a quantum harmonic oscillator. We note that for the zero-point energies of molecules, Gaussian places the zero of energy at the bottom of the internuclear potential. Thus, with this same location for the zero of energy, the vibrational partition function equates to

$$q_v = \prod_{n=1}^N \frac{e^{-\Theta_n/2T}}{1 - e^{-\Theta_n/T}}, \quad (37)$$

where N is the number of vibrational modes, Θ_n is the vibrational temperature of the n^{th} mode ($\Theta_n = \frac{\hbar\omega_n}{k_B}$), and T is temperature.

By default, Gaussian calculates the rotational partition function as a rigid rotor. For linear molecules excluding rotational symmetry,

$$q_r = \left(\frac{T}{\Theta_r} \right), \quad (38)$$

and for polyatomic molecules excluding rotational symmetry,

$$q_r = \pi^{1/2} \left(\frac{T^{3/2}}{(\Theta_{r,x}\Theta_{r,y}\Theta_{r,z})^{3/2}} \right), \quad (39)$$

where Θ_r is the rotational temperature ($\Theta_r = \frac{h^2}{8\pi^2Ik_B}$, and I is the moment of inertia (in the case of a polyatomic molecule, I_x , I_y , and I_z are the principal moments of inertia).

Gaussian displays an output for the rotational symmetry number (σ_r) of each molecule, however for all the reactants, transition states and products in our study, Gaussian displayed $\sigma_r = 1$. For this reason we calculate the rotational symmetry in Equation 32 manually⁴⁸ (the calculated symmetry numbers are listed in Table S10 in SI).

Quantum Computational Simulations

We perform quantum computational simulations with the Gaussian software package⁵¹ using the Becke-Half-and-Half-Lee-Yang-Parr (BHandHLYP) density functional^{53,54}. We chose BHandHLYP for two reasons. Firstly, it is a relatively inexpensive method that can be used for an extended transition state study such as this. Secondly, in a computational methods comparison of the well-studied reaction $\text{CH}_4 + \text{H} \rightarrow \text{CH}_3 + \text{H}_2$, BHandHLYP provided the most accurate rate coefficient compared to calculations using HF, CCSD, B3LYP, and M06-2x (see computational methods comparison in SI for more details). CAM-B3LYP also provided an accurate rate coefficient for this reaction, however the value from BHandHLYP offers a better compromise between experimental and suggested values.

Hartree-Fock (HF) methods tend to overestimate the energy barrier, whereas Density Functional Theory (DFT) methods (e.g. B3LYP) tend to underestimate the energy barrier. BHandHLYP is a hybrid functional that improves performance by using 50% HF and 50% DFT for the exchange energy calculation. All simulations are performed with the augmented correlation consistent polarized valence double zeta (aug-cc-pVDZ) basis set in order to achieve reasonable computation times.

Typically, when there is only one reaction spin configuration for a given PES, we do not specify the local spins in Gaussian when calculating the MEP. However in some cases not specifying the local spin, regardless of the number of possible spin configurations, leads to convergence issues. In these cases we specify the local spins to allow the calculation to converge. When there is more than one reaction spin configuration for a given PES, e.g., $\text{CH}_3 + {}^4\text{N} \rightarrow {}^3\text{H}_3\text{CN} \cdot \rightarrow \text{H}_2\text{CN} + \text{H}$ and $\text{CH}_3 + {}^2\text{N} \rightarrow {}^3\text{H}_3\text{CN} \cdot \rightarrow \text{H}_2\text{CN} + \text{H}$ on the triplet surface, we specify the local spins of the reactants in Gaussian to find the MEP's for each individual spin configuration.

Temperature Dependence of Rate Coefficients

Temperatures in the early Earth and Titan atmospheres fit comfortably within the range of 50–400 K^{14,55,56}. The CVT rate coefficient equation for reactions with barriers includes a temperature-dependent exponential term (see Equation 32). This exponential temperature dependence typically leads to reaction rate coefficients which vary by multiple orders of magnitude over 50–400 K. The exponential term is omitted for barrierless reactions, and thus the temperature dependence for barrierless reaction rate coefficients is much smaller. Typically rate coefficients for barrierless reactions have either no temperature dependence, or a weak temperature dependence, varying by less than a factor of a two or three from 50–400 K^{43,57–60}.

Temperature dependence for rate coefficients can be expressed using the Arrhenius equation⁶¹,

$$k(T) = \alpha \left(\frac{T}{300} \right)^\beta e^{-\gamma/T}, \quad (40)$$

where α , β , and γ are fitting parameters, which we will refer to as the Arrhenius coefficients. Units for $k(T)$ are s^{-1} for unimolecular reactions and cm^3s^{-1} for bimolecular reactions.

We calculate the rate coefficients for the reactions with

TABLE 3: Reaction rate coefficients for the atmospheric reaction network calculated in this study. All reactions are involved in HCN production in the early Earth atmosphere or are key competing reactions. Calculations are performed at the BHandHLYP/aug-cc-pVDZ level of theory. Slow reactions ($k < 10^{-21}$), either forward or reverse, are not included in this network. In the column labeled “barrier?” we specify whether the rate-limiting step (or the only step) of the reaction has an energy barrier. The error factor is the multiplicative or divisional factor from the nearest experimental or suggested value; the error factor is 1 if the calculated value is within the range of experimental or suggested values. 36% of these reactions have no experimental or suggested rate coefficients. First-order rate coefficients have units s^{-1} . Second-order rate coefficients have units cm^3s^{-1} .

Reaction equation	Forward or Reverse?	Barrier?	k(298) calculated	k(298) experimental	Error factor
$\text{H}_2\text{CN} \longleftrightarrow \text{HCN} + \text{H}$	F	Y	1.6×10^{-11}		
	R	Y	2.7×10^{-14}		
$\text{H}_2\text{CN} + \text{H} \longrightarrow \text{HCN} + \text{H}_2$	F	N	1.8×10^{-11}	8.3×10^{-11}	5
$\text{H}_2\text{CN} + {}^4\text{N} \longleftrightarrow \text{HCN} + {}^3\text{NH}$	F	Y	9.4×10^{-13}	4.4×10^{-11}	47
$2\text{H}_2\text{CN} \longleftrightarrow \text{HCN} + \text{H}_2\text{CNH}$	F	N	${}^a 3.7 \times 10^{-14}$	$3.3\text{--}8.3 \times 10^{-12}$	89
$\text{CH}_4 + \text{H} \longleftrightarrow \text{CH}_3 + \text{H}_2$	F	Y	8.1×10^{-18}	$8.2 \times 10^{-19}\text{--}3.5 \times 10^{-17}$	1
	R	Y	3.2×10^{-21}	$9.6 \times 10^{-21}\text{--}1.3 \times 10^{-20}$	3
$\text{CH}_4 + {}^2\text{N} \longleftrightarrow \text{H}_3\text{CNH} \longleftrightarrow {}^1\text{H}_2\text{CNH} + \text{H}$	F	Y	${}^b 4.7 \times 10^{-11}$	$2.4\text{--}4.5 \times 10^{-12}$	10
$\text{CH}_3 + \text{H} \longleftrightarrow \text{CH}_4$	F	N	7.9×10^{-11}	$1.5\text{--}4.7 \times 10^{-10}$	2
$\text{CH}_3 + {}^4\text{N} \longleftrightarrow {}^3\text{H}_3\text{CN} \cdot \longleftrightarrow \text{H}_2\text{CN} + \text{H}$	F	N	3.3×10^{-11}	$5.0\text{--}7.7 \times 10^{-11}$	1.5
$\text{CH}_3 + {}^2\text{N} \longleftrightarrow {}^3\text{H}_3\text{CN} \cdot \longleftrightarrow \text{H}_2\text{CN} + \text{H}$	F	N	1.0×10^{-10}		
$\text{CH}_3 + {}^2\text{N} \longleftrightarrow {}^1\text{H}_3\text{CN} \cdot \longleftrightarrow \text{H}_2\text{CN} + \text{H}$	F	N	3.1×10^{-11}		
$2\text{CH}_3 \longleftrightarrow \text{C}_2\text{H}_6$	F	N	7.3×10^{-13}	$3.5\text{--}6.5 \times 10^{-11}$	48
${}^1\text{CH}_2 + \text{H} \longleftrightarrow \text{CH}_3$	F	N	8.4×10^{-11}	5.0×10^{-11}	2
${}^1\text{CH}_2 + \text{H}_2 \longleftrightarrow \text{CH}_4$	F	N	1.0×10^{-11}	${}^c 7.0 \times 10^{-12}\text{--}1.3 \times 10^{-10}$	1
${}^1\text{CH}_2 + {}^4\text{N} \longleftrightarrow {}^4\text{H}_2\text{CN}$	F	N	1.1×10^{-10}		
${}^1\text{CH}_2 + {}^2\text{N} \longleftrightarrow {}^2\text{H}_2\text{CN}$	F	N	1.5×10^{-10}		
${}^1\text{CH}_2 + {}^1\text{CH}_2 \longleftrightarrow \text{C}_2\text{H}_4$	F	N	9.9×10^{-12}	5.0×10^{-11}	5
${}^1\text{CH}_2 + {}^3\text{CH}_2 \longleftrightarrow \text{C}_2\text{H}_4$	F	N	${}^d 3.5 \times 10^{-11}$	3.0×10^{-11}	1
${}^1\text{CH}_2 + \text{CH}_3 \longleftrightarrow \text{C}_2\text{H}_5 \cdot \longleftrightarrow \text{C}_2\text{H}_4 + \text{H}$	F	N	2.3×10^{-11}	3.0×10^{-11}	1

barriers at 50, 100, 200, 298, and 400 K and fit the results to the expression above to obtain the Arrhenius coefficients. For the sake of feasibility, we assume the rate coefficient for barrierless reactions is constant within this temperature range, as is typical⁶².

RESULTS

For detailed results, see theoretical case studies for 35 of the reactions in SI.

In Table 3, we display the reaction rate coefficients calculated using the CVT method described above at 298 K, and the comparative ranges of experimental values.

Conformance to Experiments

Of the 42 total reactions in this network, $\sim 54\%$ have been studied experimentally at or near 298 K (see the “k(298) experimental” column in Table 3 for experimental values). Another $\sim 10\%$ have been estimated based on the rate coefficients of similar bond additions and decompositions, and/or thermodynamics. 36% of the reactions have no experimental rate coefficients (those with no “k(298) experimental” value in Table 3), and in most cases, we are the first to calculate them theoretically.

$^1\text{CH}_2 + \text{CH}_4 \longleftrightarrow \text{C}_2\text{H}_6$	F	N	6.1×10^{-13}	$^e 1.9 \times 10^{-12} - 7.3 \times 10^{-11}$	3
$^3\text{CH}_2 + \text{H} \longleftrightarrow \text{CH}_3$	F	N	5.6×10^{-10}	$^f 8.3 \times 10^{-11} - 2.7 \times 10^{-10}$	2
$^3\text{CH}_2 + \text{H}_2 \longleftrightarrow \text{CH}_3 + \text{H}$	F	Y	2.5×10^{-16}	$< 5.0 \times 10^{-14} - 5.0 \times 10^{-15}$	g
	R	Y	1.4×10^{-20}		
$^3\text{CH}_2 + ^4\text{N} \longleftrightarrow ^2\text{H}_2\text{CN}$	F	N	1.3×10^{-10}		
$^3\text{CH}_2 + ^2\text{N} \longleftrightarrow ^2\text{H}_2\text{CN}$	F	N	2.7×10^{-10}		
$^3\text{CH}_2 + ^2\text{N} \longleftrightarrow ^4\text{H}_2\text{CN}$	F	N	4.3×10^{-10}		
$^3\text{CH}_2 + ^3\text{CH}_2 \longleftrightarrow \text{C}_2\text{H}_4$	F	N	4.2×10^{-11}	5.3×10^{-11}	1
$^3\text{CH}_2 + \text{CH}_3 \longleftrightarrow \text{C}_2\text{H}_5 \cdot \longleftrightarrow \text{C}_2\text{H}_4 + \text{H}$	F	N	8.8×10^{-12}	$5.0 \times 10^{-11} - 2.1 \times 10^{-10}$	6
$^3\text{CH}_2 + \text{CH}_4 \longleftrightarrow 2\text{CH}_3$	F	Y	1.4×10^{-16}	$< 5.0 \times 10^{-14} - 3.0 \times 10^{-19}$	g
	R	N	5.5×10^{-11}		
$\text{CH} + \text{H} \longleftrightarrow ^1\text{CH}_2$	F	N	1.5×10^{-10}		
$\text{CH} + \text{H} \longleftrightarrow ^3\text{CH}_2$	F	N	5.3×10^{-10}		
$\text{CH} + \text{H}_2 \longleftrightarrow \text{CH}_3$	F	N	7.9×10^{-11}	$1.0 \times 10^{-12} - 1.6 \times 10^{-10}$	1
$\text{CH} + ^4\text{N} \longleftrightarrow ^3\text{HCN} \longleftrightarrow \text{CN} + \text{H}$	F	N	1.1×10^{-10}	$2.1 \times 10^{-11} - 1.6 \times 10^{-10}$	1
$\text{CH} + ^2\text{N} \longleftrightarrow ^3\text{HCN} \longleftrightarrow \text{CN} + \text{H}$	F	N	2.7×10^{-10}		
$2\text{CH} \longleftrightarrow \text{C}_2\text{H}_2$	F	N	1.3×10^{-11}	$1.7 - 2.0 \times 10^{-10}$	13
$\text{CH} + \text{CH}_4 \longleftrightarrow \text{C}_2\text{H}_5 \cdot \longleftrightarrow \text{C}_2\text{H}_4 + \text{H}$	F	N	3.8×10^{-13}	$2.0 \times 10^{-12} - 3.0 \times 10^{-10}$	5
$^3\text{NH} + \text{H} \longleftrightarrow \text{H}_2 + ^4\text{N}$	F	Y	1.4×10^{-11}	3.2×10^{-12}	4
$^3\text{NH} + \text{H} \longleftrightarrow \text{NH}_2 \cdot \longleftrightarrow \text{H}_2 + ^2\text{N}$	R	Y	5.1×10^{-11}	$1.7 - 5.0 \times 10^{-12}$	10
$^3\text{NH} + ^4\text{N} \longleftrightarrow \text{N}_2\text{H} \cdot \longleftrightarrow \text{N}_2 + \text{H}$	F	N	4.0×10^{-11}	$2.5 - 2.6 \times 10^{-11}$	1.5
$^3\text{NH} + ^2\text{N} \longleftrightarrow \text{N}_2\text{H} \cdot \longleftrightarrow \text{N}_2 + \text{H}$	F	N	5.5×10^{-11}		

^a Simulations did not converge beyond a H-N bond distance of 1.95 Å. The calculated rate coefficient is an lower bound.

^b Simulations did not converge beyond a H-N bond distance of 2.82 Å. The calculated rate coefficient is a lower bound.

^c Experimental values are from the two-step reaction $^1\text{CH}_2 + \text{H}_2 \longrightarrow \text{CH}_4 \cdot \longrightarrow \text{CH}_3 + \text{H}$. Our theoretical work suggests the first step is the rate-limiting step, thus these values can be attributed to $^1\text{CH}_2 + \text{H}_2 \longrightarrow \text{CH}_4$.

^d Simulations did not converge beyond a C-C bond distance of 3.52 Å. The calculated rate coefficient is a lower bound.

^e Experimental values are from the two-step reaction $^1\text{CH}_2 + \text{CH}_4 \longrightarrow \text{C}_2\text{H}_6 \cdot \longrightarrow 2\text{CH}_3$. Our theoretical work suggests the first step is the rate-limiting step, thus these values can be attributed to $^1\text{CH}_2 + \text{CH}_4 \longrightarrow \text{C}_2\text{H}_6$.

^f Experimental values are from the two-step reaction $^3\text{CH}_2 + \text{H} \longrightarrow \text{CH}_3 \cdot \longrightarrow \text{CH} + \text{H}_2$. Our theoretical work suggests the first step is the rate-limiting step, thus these values can be attributed to $^3\text{CH}_2 + \text{H} \longrightarrow \text{CH}_3$.

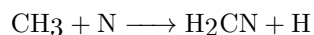
^g The theoretical value agrees with the experimental upper bounds.

It is often assumed that experiments provide the closest values to the true reaction rate coefficients. However for a single reaction, separate experiments can measure coefficients that differ by over 2 orders of magnitude (e.g. for $\text{CH} + \text{CH}_4 \longrightarrow \text{C}_2\text{H}_4 + \text{H}$, $k = 2.0 \times 10^{-12}$ to $3.0 \times 10^{-10} \text{ cm}^3\text{s}^{-1}$). This variation can be due to differing experimental methods, instrumentation, and analytical techniques. Furthermore, the reactions reported in experiments may not correspond to direct pathways. Instead there may be intermediates embedded in multiple reaction steps that correspond to the overall measured reaction rate coefficient. Theoretical analysis and mechanistic modeling can be used to sort out the most likely steps in a multiple-step reaction in order to avoid the inclusion of redundant reaction pathways in chemical networks.

In this work, we calculate the reaction rate coefficients for the reactions involved in HCN production from atmospheric nitrogen and methane radicals, as well as the most direct competing reactions. This network includes 15 reactions that have no experimental or suggested value in the literature, and six of these are directly involved in atmospheric HCN synthesis. All our calculations are performed at the same level of theory,

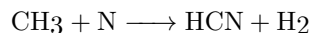
i.e. BHandHLYP/aug-cc-pVDZ, therefore we expect the error in the rate coefficients to be similar for all reactions.

The largest discrepancy between experiments and theory is for the reaction of $\text{CH}_3 + \text{N} \longrightarrow \text{products}$. Stief et al.⁶³ measured the rate coefficient of $\text{CH}_3 + \text{N} \longrightarrow \text{products}$ to be $8.6 \times 10^{-11} \text{ cm}^3\text{s}^{-1}$, and Marston et al.²⁸ reported the experimental branching ratios to be



$$\Phi \sim 0.9,$$

and



$$\Phi \sim 0.1.$$

However, we find only the first of these reactions has an efficient rate coefficient ($k = 3.3 \times 10^{-11} \text{ cm}^3\text{s}^{-1}$), and that the second reaction is very inefficient ($k \sim 10^{-28} \text{ cm}^3\text{s}^{-1}$). This result agrees with past theoretical work, which suggests the measurement of the second reaction likely corresponds to a series of reactions passing through the H_2CN intermediate⁶⁴. For more details of our analysis, see theoretical case study 4 in SI.

Our theoretical reaction rate coefficients are within an order of magnitude of the closest experimental or suggested value from the literature 93% of the time. The theoretical reaction rate coefficients for $\text{H}_2\text{CN} + {}^4\text{N} \longrightarrow \text{HCN} + {}^3\text{NH}$, $2\text{CH}_3 \longrightarrow \text{C}_2\text{H}_6$, and $2\text{H}_2\text{CN} \longrightarrow \text{HCN} + \text{H}_2\text{CNH}$, on the other hand, differ by factors of 47, 48, and 89 from the closest experimental values, respectively. In the case of $2\text{H}_2\text{CN} \longrightarrow \text{HCN} + \text{H}_2\text{CNH}$, we are unable to converge the calculations beyond a H-N bond distance of 1.95 Å, and in this case, the rate coefficients increase towards the experimental values with increasing H-N bond distance. Therefore we expect the major source of discrepancy between theory and experiment for this reaction is due to computational convergence. With regards to the other two reactions, we find the discrepancies to be due to our chosen computational method. Calculations at the CCSD/aug-cc-pVDZ level of theory bring the rate coefficient for $2\text{CH}_3 \longrightarrow \text{C}_2\text{H}_6$ to within its experimental range. CCSD calculations, however, do not universally increase accuracy. The rate coefficient for $\text{H}_2\text{CN} + {}^4\text{N} \longrightarrow \text{HCN} + {}^3\text{NH}$ when calcu-

lated using CCSD/aug-cc-pVDZ is over 3 orders of magnitude smaller than the experimental value. On the other hand, this reaction rate coefficient comes to within $\sim 80\%$ of the experimental value when using CAM-B3LYP/aug-cc-pVDZ. Because CAM-B3LYP has less short-range HF exchange than BHandHLYP⁶⁵, this method is expected to predict a smaller barrier height than BHandHLYP. Thus in this case, where BHandHLYP overestimates the barrier height (underestimates the rate coefficient) with respect to the experimental value, CAM-B3LYP brings the calculated rate coefficient closer to the experimental value. Of future interest would be to test the accuracy of all the rate coefficients in our network when calculated with CAM-B3LYP/aug-cc-pVDZ.

Temperature Dependencies

In Table 4, we display the Arrhenius coefficients for the reactions in this network for temperatures between 50 and 400 K. We also display the temperature-dependent rate coefficients for the 10 reactions that have barriers in Figure 2.

TABLE 4: Arrhenius coefficients for the 42 reactions in this network. Rate coefficients are calculated for the reactions with barriers at 50, 100, 200, 298, and 400 K, and are fit to the Arrhenius expression $k(T) = \alpha \left(\frac{T}{300}\right)^\beta e^{-\gamma/T}$. Barrierless reaction rate coefficients typically do not vary by more than a factor of 1–3 for temperatures between 50 and 400 K^{43,57–60}, therefore for feasibility of calculations we set the β and γ for these reactions to zero. For the majority of reactions, fits to the Arrhenius expression are continuous in the temperature range from 50–400 K; however, for two reactions there are discontinuities and thus these reactions have two sets of Arrhenius coefficients.

Reaction equation	Forward or Reverse?	Temperature range (K)	α	β	γ
$\text{H}_2\text{CN} \longleftrightarrow \text{HCN} + \text{H}$	F	50–400	7.9×10^{13}	0	16952
	R	50–400	6.5×10^{-11}	0.7	2318
$\text{H}_2\text{CN} + \text{H} \longrightarrow \text{HCN} + \text{H}_2$	F	50–400	1.8×10^{-11}	0	0
$\text{H}_2\text{CN} + {}^4\text{N} \longleftrightarrow \text{HCN} + {}^3\text{NH}$	F	50–279	7.8×10^{-12}	1.63	938
	F	279–400	1.2×10^{-11}	0	758
$2\text{H}_2\text{CN} \longleftrightarrow \text{HCN} + \text{H}_2\text{CNH}$	F	50–400	3.7×10^{-14}	0	0
$\text{CH}_4 + \text{H} \longleftrightarrow \text{CH}_3 + \text{H}_2$	F	50–400	5.5×10^{-11}	0.6	4689
	R	50–400	1.5×10^{-11}	-0.32	6632
$\text{CH}_4 + {}^2\text{N} \longleftrightarrow \text{H}_3\text{CNH} \longleftrightarrow {}^1\text{H}_2\text{CNH} + \text{H}$	F	50–400	4.7×10^{-10}	0	700
$\text{CH}_3 + \text{H} \longleftrightarrow \text{CH}_4$	F	50–400	7.9×10^{-11}	0	0
$\text{CH}_3 + {}^4\text{N} \longleftrightarrow {}^3\text{H}_3\text{CN} \cdot \longleftrightarrow \text{H}_2\text{CN} + \text{H}$	F	50–400	3.3×10^{-11}	0	0
$\text{CH}_3 + {}^2\text{N} \longleftrightarrow {}^3\text{H}_3\text{CN} \cdot \longleftrightarrow \text{H}_2\text{CN} + \text{H}$	F	50–400	1.0×10^{-10}	0	0
$\text{CH}_3 + {}^2\text{N} \longleftrightarrow {}^1\text{H}_3\text{CN} \cdot \longleftrightarrow \text{H}_2\text{CN} + \text{H}$	F	50–400	3.1×10^{-11}	0	0
$2\text{CH}_3 \longleftrightarrow \text{C}_2\text{H}_6$	F	50–400	7.3×10^{-13}	0	0
${}^1\text{CH}_2 + \text{H} \longleftrightarrow \text{CH}_3$	F	50–400	8.4×10^{-11}	0	0
${}^1\text{CH}_2 + \text{H}_2 \longleftrightarrow \text{CH}_4$	F	50–400	1.0×10^{-11}	0	0
${}^1\text{CH}_2 + {}^4\text{N} \longleftrightarrow {}^4\text{H}_2\text{CN}$	F	50–400	1.1×10^{-10}	0	0
${}^1\text{CH}_2 + {}^2\text{N} \longleftrightarrow {}^2\text{H}_2\text{CN}$	F	50–400	1.5×10^{-10}	0	0
${}^1\text{CH}_2 + {}^1\text{CH}_2 \longleftrightarrow \text{C}_2\text{H}_4$	F	50–400	9.9×10^{-12}	0	0
${}^1\text{CH}_2 + {}^3\text{CH}_2 \longleftrightarrow \text{C}_2\text{H}_4$	F	50–400	3.5×10^{-11}	0	0
${}^1\text{CH}_2 + \text{CH}_3 \longleftrightarrow \text{C}_2\text{H}_5 \cdot \longleftrightarrow \text{C}_2\text{H}_4 + \text{H}$	F	50–400	2.3×10^{-11}	0	0
${}^1\text{CH}_2 + \text{CH}_4 \longleftrightarrow \text{C}_2\text{H}_6$	F	50–400	6.1×10^{-13}	0	0
${}^3\text{CH}_2 + \text{H} \longleftrightarrow \text{CH}_3$	F	50–400	5.6×10^{-10}	0	0
${}^3\text{CH}_2 + \text{H}_2 \longleftrightarrow \text{CH}_3 + \text{H}$	F	50–400	5.4×10^{-11}	0	3661
	R	50–400	4.2×10^{-11}	0.82	6504
${}^3\text{CH}_2 + {}^4\text{N} \longleftrightarrow {}^2\text{H}_2\text{CN}$	F	50–400	1.3×10^{-10}	0	0

${}^3\text{CH}_2 + {}^2\text{N} \longleftrightarrow {}^2\text{H}_2\text{CN}$	F	50–400	2.7×10^{-10}	0	0
${}^3\text{CH}_2 + {}^2\text{N} \longleftrightarrow {}^4\text{H}_2\text{CN}$	F	50–400	4.3×10^{-10}	0	0
${}^3\text{CH}_2 + {}^3\text{CH}_2 \longleftrightarrow \text{C}_2\text{H}_4$	F	50–400	4.2×10^{-11}	0	0
${}^3\text{CH}_2 + \text{CH}_3 \longleftrightarrow \text{C}_2\text{H}_5 \cdot \longleftrightarrow \text{C}_2\text{H}_4 + \text{H}$	F	50–400	8.8×10^{-12}	0	0
${}^3\text{CH}_2 + \text{CH}_4 \longleftrightarrow 2 \text{CH}_3$	F	50–400	5.5×10^{-11}	1.63	3840
	R	50–400	5.5×10^{-11}	0	0
$\text{CH} + \text{H} \longleftrightarrow {}^1\text{CH}_2$	F	50–400	1.5×10^{-10}	0	0
$\text{CH} + \text{H} \longleftrightarrow {}^3\text{CH}_2$	F	50–400	5.3×10^{-10}	0	0
$\text{CH} + \text{H}_2 \longleftrightarrow \text{CH}_3$	F	50–400	7.9×10^{-11}	0	0
$\text{CH} + {}^4\text{N} \longleftrightarrow {}^3\text{HCN} \longleftrightarrow \text{CN} + \text{H}$	F	50–400	1.1×10^{-10}	0	0
$\text{CH} + {}^2\text{N} \longleftrightarrow {}^3\text{HCN} \longleftrightarrow \text{CN} + \text{H}$	F	50–400	2.7×10^{-10}	0	0
$2 \text{CH} \longleftrightarrow \text{C}_2\text{H}_2$	F	50–400	1.3×10^{-11}	0	0
$\text{CH} + \text{CH}_4 \longleftrightarrow \text{C}_2\text{H}_5 \cdot \longleftrightarrow \text{C}_2\text{H}_4 + \text{H}$	F	50–400	3.8×10^{-13}	0	0
${}^3\text{NH} + \text{H} \longleftrightarrow \text{H}_2 + {}^4\text{N}$	F	50–400	1.4×10^{-11}	0	0
${}^3\text{NH} + \text{H} \longleftrightarrow \text{NH}_2 \cdot \longleftrightarrow \text{H}_2 + {}^2\text{N}$	R	50–304	1.1×10^{-9}	0.83	909
	R	304–400	1.5×10^{-9}	0	1128
${}^3\text{NH} + {}^4\text{N} \longleftrightarrow \text{N}_2\text{H} \cdot \longleftrightarrow \text{N}_2 + \text{H}$	F	50–400	4.0×10^{-11}	0	0
${}^3\text{NH} + {}^2\text{N} \longleftrightarrow \text{N}_2\text{H} \cdot \longleftrightarrow \text{N}_2 + \text{H}$	F	50–400	5.5×10^{-11}	0	0

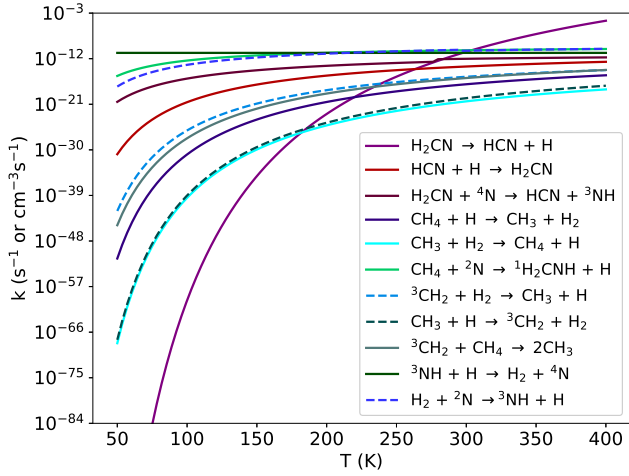
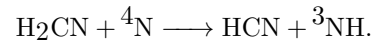
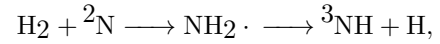
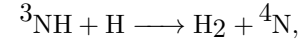


FIG. 2. Temperature dependence of the 11 reactions in our network that have barriers. Rate coefficients are calculated at 50, 100, 200, 298, and 400 K, and are fit to the Arrhenius expression $k(T) = \alpha \left(\frac{T}{300}\right)^\beta e^{-\gamma/T}$. Two of the fits have discontinuities: $\text{H}_2\text{CN} + {}^4\text{N} \longrightarrow \text{HCN} + {}^3\text{NH}$ at 279 K, and $\text{H}_2 + {}^2\text{N} \longrightarrow {}^3\text{NH} + \text{H}$ at 304 K. First-order rate coefficients have units s^{-1} . Second-order rate coefficients have units cm^3s^{-1} .

The majority of the reactions with barriers fit to one Arrhenius expression for the 50–400 K temperature range, however there were two special cases that had discontinuous fits. Both $\text{H}_2\text{CN} + {}^4\text{N} \longrightarrow \text{HCN} + {}^3\text{NH}$ and $\text{H}_2 + {}^2\text{N} \longrightarrow \text{NH}_2 \cdot \longrightarrow {}^3\text{NH} + \text{H}$ have two Gibbs maxima along their MEP’s. As temperature increases, the shorter of the Gibbs humps increases in height until it reaches the same height as the other hump at some characteristic temperature. Beyond this temperature, the previously shorter Gibbs hump surpasses the other hump in height, becoming the new location of the variational transition state. Such a drastic change in the location of the variational transition state before and after

the characteristic temperature creates a discontinuity in the temperature dependent rate coefficient, that is better fit to two separate sets of Arrhenius coefficients.

The rate coefficients of four of the reactions with barriers do not decrease rapidly with decreasing temperatures, and remain “fast” ($k > 10^{-21} \text{ cm}^3\text{s}^{-1}$) in the entire 50–400 K temperature range:

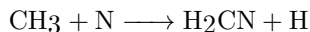


The rate coefficients of the other seven reactions with barriers drop off more rapidly for colder temperatures, and become “slow” in the ~ 100 –300 K range. One reaction’s rate coefficient has a particularly interesting temperature dependence. $\text{H}_2\text{CN} \longrightarrow \text{HCN} + \text{H}$ has a rate coefficient as high as $3.1 \times 10^{-5} \text{ s}^{-1}$ at 400 K, and as low as $4.5 \times 10^{-134} \text{ s}^{-1}$ at 50 K. Above 320 K, $\text{H}_2\text{CN} \longrightarrow \text{HCN} + \text{H}$ has the highest rate coefficient in this network.

Effects of Spin Configuration on Rate Coefficients

Both ground state (e.g. ${}^4\text{N}$, ${}^3\text{CH}_2$) and excited state (e.g. ${}^2\text{N}$, ${}^1\text{CH}_2$) species are produced during the UV photodissociation of N_2 and CH_4 . Because our network includes both ground state and excited state species, there is often more than one possible spin configuration for a given reaction. For example, the reaction

CONCLUSIONS



has three spin configurations. If the nitrogen is in the ground state, the reaction passes through the excited state $^3\text{H}_3\text{CN}$ intermediate before decaying into $\text{H}_2\text{CN} + \text{H}$ directly, or after passing through the $^3\text{H}_2\text{CNH}$ intermediate. If the nitrogen is in the excited state, the reaction can either pass through the excited state $^3\text{H}_3\text{CN}$ intermediate, or the ground state $^1\text{H}_3\text{CN}$ intermediate, before decaying into $\text{H}_2\text{CN} + \text{H}$ directly, or after passing through the $^3\text{H}_2\text{CNH}$ or $^1\text{H}_2\text{CNH}$ intermediates. In other words, on the triplet PES there are two possible reactions: $\text{CH}_3 + ^4\text{N} \longrightarrow ^3\text{H}_3\text{CN} \longrightarrow \text{H}_2\text{CN} + \text{H}$ and $\text{CH}_3 + ^2\text{N} \longrightarrow ^3\text{H}_3\text{CN} \longrightarrow \text{H}_2\text{CN} + \text{H}$, and on the singlet PES there is one reaction: $\text{CH}_3 + ^2\text{N} \longrightarrow ^1\text{H}_3\text{CN} \longrightarrow \text{H}_2\text{CN} + \text{H}$. The first steps of these reactions are the rate-limiting steps, and these steps are barrierless. All reactions have the same products, a ground state H_2CN molecule and H atom. However, the rate coefficient for $\text{CH}_3 + ^2\text{N} \longrightarrow ^3\text{H}_3\text{CN} \longrightarrow \text{H}_2\text{CN} + \text{H}$ is larger than the other two reactions by a factor of 3 (see Table 3 for calculated values).

Rate coefficients for different reaction spin configurations can also vary by several orders of magnitude, especially if a reaction barrier exists. The reaction $\text{H}_2\text{CN} + \text{N} \longrightarrow \text{HCN} + \text{NH}$ has three spin configurations that produce ground state HCN . On the singlet surface, there is $\text{H}_2\text{CN} + ^2\text{N} \longrightarrow \text{HCN} + ^1\text{NH}$, and on the triplet surface, there is $\text{H}_2\text{CN} + ^4\text{N} \longrightarrow \text{HCN} + ^3\text{NH}$ and $\text{H}_2\text{CN} + ^2\text{N} \longrightarrow \text{HCN} + ^3\text{NH}$. All these reactions have an energy barrier, but only the spin configuration involving the ^4N atom is efficient. We calculate the rate coefficient for $\text{H}_2\text{CN} + ^4\text{N} \longrightarrow \text{HCN} + ^3\text{NH}$ to be $9.4 \times 10^{-13} \text{ cm}^3\text{s}^{-1}$, which is 16 and 18 orders of magnitude larger than our calculated rate coefficients for $\text{H}_2\text{CN} + ^2\text{N} \longrightarrow \text{HCN} + ^3\text{NH}$ and $\text{H}_2\text{CN} + ^2\text{N} \longrightarrow \text{HCN} + ^1\text{NH}$, respectively.

Different spin configurations for two reactants can also lead to different products. For example, when $^1\text{CH}_2$ and CH_4 react on the singlet surface, they come together to form C_2H_6 . When the hydrogen from CH_4 bonds with the carbon of $^1\text{CH}_2$, the resultant CH_3 molecules each have an unpaired electron of opposite spin, allowing these molecules to rapidly bond to form C_2H_6 . However, when $^3\text{CH}_2$ and CH_4 react on the triplet surface, they react directly to form two CH_3 molecules, each with an unpaired electron of the same spin. The rate coefficient of $^1\text{CH}_2 + \text{CH}_4 \longrightarrow \text{C}_2\text{H}_6$ is also 5 orders of magnitude larger than $^3\text{CH}_2 + \text{CH}_4 \longrightarrow 2\text{CH}_3$. This is largely due to the fact that $^1\text{CH}_2 + \text{CH}_4 \longrightarrow \text{C}_2\text{H}_6$ is barrierless, whereas $^3\text{CH}_2 + \text{CH}_4 \longrightarrow 2\text{CH}_3$ has an energy barrier.

In this work, we use canonical variational transition state theory (CVT) to calculate 42 rate coefficients that are directly involved with or are in competition with HCN production in early Earth or Titan atmospheres. Approximately 36% of these reactions have no previously reported experimental or suggested value. To make such a large network of calculations feasible, we make use of computational quantum chemistry simulations at an accurate yet inexpensive level of theory: BHandHLYP/aug-cc-pVDZ. Moreover, we only calculate the temperature dependence of the rate coefficients for the reactions that have barriers. By using one level of theory for all reaction rate coefficient calculations, we expect the computational errors to be similar.

In this network, we focus on HCN production from methane and nitrogen radicals, which are produced in the atmosphere via UV photodissociation or lightning. Dissociation of CH_4 and N_2 produces both excited and ground state species, therefore we calculate the rate coefficients for multiple spin configurations involving these species. The reactions in our network have 1–5 spin configurations.

We list our five most important results below.

- We provide consistently calculated rate coefficients for 15 reactions that have no previously suggested values. In this sense, we fill a substantial gap in the data. These previously unknown rate coefficients include those of several key reactions in the pathway to produce atmospheric HCN (e.g. $\text{CH}_2 + \text{N} \longrightarrow \text{H}_2\text{CN}$ and $\text{H}_2\text{CN} \longrightarrow \text{HCN} + \text{H}^7$).
- Of the reactions in our network with past experimental or suggested values, 93% are within an order of magnitude of these values. The remaining 7% differ by less than 2 orders of magnitude from experimental values. These discrepancies are either due to convergence issues or our chosen computation method. When convergence isn't an issue, re-running rate coefficient calculations at the similarly expensive CAM-B3LYP/aug-cc-pVDZ level of theory or the more expensive CCSD/aug-cc-pVDZ level of theory decreases the discrepancy between theory and experimental values.
- We find the reaction of $\text{CH}_3 + \text{N} \longrightarrow \text{HCN} + \text{H}_2$ on the singlet surface to be inefficient, with a rate coefficient near $10^{-28} \text{ cm}^3\text{s}^{-1}$ (confirming the results of Cimas and Largo⁶⁴). This is in contrast to experimental results which suggest a rate coefficient to have a value near $10^{-11} \text{ cm}^3\text{s}^{-128}$. The experimental result may be due to the measurement of multi-step reaction, e.g., $\text{CH}_3 + \text{N} \longrightarrow \text{H}_2\text{CN} + \text{H}$ and $\text{H}_2\text{CN} + \text{H} \longrightarrow \text{HCN} + \text{H}_2$. However, we cannot exclude the possibility of a spin-forbidden process accounting for this experimental value.

- The effects of reaction spin configuration on the rate coefficient can be both subtle and substantial. For a given reaction, differences in rate coefficients between spin configurations can range from factors of order unity, up to 18 orders of magnitude. If there is a barrier involved with one or more of the reaction spin configurations, the difference between their reaction rate coefficients tends to be much greater than if all the reaction spin configurations are barrierless.
- Seven reaction rate coefficients in our network decrease rapidly with decreasing temperature, and become “slow” ($k < 10^{-21}$) at temperatures below ~ 100 – 300 K. One reaction, $\text{H}_2\text{CN} \longrightarrow \text{HCN} + \text{H}$, increases rapidly for increasing temperatures; above 320 K, this reaction has the highest rate coefficient in the network.

Overall, we find CVT and computational quantum chemistry simulations at the BHandHLYP/aug-cc-pVDZ level of theory to be a feasible and accurate method for calculating a large set of small-molecule, multiple-spin configuration reaction rate coefficients for a range of terrestrial atmospheric temperatures. We also note that although calculations at the CCSD/aug-cc-pVDZ level of theory often lead to improvements in the rate coefficients’

conformance to experimental values, computational cost and convergence issues made calculating all the rate coefficients at this level of theory impossible. Based on a limited number of calculations, we also find CAM-B3LYP to be an accurate alternative functional for performing CVT rate coefficient calculations and recommend it for a wider study.

ACKNOWLEDGMENTS

We thank the two anonymous referees, whose reports led to the improvement of this work. We gratefully acknowledge Anand Patel (McMaster) and Farnaz Heidar-Zadeh (Univ. of Luxembourg) whose previous work and comments helped in the development of this research. B.K.D.P. is supported by an NSERC Postgraduate Scholarship-Doctoral (PGS-D). P.W.A is supported by NSERC, the Canada Research Chairs, and Canarie. R.E.P. is supported by an NSERC Discovery Grant. We are grateful to Compute Canada for the computer time allocated for this research.

REFERENCES

- [1] Miller, S. L. The Formation of Organic Compounds on the Primitive Earth. *Ann. N. Y. Acad. Sci.* **1957**, *69*, 260–275.
- [2] Oró, J. Mechanism of Synthesis of Adenine from Hydrogen Cyanide under Possible Primitive Earth Conditions. *Nature* **1961**, *191*, 1193–1194.
- [3] Larowe, D. E.; Regnier, P. Thermodynamic Potential for the Abiotic Synthesis of Adenine, Cytosine, Guanine, Thymine, Uracil, Ribose, and Deoxyribose in Hydrothermal Systems. *Orig. Life Evol. Biosph.* **2008**, *38*, 383–397.
- [4] Cobb, A. K.; Pudritz, R. E. Nature’s Starships. I. Observed Abundances and Relative Frequencies of Amino Acids in Meteorites. *Astrophys. J.* **2014**, *783*, 140.
- [5] Pearce, B. K. D.; Pudritz, R. E. Seeding the Pregenetic Earth: Meteoritic Abundances of Nucleobases and Potential Reaction Pathways. *Astrophys. J.* **2015**, *807*, 85.
- [6] Ferris, J. P. J.; Edelson, P. C.; H., E.; Lawless, J. G. HCN: A Plausible Source of Purines, Pyrimidines and Amino Acids on the Primitive Earth. *J. Mol. Evol.* **1978**, *11*, 293–311.
- [7] Catling, D.; Kasting, J. F. In *Planets and life - the emerging science of astrobiology*; Sullivan, III, W. T., Baross, J. A., Eds.; Cambridge University Press: Cambridge, 2007; pp 91–116.
- [8] Bada, J. L. New insights into prebiotic chemistry from Stanley Millers spark discharge experiments. *Chem. Soc. Rev.* **2013**, *42*, 2186–2196.
- [9] Loison, J. C.; Hébrard, E.; Dobrijevic, M.; Hickson, K. M.; Caralp, F.; Hue, V.; Gronoff, G.; Venot, O.; Bénilan, Y. The neutral photochemistry of nitriles, amines and imines in the atmosphere of Titan. *Icarus* **2015**, *247*, 218–247.
- [10] Damer, B.; Deamer, D. W. Coupled Phases and Combinatorial Selection in Fluctuating Hydrothermal Pools: A Scenario to Guide Experimental Approaches to the Origin of Cellular Life. *Life* **2015**, *5*, 872–887.
- [11] Adriani, A.; Dinelli, B. M.; López-Puertas, M.; García-Comas, M.; Moriconi, M. L.; D’Aversa, E.; Funke, B.; Coradini, A. Distribution of HCN in Titan’s upper atmosphere from Cassini/VIMS observations at $3\ \mu\text{m}$. *Icarus* **2011**, *214*, 584–595.
- [12] Vinatier, S.; Bézard, B.; Nixon, C. A.; Mamoutkine, A.; Carlson, R. C.; Jennings, D. E.; Guandique, E. A.; Teanby, N. A.; Bjoraker, G. L.; Michael Flasar, F.; et al., Analysis of Cassini/CIRS limb spectra of Titan acquired during the nominal mission. I. Hydrocarbons, nitriles and CO_2 vertical mixing ratio profiles. *Icarus* **2010**, *205*, 559–570.
- [13] Zahnle, K. J. Photochemistry of Methane and the Formation of Hydrocyanic Acid (HCN) in the Earth’s Early Atmosphere. *J. Geophys. Res.* **1986**, *91*, 2819–2834.
- [14] Tian, F.; Kasting, J. F.; Zahnle, K. Revisiting HCN formation in Earth’s early atmosphere. *Earth Planet. Sci. Lett.* **2011**, *308*, 417–423.
- [15] Lavvas, P. P.; Coustenis, A.; Vardavas, I. M. Coupling photochemistry with haze formation in Titan’s atmosphere, Part I: Model description. *Planet. Space Sci.* **2008**, *56*, 27–66.
- [16] Lavvas, P. P.; Coustenis, A.; Vardavas, I. M. Cou-

- pling photochemistry with haze formation in Titan's atmosphere, Part II: Results and validation with Cassini/Huygens data. *Planet. Space Sci.* **2008**, *56*, 67–99.
- [17] Krasnopolsky, V. A. A photochemical model of Titan's atmosphere and ionosphere. *Icarus* **2009**, *201*, 226–256.
- [18] Hébrard, E.; Dobrijevic, M.; Loison, J. C.; Bergeat, A.; Hickson, K. M. Neutral production of hydrogen isocyanide (HNC) and hydrogen cyanide (HCN) in Titan's upper atmosphere. *Astron. Astrophys.* **2012**, *541*, A21.
- [19] Pople, J. A. Nobel Lecture: Quantum chemical models. *Rev. Mod. Phys.* **1999**, *71*, 1267–1274.
- [20] Pople, J. A. Theoretical Models for Chemistry. Proceedings of the Summer Research Conference on Theoretical Chemistry, Energy Structure and Reactivity. New York, 1973; pp 51–61.
- [21] Ferus, M.; Pietrucci, F.; Saitta, A. M.; Knížek, A.; Kubelík, P.; Ivanek, O.; Shestivska, V.; Civiš, S. Formation of nucleobases in a MillerUrey reducing atmosphere. *Proc. Nat. Acad. Sci. U.S.A.* **2017**, *114*, 4306–4311.
- [22] Cobb, A. K.; Pudritz, R. E.; Pearce, B. K. D. Nature's Starships II. Simulating the Synthesis of Amino Acids in Meteorite Parent Bodies. *Astrophys. J.* **2015**, *809*, 6.
- [23] Martins, Z.; Price, M. C.; Goldman, N.; Sephton, M. A.; Burchell, M. J. Shock synthesis of amino acids from impacting cometary and icy planet surface analogues. *Nat. Geosci.* **2013**, *6*, 1045–1049.
- [24] Lellouch, E.; Romani, P. N.; Rosenqvist, J. The Vertical Distribution and Origin of HCN in Neptune's Atmosphere. *Icarus* **1994**, *108*, 112–136.
- [25] Cleaves, H. J.; Neish, C.; Callahan, M. P.; Parker, E.; Fernández, F. M.; Dworkin, J. P. Amino acids generated from hydrated Titan tholins: Comparison with Miller-Urey electric discharge products. *Icarus* **2014**, *237*, 182–189.
- [26] Shi, X.; Yin, Q.-Z.; Gao, H.; Chang, Y.-C.; Jackson, W. M.; Wiens, R. C.; Ng, C.-Y. Branching Ratios in Vacuum Ultraviolet Photodissociation of CO and N₂: Implications for Oxygen and Nitrogen Isotopic Compositions of the Solar Nebula. *Astrophys. J.* **2017**, *850*, 48.
- [27] Gans, B.; Boyé-Péronne, S.; Broquier, M.; Delsaut, M.; Douin, S.; Fellows, C. E.; Halvick, P.; Loison, J.-C.; Lucchese, R. R.; Gaucyacq, D. Photolysis of methane revisited at 121.6 nm and at 118.2 nm: quantum yields of the primary products, measured by mass spectrometry. *Phys. Chem. Chem. Phys.* **2011**, *13*, 8140–8152.
- [28] Marston, G.; Nesbitt, F. L.; Stief, L. J. Branching ratios in the N+CH₃ reaction: Formation of the methylene amidogen (H₂CN) radical. *J. Chem. Phys.* **1989**, *91*, 3483–3491.
- [29] Devriendt, K.; Van Poppel, M.; Boullart, W.; Peeters, J. Kinetic Investigation of the CH₂(\tilde{X}^3B_1) + H \longrightarrow CH(X²Π) + H₂ Reaction in the Temperature Range 400 K < T < 1000 K. *J. Phys. Chem.* **1995**, *99*, 16953–16959.
- [30] Boullart, W.; Peeters, J. Product distributions of the C₂H₂ + O and HCCO + H reactions. Rate constant of methylene(\tilde{X}^3B_1) + H. *J. Phys. Chem.* **1992**, *96*, 9810–9816.
- [31] Böhland, T.; Temps, F.; Wagner, H. G. A Direct Study of the Reactions of CH₂(\tilde{X}^3B_1) Radicals with H and D Atoms. *J. Phys. Chem.* **1987**, *91*, 1205–1209.
- [32] Zabarnick, S.; Fleming, J. W.; Lin, M. C. Kinetic study of the reaction CH(X²Π) + H₂ \longleftrightarrow CH₂(\tilde{X}^3B_1) + H in the temperature range 372 to 675 K. *J. Phys. Chem.* **1986**, *85*, 4373–4376.
- [33] Böhland, T.; Temps, F. Direct Determination of the Rate Constant for the Reaction CH₂ + H \longrightarrow CH + H₂. *Ber. Bunsenges. Phys. Chem.* **1984**, *88*, 459.
- [34] Grebe, J.; Homann, K. H. Kinetics of the Species OH(A²Σ⁺), OH(X₂Π) and CH(X²Π) in the System C₂H₂/O/H. *Ber. Bunsenges. Phys. Chem.* **1982**, *86*, 581.
- [35] Becker, K. H.; Kurtenbach, R.; Wiesen, P. Temperature and pressure dependence of the reaction CH + H₂. *J. Chem. Phys.* **1991**, *95*, 2390–2394.
- [36] Braun, W.; Bass, A. M.; Pilling, M. Flash Photolysis of Ketene and Diazomethane: The Production and Reaction Kinetics of Triplet and Singlet Methylene. *J. Chem. Phys.* **1970**, *52*, 5131–5143.
- [37] Langford, A. O.; Petek, H.; Moore, C. B. Collisional removal of CH₂(¹A₁): Absolute rate constants for atomic and molecular collisional partners at 295 K. *J. Chem. Phys.* **1983**, *78*, 6650–6659.
- [38] Ashfold, M. N. R.; Fullstone, M. A.; Hancock, G.; Ketley, G. W. Singlet Methylene Kinetics: Direct Measurements of Removal Rates of \tilde{a}^1A_1 and \tilde{b}^1B_1 CH₂ and CD₂. *Chem. Phys.* **1981**, *55*, 245–257.
- [39] Umemoto, H.; Nakae, T.; Hashimoto, H.; Kongo, K.; Kawasaki, M. Reactions of N(2²D) with methane and deuterated methanes. *J. Chem. Phys.* **1998**, *109*, 5844–5848.
- [40] Truhlar, D. G.; Garrett, B. C. Variational Transition State Theory. *Annu. Rev. Phys. Chem.* **1984**, *35*, 159–189.
- [41] Truhlar, D. G. In *Theory of Chemical Reaction Dynamics*; Baer, M., Ed.; CRC Press: Boca Raton, FL, 1985; pp 65–137.
- [42] Maity, D. K.; Duncan, W. T.; Truong, T. N. Direct ab Initio Dynamics Studies of the Hydrogen Abstraction Reactions of Hydrogen Atom with Fluoromethanes. *J. Phys. Chem. A* **1999**, *103*, 2152–2159.
- [43] Li, H.; Chen, B.-Z.; Huang, M.-B. CASPT2 investigation of ethane dissociation and methyl recombination using canonical variational transition state theory. *Int. J. Chem. Kinet.* **2008**, *40*, 161–173.
- [44] Eyring, H. The Activated Complex in Chemical Reactions. *J. Chem. Phys.* **1935**, *3*, 107.
- [45] Steinfeld, J. I.; Francisco, J. S.; Hase, W. L. *Chemical Kinetics and Dynamics*; Prentice-Hall: New Jersey, 1989.
- [46] Hänggi, P.; Talkner, P.; Borkovec, M. Reaction-rate theory: fifty years after Kramers. *Rev. Mod. Phys.* **1990**, *62*, 251–341.
- [47] You, X.; Wang, H.; Goos, E.; Sung, C.-J.; Klippenstein, S. J. Reaction Kinetics of CO + HO₂ to Products: Ab Initio Transition State Theory Study with Master Equation Modeling. *J. Phys. Chem. A* **2007**, *111*, 4031–4042.
- [48] Fernández-Ramos, A.; Ellingson, B. A.; Meana-Pañeda, R.; Marques, J. M. C.; Truhlar, D. G. Symmetry numbers and chemical reaction rates. *Theor. Chem. Account* **2007**, *118*, 813–826.
- [49] Robertson, S. H.; Wagner, A. F.; Wardlaw, D. M.

- Canonical flexible transition state theory revisited. *J. Chem. Phys.* **1995**, *103*, 2917–2928.
- [50] Truhlar, D. G.; Garrett, B. C. Variational Transition-State Theory. *Acc. Chem. Res.* **1980**, *13*, 440–448.
- [51] Frisch, M. J.; Trucks, G. W.; Schlegel, H. B.; Scuseria, G. E.; Robb, M. A.; Cheeseman, J. R.; Scalmani, G.; Barone, V.; Petersson, G. A.; Nakatsuji, H.; et al., *Gaussian 09*, Revision E.01; Gaussian, Inc.: Wallingford, CT, 2009.
- [52] Ochterski, J. W. *Thermochemistry in Gaussian*; Gaussian Inc.: Wallingford, CT, 2000; pp 1–19.
- [53] Becke, A. D. A new mixing of Hartree-Fock and local density-functional theories. *J. Chem. Phys.* **1993**, *98*, 1372–1377.
- [54] Lee, C.; Yang, W.; Parr, R. G. Development of the Colle-Salvetti correlation-energy formula into a functional of the electron density. *Phys. Rev. B* **1988**, *37*, 785–789.
- [55] Hörst, S. M. Titan’s atmosphere and climate. *J. Geophys. Res. Planets* **2017**, *122*, 432–482.
- [56] Cockell, C. S. *Astrobiology: Understanding Life in the Universe*; Wiley-Blackwell: New Jersey, 2015.
- [57] Clary, D. C. Fast Chemical Reactions: Theory Challenges Experiment. *Annu. Rev. Phys. Chem.* **1990**, *41*, 61–90.
- [58] Hase, W. L.; Mondro, S. L.; Duchovic, R. J.; Hirst, D. M. Thermal Rate Constant for $\text{H} + \text{CH}_3 \longrightarrow \text{CH}_4$ Recombination. 3. Comparison of Experiment and Canonical Variational Transition State Theory. *J. Am. Chem. Soc.* **1987**, *109*, 2916–2922.
- [59] Jasper, A. W.; Klippenstein, S. J.; Harding, L. B. Secondary Kinetics of Methanol Decomposition: Theoretical Rate Coefficients for ${}^3\text{CH}_2 + \text{OH}$, ${}^3\text{CH}_2 + {}^3\text{CH}_2$, and ${}^3\text{CH}_2 + \text{CH}_3$. *J. Phys. Chem. A* **2007**, *111*, 8699–8707.
- [60] Daranlot, J.; Hu, X.; Xie, C.; Loison, J.-C.; Caubet, P.; Costes, M.; Wakelam, V.; Xie, D.; Guo, H.; Hickson, K. Low temperature rate constants for the $\text{N}({}^4\text{S}) + \text{CH}(\text{X}^2\Pi_r)$ reaction. Implications for N_2 formation cycles in dense interstellar clouds. *Phys. Chem. Chem. Phys.* **2013**, *15*, 13888–13896.
- [61] Semenov, D.; Hersant, F.; Wakelam, V.; Dutrey, A.; Chapillon, E.; Guilloteau, S.; Henning, T.; Launhardt, R.; Piétu, V.; Schreyer, K. Chemistry in disks. IV. Benchmarking gas-grain chemical models with surface reactions. *Astron. Astrophys.* **2010**, *522*, A42.
- [62] Baulch, D. L.; Cobos, C. J.; Cox, R. A.; Esser, C.; Frank, P.; Just, T.; Kerr, J. A.; Pilling, M. J.; Troe, J.; Walker, R. W.; et al., Evaluated kinetic data for combustion modelling. *J. Phys. Chem. Ref. Data* **1992**, *21*, 411–429.
- [63] Stief, L. J.; Marston, G.; Nava, D. F.; Payne, W. A.; Nesbitt, F. L. Rate constant for the reaction of $\text{N}({}^4\text{S})$ with CH_3 AT 298 K. *Chem. Phys. Lett.* **1988**, *147*, 570–574.
- [64] Cimas, A.; Largo, A. The Reaction of Nitrogen Atoms with Methyl Radicals: Are Spin-Forbidden Channels Important? *J. Phys. Chem. A* **2006**, *110*, 10912–10920.
- [65] Yanai, T.; Tew, D. P.; Handy, N. C. A new hybrid exchange-correlation functional using the Coulomb-attenuating method (CAM-B3LYP). *Chem. Phys. Lett.* **2004**, *393*, 51–57.
- [66] Manion, J. A.; Huie, R. E.; Levin, R. D.; Burgess Jr., D. R.; Orkin, V. L.; Tsang, W.; McGivern, W. S.; Hudgens, J. W.; Knyazev, V. D.; Atkinson, D. B.; et al., *NIST Chemical Kinetics Database*; NIST Standard Reference Database Number 17, Version 7.0 (Web Version), Release 1.6.8, Data version 2015.09, National Institute of Standards and Technology: Gaithersburg, MD, <http://kinetics.nist.gov/>, (retrieved May 10, 2018).
- [67] Tomczek, J.; Gradoń, B. The role of N_2O and NNH in the formation of NO via HCN in hydrocarbon flames. *Combust. Flame* **2003**, *133*, 311–322.
- [68] Nesbitt, F. L.; Marston, G.; Stief, L. J. Kinetic Studies of the Reactions of H_2CN and D_2CN Radicals with N and H . *J. Phys. Chem.* **1990**, *94*, 4946–4951.
- [69] Horne, D. G.; Norrish, R. G. W. The Photolysis of Acyclic Azines and the Electronic Spectra of $\text{R}_1\text{R}_2\text{CN}$ Radicals. *Proc. R. Soc. Lond. A Math. Phys. Sci.* **1970**, *315*, 301–322.
- [70] Lawrence, Jr., R. H.; Firestone, R. F. Kinetics of thermal deuterium atom reactions with methane and ethane. *J. Am. Chem. Soc.* **1966**, *88*, 4564–4570.
- [71] Jones, W. E.; Ma, J. L. An electron spin resonance study of the reactions of hydrogen atoms with halocarbons. *Can. J. Chem.* **1986**, *64*, 2192–2195.
- [72] Takayanagi, T.; Kurosaki, Y.; Sato, K.; Misawa, K.; Kobayashi, Y.; Tsunashima, S. Kinetic Studies on the $\text{N}({}^2\text{D}, {}^2\text{P}) + \text{CH}_4$ and CD_4 Reactions: The Role of Nonadiabatic Transitions on Thermal Rate Constants. *J. Chem. Phys. A* **1999**, *103*, 250–255.
- [73] Fell, B.; Rivas, I. V.; McFadden, D. L. Kinetic Study of Electronically Metastable Nitrogen Atoms, $\text{N}({}^2\text{D}_J)$, by Electron Spin Resonance Absorption. *J. Phys. Chem.* **1981**, *85*, 224–228.
- [74] Umemoto, H.; Hachiya, N.; Matsunaga, E.; Suda, A.; Kawasaki, M. Rate constants for the deactivation of $\text{N}({}^2\text{D})$ by simple hydride and deuteride molecules. *Chem. Phys. Lett.* **1998**, *296*, 203–207.
- [75] Black, G.; Slinger, T. G.; St. John, G. A.; Young, R. A. Vacuum-Ultraviolet Photolysis of N_2O . IV. Deactivation of $\text{N}({}^2\text{D})$. *J. Chem. Phys.* **1969**, *51*, 116–121.
- [76] Herron, J. T. Evaluated Chemical Kinetics Data for Reactions of $\text{N}({}^2\text{D})$, $\text{N}({}^2\text{P})$ and $\text{N}_2(\text{A}^3\Sigma_u^+)$ in the Gas Phase. *J. Phys. Chem. Ref. Data* **1999**, *28*, 1453–1483.
- [77] Brouard, M.; Macpherson, M. T.; Pilling, M. J. Experimental and RRKM Modeling Study of the $\text{CH}_3 + \text{H}$ and $\text{CH}_3 + \text{D}$ Reactions. *J. Phys. Chem.* **1989**, *93*, 4047–4059.
- [78] Cheng, J.-T.; Yeh, C.-T. Pressure Dependence of the Rate Constant of the Reaction $\text{H} + \text{CH}_3 \longrightarrow \text{CH}_4$. *J. Phys. Chem.* **1977**, *81*, 1982–1984.
- [79] Cheng, J.-T.; Lee, Y.-S.; Yeh, C.-T. The Triplet Mercury Photosensitized Decomposition of Ethane at High Intensity. *J. Phys. Chem.* **1977**, *81*, 687–690.
- [80] Sworski, T. J.; Hochanadel, C. J.; Ogren, P. J. Flash Photolysis of H_2O Vapor in CH_4 . H and OH Yields and Rate Constants for CH_3 Reactions with H and OH . *J. Phys. Chem.* **1980**, *84*, 129–134.
- [81] Patrick, R.; Pilling, M. J.; Rogers, G. J. A high pressure rate constant for $\text{CH}_3 + \text{H}$ and an analysis of the kinetics of the $\text{CH}_3 + \text{H} \longrightarrow \text{CH}_4$ reaction. *Chem. Phys.* **1980**, *53*, 279–291.
- [82] Michael, J. V.; Osborne, D. T.; Suess, G. N. Reaction $\text{H} + \text{C}_2\text{H}_4$: Investigation into the effects of pressure, stoichiometry, and the nature of the third body species. *J. Chem. Phys.* **1973**, *58*, 2800–2806.
- [83] Cobos, C. J.; Troe, J. The Dissociation-Recombination

- System $\text{CH}_4 + \text{M} \longleftrightarrow \text{CH}_3 + \text{H} + \text{M}$: Reevaluated Experiments from 300 to 3000 K. *Z. Phys. Chem. N. F.* **1990**, *167*, 129–149.
- [84] Tsang, W. Rate Constants for the Decomposition and Formation of Simple Alkanes Over Extended Temperature and Pressure Ranges. *Combust. Flame* **1989**, *78*, 71–86.
- [85] Kobrinsky, P. C.; Pacey, P. D. The Reaction of Methyl Radicals with Molecular Hydrogen. *Can. J. Chem.* **1974**, *52*, 3665–3670.
- [86] Tsang, W.; Hampson, R. F. Chemical Kinetic Data Base for Combustion Chemistry. Part I. Methane and Related Compounds. *J. Phys. Chem. Ref. Data* **1986**, *15*, 1087–1279.
- [87] Miller, J. A.; Bowman, C. T. Mechanism and Modeling of Nitrogen Chemistry in Combustion. *Prog. Energy Combust. Sci.* **1989**, *15*, 287–338.
- [88] Walter, D.; Grotheer, H.-H.; Davies, J. W.; Pilling, M. J.; Wagner, A. F. Experimental and theoretical study of the recombination reaction $\text{CH}_3 + \text{CH}_3 \longrightarrow \text{C}_2\text{H}_6$. Twenty-Third Symposium (International) on Combustion. Seattle, 1991; pp 107–114.
- [89] Macpherson, M. T.; Pilling, M. J.; Smith, M. J. C. Determination of the absorption cross section for methyl at 216.36 nm and the absolute rate constant for methyl radical recombination over the temperature range 296–577 K. *J. Phys. Chem.* **1985**, *89*, 2268–2274.
- [90] Du, H.; Hessler, J. P.; Ogren, P. J. Recombination of Methyl Radicals. 1. New Data between 1175 and 1750 K in the Falloff Region. *J. Phys. Chem.* **1996**, *100*, 974–983.
- [91] Slagle, D., I. R. Gutman; Davies, J. W.; Pilling, M. J. Study of the recombination reaction $\text{CH}_3 + \text{CH}_3 \longrightarrow \text{C}_2\text{H}_6$. 1. Experiment. *J. Phys. Chem.* **1988**, *92*, 2455–2462.
- [92] Sangwan, M.; Yan, C.; Chesnokov, E. N.; Krasnoperov, L. N. Reaction $\text{CH}_3 + \text{CH}_3 \longrightarrow \text{C}_2\text{H}_6$ Studied over the 292–714 K Temperature and 1–100 bar Pressure Ranges. *J. Phys. Chem. A* **2015**, *119*, 7847–7857.
- [93] Pagsberg, J., P. Munk; Sillesen, A.; Anastasi, C. UV spectrum and kinetics of hydroxymethyl radicals. *Chem. Phys. Lett.* **1988**, *146*, 375–381.
- [94] Hippler, H.; Luther, K.; Ravishankara, A. R.; Troe, J. High-Pressure Effects in the Recombination Reaction $\text{CH}_3 + \text{CH}_3 \longrightarrow \text{C}_2\text{H}_6$. *Z. Phys. Chem. N. F.* **1984**, *142*, 1–12.
- [95] Fahr, A.; Laufer, A.; Klein, R.; Braun, W. Reaction Rate Determinations of Vinyl Radical Reactions with Vinyl, Methyl, and Hydrogen Atoms. *J. Phys. Chem.* **1991**, *95*, 3218–3224.
- [96] Wang, B.; Fockenberg, C. Direct Measurement of the Rate Constant for the $\text{CH}_2(\tilde{\text{X}}^3\text{B}_1) + \text{CH}_3$ Reaction at 300 K. *J. Phys. Chem. A* **2001**, *105*, 8449–8455.
- [97] Arthur, N. L. Methyl-radical absorption cross-section at 216.4 nm and rate constant for methyl-radical recombination. *J. Chem. Soc., Faraday Trans. 2* **1986**, *82*, 331–336.
- [98] Anastasi, C.; Arthur, N. L. Rate constants for the reactions of CH_3 radicals with C_2H_5 , $i\text{-C}_3\text{H}_7$ and $t\text{-C}_4\text{H}_9$ radicals. *J. Chem. Soc., Faraday Trans. 2* **1987**, *83*, 277–287.
- [99] Darwin, D. C.; Moore, C. B. Reaction Rate Constants (295 K) for 3CH_2 with H_2S , SO_2 , and NO_2 : Upper Bounds for Rate Constants with Less Reactive Partners. *J. Phys. Chem.* **1995**, *99*, 13467–13470.
- [100] Pilling, M. J.; Robertson, J. A. Flash photolysis of ketene. Photolysis mechanism and rate constants for singlet and triplet methylene. *J. Chem. Soc., Faraday Trans. 1* **1977**, *73*, 968–984.
- [101] Deters, R.; Otting, M.; Wagner, H. G.; Temps, F.; Dobẽ, S. Rate constant for the reaction $\text{CH}_3 + \text{CH}_2(\tilde{\text{X}}^3\text{B}_1)$ at 298 K. *Ber. Bunsenges. Phys. Chem.* **1998**, *102*, 978–981.
- [102] Laufer, A. H.; Bass, A. M. Mechanism and rate constant of the reaction between methylene and methyl radicals. *J. Phys. Chem.* **1975**, *79*, 1635–1638.
- [103] Pilling, M. J.; Robertson, J. A. A rate constant for $\text{CH}_2(\tilde{\text{X}}^3\text{B}_1) + \text{CH}_3$. *Chem. Phys. Lett.* **1975**, *33*, 336–339.
- [104] Böhland, T.; Dobẽ, S.; Temps, F.; Wagner, H. G. Kinetics of the Reactions between $\text{CH}_2(\tilde{\text{X}}^3\text{B}_1)$ Radicals and Saturated Hydrocarbons in the Temperature Range 296 K $\leq T \leq 707$ K. *Ber. Bunsenges. Phys. Chem.* **1985**, *89*, 1110–1116.
- [105] Brownsword, R. A.; Canosa, A.; Rowe, B. R.; Sims, I. R.; Smith, I. W. M.; Stewart, D. W. A.; Symonds, A. C.; Travers, D. Kinetics over a wide range of temperature (13–744 K): Rate constants for the reactions of $\text{CH}(\nu=0)$ with H_2 and D_2 and for the removal of $\text{CH}(\nu=1)$ by H_2 and D_2 . *J. Chem. Phys.* **1997**, *106*, 7662–7677.
- [106] Fulle, D.; Hippler, H. The temperature and pressure dependence of the reaction $\text{CH} + \text{H} \longleftrightarrow \text{CH}_3 \longleftrightarrow \text{CH}_2 + \text{H}$. *J. Chem. Phys.* **1997**, *106*, 8691–8698.
- [107] Berman, M. R.; Lin, M. C. Kinetics and mechanisms of the reactions of CH and CD with H_2 and D_2 . *J. Chem. Phys.* **1984**, *81*, 5743–5752.
- [108] McIlroy, A.; Tully, F. P. $\text{CH} + \text{H}_2$ reaction kinetics: Temperature and pressure dependence and Rice-Ramsperger-Kassel-Marcus-master-equation calculation. *J. Chem. Phys.* **1993**, *99*, 3597–3603.
- [109] Butler, J. E.; Goss, L. P.; Lin, M. C.; Hudgens, J. W. Production, detection and reactions of the CH radical. *Chem. Phys. Lett.* **1979**, *63*, 104–107.
- [110] Bosnali, M. W.; Perner, D. Notizen: Reaktionen von pulsradiolytisch erzeugtem $\text{CH}(\tilde{\text{X}}^2\Pi)$ mit Methan und anderen Substanzen. *Z. Naturforsch.* **1971**, *26*, 1768–1769.
- [111] Braun, W.; McNesby, J. R.; Bass, A. M. Flash Photolysis of Methane in the Vacuum Ultraviolet. II. Absolute Rate Constants for Reactions of CH with Methane, Hydrogen, and Nitrogen. *J. Chem. Phys.* **1967**, *46*, 2071–2080.
- [112] Brownsword, R. A.; Gatenby, S. D.; Herbert, L. B.; Smith, I. W. M.; Stewart, D. W. A.; Symonds, A. C. Kinetics of reactions between neutral free radicals. Rate constants for the reaction of CH radicals with N atoms between 216 and 584 K. *J. Chem. Soc. Faraday Trans.* **1996**, *92*, 723–727.
- [113] Messing, I.; Filseth, S. V.; Sadowski, C. M.; Carrington, D. Absolute rate constants for the reactions of CH with O and N atoms. *J. Chem. Phys.* **1981**, *74*, 3874–3881.
- [114] Braun, W.; Welge, K. H.; McNesby, J. R. Flash Photolysis of Methane in the Vacuum Ultraviolet. I. End-Product Analysis. *J. Chem. Phys.* **1966**, *45*, 2650–2656.

- [115] Butler, J. E.; Fleming, J. E.; Goss, L. P.; Lin, M. C. Kinetics of CH Radical Reactions with Selected Molecules at Room Temperature. *J. Chem. Phys.* **1981**, *56*, 355–365.
- [116] Berman, M. R.; Lin, M. C. Kinetics and mechanisms of the reactions of CH with CH₄, C₂H₆ and n-C₄H₁₀. *J. Chem. Phys.* **1983**, *82*, 435–442.
- [117] Blitz, M. A.; Johnson, D. G.; Pesa, M.; Pilling, M. J.; Robertson, S. H.; Seakins, P. W. Reaction of CH radicals with methane isotopomers. *J. Chem. Soc. Faraday Trans.* **1997**, *93*, 1473–1479.
- [118] Canosa, A.; Sims, I. R.; Travers, D.; Smith, I. W. M.; Rowe, B. R. Reactions of the methylidene radical with CH₄, C₂H₂, C₂H₄, C₂H₆, and but-1-ene studied between 23 and 295K with a CRESU apparatus. *Astron. Astrophys.* **1997**, *323*, 644–651.
- [119] Thiesemann, H.; MacNamara, J.; Taatjes, C. A. Deuterium Kinetic Isotope Effect and Temperature Dependence in the Reactions of CH[²Π] with Methane and Acetylene. *J. Phys. Chem. A* **1997**, *101*, 1881–1886.
- [120] Adam, L.; Hack, W.; Zhu, H.; Qu, Z.-W.; Schinke, R. Experimental and theoretical investigation of the reaction NH(X³Σ⁻) + H(²S) → N(⁴S) + H₂(X¹Σ⁺_g). *J. Chem. Phys.* **2005**, *122*, 114301.
- [121] Hack, W.; Wagner, H. G.; Zasyplin, A. Elementary reactions of NH(a¹Δ) and NH(X³Σ) with N, O and NO. *Ber. Bunsenges. Phys. Chem.* **1994**, *98*, 156–164.
- [122] Konnov, A. A.; De Ruyck, J. Kinetic Modeling of the Decomposition and Flames of Hydrazine. *Combust. Flame* **2001**, *124*, 106–126.
- [123] Black, G.; Sharpless, R. L.; Slinger, T. G.; Lorents, D. C. Quantum yields for the production of O(¹S), N(²D), and N₂(A³Σ_u⁺) from the vacuum uv photolysis of N₂O. *J. Chem. Phys.* **1975**, *62*, 4266–4273.
- [124] Suzuki, T.; Shihira, Y.; Sato, T.; Umemoto, H.; Tsunashima, S. Reactions of N(²D) and N(²P) with H₂ and D₂. *J. Chem. Soc. Faraday Trans.* **1993**, *89*, 995–999.
- [125] Umemoto, H.; Hachiya, N.; Matsunaga, E.; Suda, A.; Kawasaki, M. Rate constants for the deactivation of N(²D) by simple hydride and deuteride molecules. *Chem. Phys. Lett.* **1998**, *296*, 203–207.
- [126] Piper, L. G.; Donahue, M. E.; Rawlins, W. T. Rate Coefficients for N(²D) Reactions. *J. Phys. Chem.* **1987**, *91*, 3883–3888.
- [127] Husain, D.; Mitra, S. K.; Young, A. N. Kinetic Study of Electronically Excited Nitrogen Atoms, N(²D_J, 2²P_J), by Attenuation of Atomic Resonance Radiation in the Vacuum Ultra-violet. *J. Chem. Soc., Faraday Trans. 2* **1974**, *70*, 1721–1731.
- [128] Whitefield, P. D.; Hovis, F. E. Rate Constants for the Reactions of N(²D) atoms with O₂, H₂ and HF. *Chem. Phys. Lett.* **1987**, *135*, 454–458.
- [129] Husain, D.; Kirsch, L. J.; Wiesenfeld, J. R. Collisional quenching of electronically excited nitrogen atoms, N(²D_J, 2²P_J) by time-resolved atomic absorption spectroscopy. *Faraday Discuss. Chem. Soc.* **1972**, *53*, 201–210.
- [130] Barker, J. R.; Keil, D. G.; Michael, J. V.; Osborne, D. T. Reaction H+C₂H₄: Comparison of Three Experimental Techniques. *J. Chem. Phys.* **1970**, *52*, 2079–2088.
- [131] Kerkeni, B.; Clary, D. C. Kinetic Isotope Effects in the Reactions of D Atoms with CH₄, C₂H₆, and CH₃OH: Quantum Dynamics Calculations. *J. Phys. Chem. A* **2004**, *108*, 8966–8972.
- [132] Truong, T. N.; Duncan, W. A new direct ab initio dynamics method for calculating thermal rate constants from density functional theory. *J. Chem. Phys.* **1994**, *101*, 7408–7414.
- [133] Truong, T. N. A direct ab initio dynamics approach for calculating thermal rate constants using variational transition state theory and multidimensional semiclassical tunneling methods. An application to the CH₄ + H ↔ CH₃ + H₂ reaction. *J. Chem. Phys.* **1994**, *100*, 8014–8025.
- [134] Espinosa-García, J.; Corchado, J. C. Recalibration of Two Earlier Potential Energy Surfaces for the CH₄ + H → CH₃ + H₂ Reaction. Application of Variational Transition-State Theory and Analysis of the Kinetic Isotope Effects Using Rectilinear and Curvilinear Coordinates. *J. Phys. Chem.* **1996**, *100*, 16561–16567.
- [135] Jordan, M. J. T.; Gilbert, R. G. Classical trajectory studies of the reaction CH₄ + H → CH₃ + H₂. *J. Chem. Phys.* **1995**, *102*, 5669–5682.
- [136] Joseph, T.; Steckler, R.; Truhlar, D. G. A new potential energy surface for the CH₃ + H₂ ↔ CH₄ + H reaction: Calibration and calculations of rate constants and kinetic isotope effects by variational transition state theory and semiclassical tunneling calculations. *J. Chem. Phys.* **1987**, *87*, 7036–7049.
- [137] Kerkeni, B.; Clary, D. C. Ab initio rate constants from hyperspherical quantum scattering: Application to H + CH₄ → H₂ + CH₃. *J. Chem. Phys.* **2004**, *120*, 2308–2318.
- [138] Clark, T. C.; Dove, J. E. Examination of Possible Non-Arrhenius Behavior in the reactions. *Can. J. Chem.* **1973**, *51*, 2147–2154.
- [139] Pu, J.; Truhlar, D. G. Parametrized direct dynamics study of rate constants of H with CH₄ from 250 to 2400 K. *J. Chem. Phys.* **2002**, *116*, 1468–1478.
- [140] Berry, R. J.; Ehlers, C. J.; Burgess, Jr., D. R.; Zachariah, M. R.; Marshall, P. A computational study of the reactions of atomic hydrogen with fluoromethanes: kinetics and product channels. *Chem. Phys. Lett.* **1997**, *269*, 107–116.
- [141] Bryukov, M. G.; Slagle, I. R.; Knyazev, V. D. Kinetics of Reactions of H Atoms With Methane and Chlorinated Methanes. *J. Phys. Chem. A* **2001**, *105*, 3107–3122.
- [142] Gonzalez, C.; McDouall, J. J. W.; Schlegel, H. B. Ab Initio Study of the Reactions between Methane and OH, H, and ³O. *J. Phys. Chem.* **1990**, *94*, 7467–7471.
- [143] Alves, T. V.; de Oliveira Filho, A. G. S.; Ornellas, F. R. The reaction of methyl radical with nitrogen atom on the triplet potential energy surface: A CCSD(T)/CBS characterization. *Chem. Phys. Lett.* **2008**, *457*, 36–41.
- [144] Hase, W. L.; Duchovic, R. J. Thermal rate constant for H + CH₃ → CH₄ recombination. Comparison of quasiclassical trajectory and variational transition state theory. *J. Chem. Phys.* **1985**, *83*, 3448–3453.
- [145] Pilling, M. J. Association reactions of atoms and radicals. *Int. J. Chem. Kinet.* **1989**, *21*, 267–291.
- [146] Forst, W. Microcanonical Variational Theory of Radical Recombination by Inversion of Interpolated Partition Function, with Examples: CH₃ + H, CH₃ + CH₃. *J. Phys. Chem.* **1991**, *95*, 13612–3620.
- [147] Troe, J.; Ushakov, V. G. The dissocia-

- tion/recombination reaction $\text{CH}_4(^+M) \longleftrightarrow \text{CH}_3 + \text{H}(^+M)$: A case study for unimolecular rate theory. *J. Chem. Phys.* **2012**, *136*, 214309.
- [148] Harding, L. B.; Georgievskii, Y.; Klippenstein, S. J. Predictive Theory for Hydrogen Atom-Hydrocarbon Radical Association Kinetics. *J. Phys. Chem. A* **2005**, *109*, 4646–4656.
- [149] Takahashi, J.; Momose, T.; Shida, T. Thermal rate constants for $\text{SiH}_4 \longleftrightarrow \text{SiH}_3 + \text{H}$ and $\text{CH}_4 \longleftrightarrow \text{CH}_3 + \text{H}$ by Canonical Variational Transition State Theory. *Bull. Chem. Soc. Jpn.* **1994**, *67*, 74–85.
- [150] Wardlaw, D. M.; Marcus, R. A. Unimolecular reaction rate theory for transition states of any looseness. 3. Application to methyl radical recombination. *J. Phys. Chem.* **1986**, *90*, 5383–5393.
- [151] Darvesh, K. V.; Boyd, R. J.; Pacey, P. D. Recombination of Methyl Radicals: Ab Initio Potential and Transition-State Theory Calculations. *J. Phys. Chem.* **1989**, *93*, 4772–4779.
- [152] Pesa, M.; Pilling, M.; Robertson, S. H.; Wardlaw, D. M. Application of the Canonical Flexible Transition State Theory to CH_3 , CF_3 , and CCl_3 Recombination Reactions. *J. Phys. Chem. A* **1998**, *102*, 8526–8536.
- [153] Klippenstein, S. J.; Harding, L. B. A Direct Transition State Theory Based Study of Methyl Radical Recombination Kinetics. *J. Phys. Chem. A* **1999**, *103*, 9388–9398.
- [154] Klippenstein, S. J.; Georgievskii, Y.; Harding, L. B. Predictive theory for the combination kinetics of two alkyl radicals. *Phys. Chem. Chem. Phys.* **2006**, *8*, 1133–1147.
- [155] Wagner, A. F.; Wardlaw, D. M. Study of the recombination reaction $\text{CH}_3 + \text{CH}_3 \longrightarrow \text{C}_2\text{H}_6$. 2. Theory. *J. Phys. Chem.* **1988**, *92*, 2462–2471.
- [156] Wang, B.; Hou, H.; Yoder, L. M.; Muckerman, J. T.; Fockenberg, C. Experimental and Theoretical Investigations on the Methyl-Methyl Recombination Reaction. *J. Phys. Chem. A* **2003**, *107*, 11414–11426.
- [157] Lorant, F.; Behar, F.; Goddard, III, W.; Tang, Y. Ab Initio Investigation of Ethane Dissociation Using Generalized Transition State Theory. *J. Phys. Chem. A* **2001**, *105*, 7896–7904.
- [158] Lu, K.-W.; Matsui, H.; Huang, C.-L.; Raghunath, P.; Wang, N.-S.; Lin, M. C. Shock Tube Study on the Thermal Decomposition of CH_3OH . *J. Phys. Chem.* **2010**, *114*, 5493–5502.
- [159] Herbst, E.; Terzieva, R.; Talbi, D. Calculations on the rates, mechanisms, and interstellar importance of the reactions between C and NH_2 and between N and CH_2 . *Mon Not R Astron Soc* **2000**, *311*, 869–876.
- [160] Mayneris, J.; Saracibar, A.; Goldfield, E. M.; González, M.; García, E.; Gray, S. K. Theoretical Study of the Complex-Forming $\text{CH} + \text{H}_2 \longrightarrow \text{CH}_2 + \text{H}$ Reaction. *J. Phys. Chem. A* **2006**, *110*, 5542–5548.
- [161] Caridade, P. J. S. B.; Rodrigues, S. P. J.; Sousa, F.; Varandas, A. J. C. Unimolecular and Bimolecular Calculations for HN_2 . *J. Phys. Chem. A* **2005**, *109*, 2356–2363.
- [162] Xu, Z.-F.; Fang, D.-C.; Fu, X.-Y. Ab Initio Studies on the Dynamical Properties of the Reaction $\text{NH}(\text{X}^3\Sigma^-) + \text{H} \longrightarrow \text{N}(^4\text{S}) + \text{H}_2$. *J. Phys. Chem. A* **1997**, *101*, 4432–4436.
- [163] Pascual, R. Z.; Schatz, G. C.; Lendvay, G.; Troya, D. Quasiclassical Trajectory and Transition State Theory Studies of the $\text{N}(^4\text{S}) + \text{H}_2 \longleftrightarrow \text{NH}(\text{X}^3\Sigma^-) + \text{H}$ Reaction. *J. Chem. Phys.* **2002**, *106*, 4125–4136.
- [164] Takayanagi, T.; Kobayashi, H.; Tsunashima, S. Reaction dynamics for the $\text{N}(^2\text{D}) + \text{H}_2$ reaction. *J. Chem. Soc. Faraday Trans.* **1996**, *92*, 1311–1314.
- [165] Kobayashi, H.; Takayanagi, T.; Yokoyama, K.; Sato, T.; Tsunashima, S. Quasiclassical Trajectory Studies of $\text{N}(^2\text{D}) + \text{H}_2$ Reaction on a Fitted ab initio Potential-energy Surface. *J. Chem. Soc. Faraday Trans.* **1995**, *91*, 3771–3777.
- [166] Pederson, L. A.; Schatz, G. C.; Ho, T.-S.; Hollebeek, T.; Rabitz, H.; Harding, L. B.; Lendvay, G. Potential energy surface and quasiclassical trajectory studies of the $\text{N}(^2\text{D}) + \text{H}_2$ reaction. *J. Chem. Phys.* **1999**, *110*, 9091–9100.
- [167] Ouk, C.-M.; Zvereva-Loëte, N.; Scribano, Y.; Bussery-Honvault, B. Transition State Theory Thermal Rate Constants and RRKM-Based Branching Ratios for the $\text{N}(^2\text{D}) + \text{CH}_4$ Reaction Based on Multi-State and Multi-Reference Ab Initio Calculations of Interest for the Titan’s Chemistry. *J. Comput. Chem.* **2012**, *33*, 2211–2224.
- [168] Balucani, N.; Bergeat, A.; Cartechini, L.; Volpi, G. G.; Skouteris, D.; Rosi, M. Combined Crossed Molecular Beam and Theoretical Studies of the $\text{N}(^2\text{D}) + \text{CH}_4$ Reaction and Implications for Atmospheric Models of Titan. *J. Phys. Chem. A* **2009**, *113*, 11138–11152.
- [169] Ouk, C.-M.; Zvereva-Loëte, N.; Bussery-Honvault, B. Towards a converged barrier height for the entrance channel transition state of the $\text{N}(^2\text{D}) + \text{CH}_4$ reaction and its implication for the chemistry in Titan’s atmosphere. *Chem. Phys. Lett.* **2011**, *515*, 13–18.
- [170] Chiba, S.; Yoshida, F. Theoretical study of $\text{N}(^4\text{S}, ^2\text{D}) + \text{CH}_3(^2\text{A}_2)$ reaction mechanisms revisited: The importance of spin-forbidden and roaming dynamics processes. *Chem. Phys. Lett.* **2014**, *595-596*, 103–108.
- [171] Becerra, R.; Canosa-Mas, C. E.; Frey, H. M.; Walsh, R. Studies of Methylene Chemistry by Pulsed Laser-induced Decomposition of Ketene. *J. Chem. Soc., Faraday Trans. 2* **1987**, *83*, 435–448.
- [172] Yu, A.; Chen, C.; Huang, M. An ab initio study on the reaction of $\text{CH}(\text{X}^2\Pi)$ with CH_4 . *Can. J. Chem.* **1993**, *71*, 512–519.
- [173] Wang, Z.-X.; Chen, C.; Huang, M. Theoretical study on the insertion reaction of $\text{CH}(\text{X}^2\Pi)$ with CH_4 . *Can. J. Chem.* **1997**, *75*, 996–1001.
- [174] Donovan, R. J.; Husain, D. Recent Advances in the Chemistry of Electronically Excited Atoms. *Chem. Rev.* **1970**, *70*, 489–516.

SUPPORTING INFORMATION

Experimental Data

Experiments and reviews have measured and suggested reaction rate coefficients for several of the reactions in this network at or near ~ 298 K. These values are listed in Table S1.

TABLE S1: All available experimental or recommended reaction rate coefficients for the reactions in this study. For brevity, only the 13 most recent experimental rate coefficients are listed for $\text{CH}_3 + \text{CH}_3 \longrightarrow \text{C}_2\text{H}_6$, for a complete listing, we refer the reader to the NIST Chemical Kinetics Database⁶⁶. First-order rate coefficients have units s^{-1} . Second-order rate coefficients have units cm^3s^{-1} .

k(298K)	Technique	Temp. (K)	Pressure (Torr)	Reference(s)
$\text{H}_2\text{CN} + \text{H} \longrightarrow \text{HCN} + \text{H}_2$ 8.3×10^{-11}	Z	independent		Tomeczek and Gradoń ⁶⁷
$\text{H}_2\text{CN} + {}^4\text{N} \longrightarrow \text{HCN} + {}^3\text{NH}$ 4.4×10^{-11}	M	298	1	Nesbitt et al. ⁶⁸
$2\text{H}_2\text{CN} \longrightarrow \text{HCN} + \text{H}_2\text{CNH}$ $3.3\text{--}8.3 \times 10^{-12}$	M	300	120–480	Horne and Norrish ⁶⁹
$\text{CH}_4 + \text{H} \longrightarrow \text{CH}_3 + \text{H}_2$ 3.5×10^{-17}	M	298		Lawrence and Firestone ⁷⁰
	M	298	0.55	Jones and Ma ⁷¹
	S	300		Baulch et al. ⁶²
$\text{CH}_4 + {}^2\text{N} \longrightarrow \text{H}_2\text{CNH} + \text{H}$ ${}^a 4.5 \times 10^{-12}$	M	298	700	Takayanagi et al. ⁷² , Umemoto et al. ³⁹
${}^a 3.7 \times 10^{-12}$	M	300	6	Fell et al. ⁷³ , Umemoto et al. ³⁹
${}^a 2.7 \times 10^{-12}$	M	295	20	Umemoto et al. ⁷⁴ , Umemoto et al. ³⁹
${}^a 2.4 \times 10^{-12}$	M	300	3–5	Black et al. ⁷⁵ , Umemoto et al. ³⁹
${}^a 3.2 \times 10^{-12}$	S	298		Herron ⁷⁶ , Umemoto et al. ³⁹
$\text{CH}_4 + {}^2\text{N} \longrightarrow \text{CH}_3 + {}^3\text{NH}$ ${}^b 1.7 \times 10^{-12}$	M	298	700	Takayanagi et al. ⁷² , Umemoto et al. ³⁹
${}^b 1.4 \times 10^{-12}$	M	300	6	Fell et al. ⁷³ , Umemoto et al. ³⁹
${}^b 1.0 \times 10^{-12}$	M	295	20	Umemoto et al. ⁷⁴ , Umemoto et al. ³⁹
${}^b 9.0 \times 10^{-13}$	M	300	3–5	Black et al. ⁷⁵ , Umemoto et al. ³⁹
${}^b 1.2 \times 10^{-12}$	S	298		Herron ⁷⁶ , Umemoto et al. ³⁹
$\text{CH}_3 + \text{H} \longrightarrow \text{CH}_4$ 4.7×10^{-10}	M	300	high-pressure limit	Brouard et al. ⁷⁷
3.3×10^{-10}	M	308	high-pressure limit	Cheng and Yeh ⁷⁸
2.5×10^{-10}	M	308	300	Cheng et al. ⁷⁹
2.0×10^{-10}	M	296	735–755	Sworski et al. ⁸⁰
1.5×10^{-10}	M	300	high-pressure limit	Patrick et al. ⁸¹
3.4×10^{-10}	F	298	high-pressure limit	Michael et al. ⁸²
3.5×10^{-10}	S	independent	high-pressure limit	Cobos and Troe ⁸³
3.5×10^{-10}	S	independent	high-pressure limit	Baulch et al. ⁶²
2.0×10^{-10}	S	298	high-pressure limit	Tsang ⁸⁴
$\text{CH}_3 + \text{H}_2 \longrightarrow \text{CH}_4 + \text{H}$ ${}^c 1.3 \times 10^{-20}$	M	300		Kobrinisky and Pacey ⁸⁵
1.2×10^{-20}	S	300		Tsang and Hampson ⁸⁶
9.6×10^{-21}	S	300		Baulch et al. ⁶²
$\text{CH}_3 + {}^4\text{N} \longrightarrow \text{HCN} + \text{H}_2$ 8.6×10^{-12}	M	298	0.3–1.6	Marston et al. ²⁸ , Stief et al. ⁶³
$\text{CH}_3 + {}^4\text{N} \longrightarrow \text{H}_2\text{CN} + \text{H}$ 7.7×10^{-11}	M	298	0.3–1.6	Marston et al. ²⁸ , Stief et al. ⁶³
5.0×10^{-11}	S	independent		Miller and Bowman ⁸⁷
$2\text{CH}_3 \longrightarrow \text{C}_2\text{H}_6$ 6.5×10^{-11}	M	300	high-pressure limit	Walter et al. ⁸⁸

6.5×10^{-11}	M	298	high-pressure limit	Macpherson et al. ⁸⁹
6.0×10^{-11}	M	298	high-pressure limit	Du et al. ⁹⁰
6.0×10^{-11}	M	298	high-pressure limit	Slagle et al. ⁹¹
$^d 5.9 \times 10^{-11}$	M	292	758	Sangwan et al. ⁹²
5.8×10^{-11}	M	298	750	Pagsberg et al. ⁹³
5.5×10^{-11}	M	298	high-pressure limit	Hippler et al. ⁹⁴
5.2×10^{-11}	M	298	100	Fahr et al. ⁹⁵
4.6×10^{-11}	M	300	1	Wang et al. ⁹⁶
4.0×10^{-11}	M	302	81–571	Arthur ⁹⁷
3.5×10^{-11}	M	308	86	Anastasi and Arthur ⁹⁸
6.0×10^{-11}	S	independent	high-pressure limit	Baulch et al. ⁶²
4.4×10^{-11}	S	298	high-pressure limit	Tsang ⁸⁴
$^1\text{CH}_2 + \text{H} \longrightarrow \text{CH} + \text{H}_2$				
5.0×10^{-11}	S			Tsang and Hampson ⁸⁶
$^1\text{CH}_2 + \text{H}_2 \longrightarrow \text{CH}_4 \cdot \longrightarrow \text{CH}_3 + \text{H}$				
1.3×10^{-10}	M	295	6	Langford et al. ³⁷
1.1×10^{-10}	M	298	10^{-4} –10	Ashfold et al. ³⁸
7.0×10^{-12}	M	298	10	Braun et al. ³⁶
1.2×10^{-10}	S			Tsang and Hampson ⁸⁶
1.2×10^{-10}	S	independent		Baulch et al. ⁶²
$^1\text{CH}_2 + ^1\text{CH}_2 \longrightarrow \text{C}_2\text{H}_2 + 2\text{H}$				
5.0×10^{-11}	S			Tsang and Hampson ⁸⁶
$^1\text{CH}_2 + ^3\text{CH}_2 \longrightarrow \text{C}_2\text{H}_2 + \text{H}_2$				
3.0×10^{-11}	S			Tsang and Hampson ⁸⁶
$^1\text{CH}_2 + \text{CH}_3 \longrightarrow \text{C}_2\text{H}_4 + \text{H}$				
3.0×10^{-11}	S			Tsang and Hampson ⁸⁶
$^1\text{CH}_2 + \text{CH}_4 \longrightarrow 2\text{CH}_3$				
7.3×10^{-11}	M	298	10^{-4} –10	Ashfold et al. ³⁸
7.0×10^{-11}	M	295	6	Langford et al. ³⁷
1.9×10^{-12}	M	298	5–20	Braun et al. ³⁶
7.1×10^{-11}	S			Tsang and Hampson ⁸⁶
$^3\text{CH}_2 + \text{H} \longrightarrow \text{CH}_3 \cdot \longrightarrow \text{CH} + \text{H}_2$				
2.7×10^{-10}	M	285	2	Boullart and Peeters ³⁰
2.7×10^{-10}	M	298	2	Böhland and Temps ³³
$^e 2.6 \times 10^{-10}$	M	300	2	Devriendt et al. ²⁹
1.8×10^{-10}	M	298	1–2	Böhland et al. ³¹
$^c 1.4 \times 10^{-10}$	M	300	100	Zabarnick et al. ³²
8.3×10^{-11}	M	298	2	Grebe and Homann ³⁴
2.0×10^{-10}	S	300		Baulch et al. ⁶²
2.7×10^{-10}	S	298		Tsang and Hampson ⁸⁶
$^3\text{CH}_2 + \text{H}_2 \longrightarrow \text{CH}_3 + \text{H}$				
$< 5.0 \times 10^{-14}$	M	298	10	Braun et al. ³⁶
$< 6.9 \times 10^{-15}$	M	295	8	Darwin and Moore ⁹⁹
$< 5.0 \times 10^{-15}$	M		10	Pilling and Robertson ¹⁰⁰
$^3\text{CH}_2 + ^3\text{CH}_2 \longrightarrow \text{C}_2\text{H}_2 + 2\text{H}$				
5.3×10^{-11}	M	298	20–700	Braun et al. ³⁶
5.3×10^{-11}	S	300		Baulch et al. ⁶²
$^3\text{CH}_2 + \text{CH}_3 \longrightarrow \text{C}_2\text{H}_5 \cdot \longrightarrow \text{C}_2\text{H}_4 + \text{H}$				
2.1×10^{-10}	M	300	1	Wang and Fockenberg ⁹⁶
1.1×10^{-10}	M	298	1	Deters et al. ¹⁰¹
1.0×10^{-10}	M	308	50–700	Lauffer and Bass ¹⁰²
5.0×10^{-11}	M		200	Pilling and Robertson ¹⁰³
7.0×10^{-11}	S	independent		Baulch et al. ⁶²
7.0×10^{-11}	S	298		Tsang and Hampson ⁸⁶
$^3\text{CH}_2 + \text{CH}_4 \longrightarrow 2\text{CH}_3$				
$< 5.0 \times 10^{-14}$	M	298	10	Braun et al. ³⁶
$^f 3.1 \times 10^{-19}$	M	298	2–3	Böhland et al. ¹⁰⁴
$< 3.0 \times 10^{-19}$	S	298		Tsang and Hampson ⁸⁶
$\text{CH} + \text{H}_2 \longrightarrow \text{CH}_3$				
1.6×10^{-10}	M	294	high-pressure limit	Brownsword et al. ¹⁰⁵

5.1×10^{-11}	M	300	750	Fulle and Hippler ¹⁰⁶
4.5×10^{-11}	M	298	591	Becker et al. ³⁵
4.5×10^{-11}	M	279	600	Berman and Lin ¹⁰⁷
3.0×10^{-11}	M	294	750	McIlroy and Tully ¹⁰⁸
2.3×10^{-11}	M	298	100	Butler et al. ¹⁰⁹
1.7×10^{-11}	M			Bosnali and Perner ¹¹⁰
1.0×10^{-12}	M	298	1–9	Braun et al. ¹¹¹
$\text{CH} + \text{H}_2 \longrightarrow \text{CH}_3 \cdot \longrightarrow {}^3\text{CH}_2 + \text{H}$				
^c 9.1×10^{-13}	M	300	100	Zabarnick et al. ³²
1.2×10^{-12}	M	294	400	Brownsword et al. ¹⁰⁵
4.5×10^{-11}	M	298	591	Becker et al. ³⁵
$\text{CH} + {}^4\text{N} \longrightarrow {}^3\text{HCN} \longrightarrow \text{CN} + \text{H}$				
1.6×10^{-10}	M	298	4	Brownsword et al. ¹¹²
$1.2\text{--}1.4 \times 10^{-10}$	M	296	5	Daranlot et al. ⁶⁰
2.1×10^{-11}	M	298	5–15	Messing et al. ¹¹³
$2\text{CH} \longrightarrow \text{C}_2\text{H}_2$				
2.0×10^{-10}	M	298	1–330	Braun et al. ¹¹¹
1.7×10^{-10}	M	298	1–500	Braun et al. ¹¹⁴
$\text{CH} + \text{CH}_4 \longrightarrow \text{C}_2\text{H}_4 + \text{H}$				
3.0×10^{-10}	M	298	30–100	Butler et al. ¹⁰⁹
1.0×10^{-10}	M	298	100	Butler et al. ¹¹⁵
9.8×10^{-11}	M	298	100	Berman and Lin ¹¹⁶
9.1×10^{-11}	M	298	50–300	Blitz et al. ¹¹⁷
8.9×10^{-11}	M	295	9–12	Canosa et al. ¹¹⁸
6.7×10^{-11}	M	298	100	Thiesemann et al. ¹¹⁹
3.3×10^{-11}	M			Bosnali and Perner ¹¹⁰
2.5×10^{-12}	M	298	100	Braun et al. ¹¹¹
2.0×10^{-12}	M	298	1–500	Braun et al. ¹¹⁴
9.8×10^{-11}	S	298		Baulch et al. ⁶²
${}^3\text{NH} + \text{H} \longrightarrow \text{H}_2 + {}^4\text{N}$				
3.2×10^{-12}	M	298	2–8	Adam et al. ¹²⁰
${}^3\text{NH} + {}^4\text{N} \longrightarrow \text{N}_2 + \text{H}$				
2.5×10^{-11}	M	298	11–15	Hack et al. ¹²¹
2.6×10^{-11}	S	300		Konnov and De Ruyck ¹²²
${}^2\text{N} + \text{H}_2 \longrightarrow \text{NH}_2 \cdot \longrightarrow {}^3\text{NH} + \text{H}$				
5.0×10^{-12}	M	300	3–5	Black et al. ⁷⁵
3.5×10^{-12}	M	300	6	Fell et al. ⁷³
2.7×10^{-12}	M	300	2–5	Black et al. ¹²³
2.4×10^{-12}	M	300	753	Suzuki et al. ¹²⁴
2.3×10^{-12}	M	295	30	Umemoto et al. ¹²⁵
2.3×10^{-12}	M	300	1–3	Piper et al. ¹²⁶
2.1×10^{-12}	M	300	26	Husain et al. ¹²⁷
1.8×10^{-12}	M	298	1	Whitefield et al. ¹²⁸
1.7×10^{-12}	M	300	50	Husain et al. ¹²⁹
2.2×10^{-12}	S	200–300		Herron ⁷⁶

^a Experimental value of $\text{CH}_4 + {}^2\text{N} \longrightarrow \text{products}$, multiplied by a branching ratio of 0.8³⁹.

^b Experimental value of $\text{CH}_4 + {}^2\text{N} \longrightarrow \text{products}$, multiplied by a branching ratio of 0.3³⁹.

^c Experiments performed at 372 K and extrapolated to 300 K.

^d Value taken as average of two identical experiments.

^e Experiments performed at ≥ 400 K and extrapolated to 300 K.

^f Experiments performed at ≥ 413 K and extrapolated to 300 K.

Z: Zero activation energy value. Calculated by numerical modeling using the chemical compositions of the flames of $\text{CH}_4 + \text{air}$.

M: Monitoring decay of reactants and/or production of products.

S: Suggested value based on experiments and/or evaluations at a range of temperatures.

F: Fitting of simulated concentration profiles to absolute concentration profiles from experiments reported by Barker et al.¹³⁰.

Previous Theoretical Data

Previous theoretical studies have been performed on the reactions in this network. In Table S2, we list the

theoretical rate coefficients and the methods that were employed to calculate them.

TABLE S2: Previous theoretical rate coefficients for the reactions in this study. For sources that performed multiple rate coefficient calculations with different theoretical and/or computational methods, we list the range of their results here. First-order rate coefficients have units s^{-1} . Second-order rate coefficients have units cm^3s^{-1} .

k(298K)	Theory	Computational Method	Reference(s)
$\text{CH}_4 + \text{H} \longrightarrow \text{CH}_3 + \text{H}_2$			
4.1×10^{-21} – 2.2×10^{-18}	TST, quantum dynamics	CCSD(T)/cc-pVTZ ^a	Kerkeni and Clary ¹³¹
8.4×10^{-19} – 2.1×10^{-18}	CVT + SCT ^b	BH&HLYP/6-311G(d,p), PMP4/6-311+G(2df,2pd) ^c	Truong and Duncan ¹³²
1.6×10^{-18}	CVT + SCT	PMP4/cc-pVTZ ^d	Maity et al. ⁴²
1.3×10^{-18}	CVT + SCT ^e	QCISD/6-311G(d,p)	Truong ¹³³
9.8×10^{-19}	CVT + μOMT		Espinosa-García and Corchado ¹³⁴
			Jordan and Gilbert ¹³⁵
6.5×10^{-19}	CVT + μOMT		Espinosa-García and Corchado ¹³⁴
			Joseph et al. ¹³⁶
3.0×10^{-21} – 6.0×10^{-19}	TST, quantum dynamics	CCSD(T)/cc-pVTZ ^a	Kerkeni and Clary ¹³⁷
3.8×10^{-19}	BEBO		Clark and Dove ¹³⁸
8.7×10^{-21} – 2.4×10^{-19}	TST, CVT, CVT + SCT		Pu and Truhlar ¹³⁹
1.8×10^{-21} – 1.6×10^{-19}	TST	G2(MP2) ^f , BAC-MP4 ^g	Berry et al. ¹⁴⁰
8.1×10^{-20}	TST + tunneling	UMP2/6-31G-(d,p)	Bryukov et al. ¹⁴¹
4.6×10^{-20}	TST + WTC	PMP4SDTQ/6-311G ^{**h}	Gonzalez et al. ¹⁴²
$\text{CH}_3 + \text{H}_2 \longrightarrow \text{CH}_4 + \text{H}$			
1.2×10^{-19}	CVT + μOMT		Espinosa-García and Corchado ¹³⁴
			Joseph et al. ¹³⁶
1.1×10^{-19}	CVT + SCT	PMP4/cc-pVTZ ^d	Maity et al. ⁴²
1.5 – 8.2×10^{-20}	CVT + SCT ^b	BH&HLYP/6-311G(d,p), PMP4/6-311+G(2df,2pd) ^c	Truong and Duncan ¹³²
8.0×10^{-20}	CVT + μOMT		Espinosa-García and Corchado ¹³⁴
			Jordan and Gilbert ¹³⁵
5.2×10^{-20}	CVT + SCT ^e	QCISD/6-311G(d,p)	Truong ¹³³
1.7×10^{-20}	TST + tunneling	UMP2/6-31G-(d,p)	Bryukov et al. ¹⁴¹
$\text{CH}_3 + {}^4\text{N} \longrightarrow \text{H}_3\text{CN} \cdot \longrightarrow \text{H}_2\text{CN} + \text{H}$			
1.9×10^{-10}	CVT + RRKM	CCSD(T)/CBS	Alves et al. ¹⁴³
9.1×10^{-12}	μVT + RRKM	CCSD(T)/cc-pVTZ ⁱ	Cimas and Largo ⁶⁴
$\text{CH}_4 + {}^2\text{N} \longrightarrow \text{products}$			
8.5×10^{-14}	CVT	CASSCF(5,5)/6-311G ^{**}	Takayanagi et al. ⁷²
$\text{CH}_3 + \text{H} \longrightarrow \text{CH}_4$			
6.7×10^{-10}	CVT	MP4/6-31G ^{**}	Hase and Duchovic ¹⁴⁴
^j 4.7×10^{-10}	CVT + RRKM		Pilling ¹⁴⁵
^j 4.3 – 4.7×10^{-10}	μVT + RRKM, CVT + RRKM		Forst ¹⁴⁶
^j 3.3×10^{-10}	SACM/CT	CASPT2/cc-pVDZ ^k	Troe and Ushakov ¹⁴⁷
^j 3.2×10^{-10}	VRC-TST	CASPT2/cc-pVDZ ^k	Harding et al. ¹⁴⁸
2.0 – 2.7×10^{-10}	CVT	MP4/6-31G ^{**} , MRD-CI/6-31G ^{**}	Hase et al. ⁵⁸
2.1×10^{-10}	CVT	MCSCF-CI/DZP ^l	Takahashi et al. ¹⁴⁹
$2 \text{CH}_3 \longrightarrow \text{C}_2\text{H}_6$			
1.8×10^{-10} – 4.6×10^{-9}	CVT	CASPT2/ANO-L ^m	Li et al. ⁴³
^j 6.9 – 8.4×10^{-11}	LTS	MC	Wardlaw and Marcus ¹⁵⁰
8.3×10^{-11}	CVT	MRD-CI/DZ	Darvesh et al. ¹⁵¹
^j 7.2×10^{-11}	FTST	MC	Pesa et al. ¹⁵²
^j 5.8 – 6.7×10^{-11}	μVT + RRKM		Forst ¹⁴⁶
^j 6.3×10^{-11}	CVT	CAS+1+2/cc-pVDZ	Klippenstein and Harding ¹⁵³
	CVT + RRKM		
5.8×10^{-11}	VRC-TST	CASPT2/cc-pVDZ ^k	Klippenstein et al. ¹⁵⁴
^j 5.8×10^{-11}	RRKM + FTST		Wagner and Wardlaw ¹⁵⁵
^j 5.6×10^{-11}	CVT	MRCI+Q/aug-cc-pVTZ	Wang et al. ¹⁵⁶
2.0×10^{-11}	CVT	B3LYP/6-31G ^{**}	Lorant et al. ¹⁵⁷
${}^3\text{CH}_2 + \text{H}_2 \longrightarrow \text{CH}_3 + \text{H}$			
1.5×10^{-18}	TST	G2M(RCC2) ⁿ	Lu et al. ¹⁵⁸

${}^3\text{CH}_2 + {}^4\text{N} \longrightarrow \text{H}_2\text{CN} \cdot \longrightarrow \text{HCN} + \text{H}$	7.9×10^{-11}	quantum dynamics	MP4SDTQ/6-311++G(3df,3pd) ^o	Herbst et al. ¹⁵⁹
${}^3\text{CH}_2 + {}^3\text{CH}_2 \longrightarrow \text{C}_2\text{H}_2 + 2\text{H}$	1.5×10^{-10}	VRC-TST	CASPT2/aug-cc-pVTZ ^p	Jasper et al. ⁵⁹
${}^3\text{CH}_2 + \text{CH}_3 \longrightarrow \text{C}_2\text{H}_4 + \text{H}$	2.2×10^{-10}	VRC-TST	CASPT2/aug-cc-pVTZ ^p	Jasper et al. ⁵⁹
$\text{CH} + \text{H}_2 \longrightarrow \text{CH}_3$	${}^j 7.8 \times 10^{-11}$	RRKM		McIlroy and Tully ¹⁰⁸
$\text{CH} + \text{H}_2 \longrightarrow \text{CH}_3 \cdot \longrightarrow {}^3\text{CH}_2 + \text{H}$	3.3×10^{-11}	QCT	MRCI/aug-cc-pVTZ	Mayneris et al. ¹⁶⁰
$\text{CH} + \text{N} \longrightarrow {}^3\text{HCN} \cdot \longrightarrow \text{CN} + \text{H}$	1.2×10^{-10}	quantum dynamics	MRCI+Q/AVTZ	Daranlot et al. ⁶⁰
${}^3\text{NH} + {}^4\text{N} \longrightarrow \text{N}_2 + \text{H}$	1.9×10^{-11}	QCT	MRCI/aug-cc-pVQZ	Caridade et al. ¹⁶¹
${}^3\text{NH} + \text{H} \longrightarrow \text{H}_2 + {}^4\text{N}$	1.5×10^{-12}	CT	MRCI/aug-cc-pVQZ	Adam et al. ¹²⁰
	$1.3\text{--}5.2 \times 10^{-12}$	CVT	MP-SAC4/6-311G**	Xu et al. ¹⁶²
	$2.0\text{--}5.5 \times 10^{-13}$	QCT, CVT	MCQDPT2/6-311++G** ^q	Pascual et al. ¹⁶³
${}^2\text{N} + \text{H}_2 \longrightarrow \text{NH}_2 \cdot \longrightarrow {}^3\text{NH} + \text{H}$	$2.5\text{--}3.3 \times 10^{-12}$	quantum dynamics, QCT	FOCI/TZP	Takayanagi et al. ¹⁶⁴
	$2.7\text{--}2.9 \times 10^{-12}$	QCT	FOCI/TZP	Kobayashi et al. ¹⁶⁵
	$1.8\text{--}2.7 \times 10^{-12}$	QCT, CVT		Suzuki et al. ¹²⁴
	8.9×10^{-13}	QCT	MRCI/aug-pVTZ	Pederson et al. ¹⁶⁶

^a Single point energies are based on optimized geometries calculated at the MP2/cc-pVTZ level.

^b Energy barrier scaled by a factor of 1.174.

^c Single point energies are based on optimized geometries calculated at the BHandHLYP/6-311G(d,p) level.

^d Single point energies are based on optimized geometries calculated at the BHandHLYP/cc-pVDZ level.

^e Energy barrier scaled by a factor of 0.86.

^f Single point energies are based on optimized geometries calculated at the MP2/6-31G(d) level.

^g Single point energies are based on optimized geometries calculated at the HF/6-31G(d) level.

^h Single point energies are based on optimized geometries calculated at the UMP2/6-31G** level.

ⁱ Single point energies are based on optimized geometries calculated at the B3LYP/cc-pVTZ level.

^j Values calculated in the high-pressure limit ($p \rightarrow \infty$).

^k Single point energies are based on optimized geometries calculated at the B3LYP/6-31G* level, and corrections are applied at the CAS+1+2+QC/aug-cc-pVTZ level.

^l CI calculations are based on optimized geometries calculated at the UHF/DZP level.

^m Single point energies are based on optimized geometries calculated at the CASSCF/ANO-L level.

ⁿ Single point energies are based on optimized geometries calculated at the B3LYP/6-311++G(3df, 2p) level.

^o Single point energies are based on optimized geometries calculated at the MP2/6-31G(d,p) level.

^p Single point energies are based on optimized geometries calculated at the B3LYP/6-311++G(d,p) level.

^q Single point energies are based on optimized geometries calculated at the FORS-MCSCF(7,6)/6-311++G** level.

TST: Transition state theory.

CVT: Canonical variational transition state theory.

SCT: Small curvature tunneling approximation

μ OMT: Microcanonical optimized multidimensional tunneling.

BEBO: bond-energy-bond-order method.

WTC: Wigner tunneling correction.

RRKM: Rice-Ramsperger-Kassel-Marcus theory.

μ VT: Microcanonical variational transition state theory.

SACM/CT: Statistical adiabatic channel model/classical trajectories approach.

VRC-TST: Variable reaction coordinate transition state theory.

LTS: Loose transition state model.

MC: Monte Carlo simulations.

FTST: Flexible transition state theory.

QCT: Quasi-classical trajectory method

CT: Classical trajectory method

Example Calculation and Computational Methods Comparison

theoretically^{42,62,70,71,132–140,142}. A pair of experiments at 298 K place its rate coefficient between $1.7\text{--}3.5 \times 10^{-17}$

The $\text{CH}_4 + \text{H} \longrightarrow \text{CH}_3 + \text{H}_2$ abstraction reaction has been thoroughly studied both experimentally and

$\text{cm}^3\text{s}^{-170,71}$. However, based on a range of experiments and evaluations over a wider temperature range (300–2000 K), it has been suggested the rate coefficient is closer to $8.2 \times 10^{-19} \text{ cm}^3\text{s}^{-162}$. Previous theoretical studies have calculated its rate coefficient to be between 1.8×10^{-21} and $2.2 \times 10^{-18} \text{ cm}^3\text{s}^{-1}$ (see Table S2).

The geometry of this reaction progresses as follows: A single H atom approaches a CH_4 molecule directly in line with one of its H atoms and its central C atom. The H-C bond in methane then stretches until its H atom bonds with the adjacent H atom. The two newly formed molecules, H_2 and CH_3 then separate. The geometry of the transition state is depicted in Figure S2.

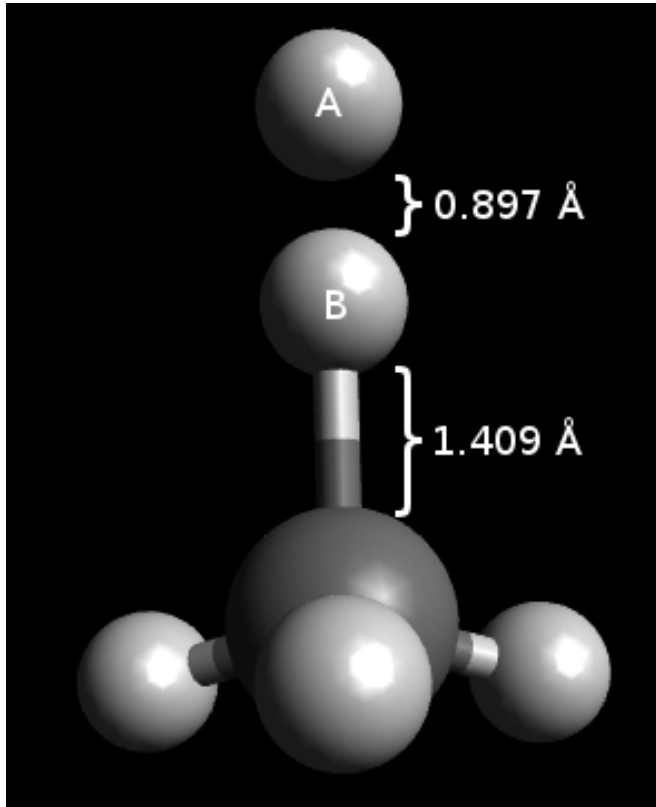


FIG. S1. Geometry of the conventional transition state for $\text{CH}_4 + \text{H} \rightarrow \text{CH}_3 + \text{H}_2$ at the BHandHLYP/aug-cc-pVDZ level of theory. In the reactant state, hydrogen B is 1.09 \AA from the central carbon. In the product state hydrogen B is 0.754 \AA from hydrogen A.

In Figure S2, we show $\Delta G_{GT}(298.15\text{K}, s)$ with the reaction coordinate representing the C-H bond distance. At the BHandHLYP/aug-cc-pVDZ level of theory, the maximum ΔG occurs at a C-H distance of 1.44 \AA , which is slightly farther along the reaction coordinate than the conventional transition state (1.409 \AA).

We calculate the rate coefficient for this reaction using 6 different computational methods, and display them in Table S3.

Rate coefficient calculations using BHandHLYP and CAM-B3LYP methods are within the experimental and

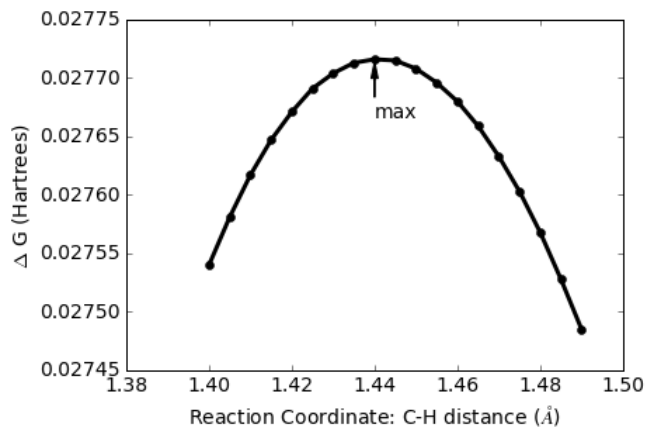


FIG. S2. Gibbs free energy difference as a function of the reaction coordinate (C-H bond distance) for $\text{CH}_4 + \text{H} \rightarrow \text{CH}_3 + \text{H}_2$ at the BHandHLYP/aug-cc-pVDZ level of theory. The maximum ΔG occurs at 1.44 \AA . ΔG is calculated as the Gibbs free energy at the reaction coordinate minus the Gibbs free energy of the reactants placed 100 \AA apart.

TABLE S3. Calculated rate coefficients for $\text{CH}_4 + \text{H} \rightarrow \text{CH}_3 + \text{H}_2$ using 6 different computational methods with the aug-cc-pVDZ basis set. Experimental and suggested values range from 8.2×10^{-19} to $3.5 \times 10^{-17} \text{ cm}^3\text{s}^{-162,70,71}$. The error factor is the multiplicative or divisional factor from the nearest experimental or suggested value; the error factor is 1 if the calculated value is within the range of experimental or suggested values. Rate coefficients have units cm^3s^{-1} .

Computational Method	$k(298)$	Error factor
HF	3.5×10^{-25}	2×10^6
M06-2x	5.7×10^{-20}	14
CCSD	9.9×10^{-20}	8
BHandHLYP	8.1×10^{-18}	1
CAM-B3LYP	3.1×10^{-17}	1
B3LYP	3.9×10^{-16}	11

suggested range. Calculations using HF grossly over-estimate the energy barrier, and provide a rate coefficient several orders of magnitude lower than the experimental and suggested range. M06-2x and CCSD methods also provide values lower than the experimental and suggested range, however only by approximately an order of magnitude. Calculations using B3LYP under-estimate the energy barrier, leading to a value approximately an order of magnitude higher than the experimental and suggested range.

The calculated rate coefficient using the BHandHLYP functional sits in the middle of the range of experimental and suggested values, whereas the rate coefficient calculated using CAM-B3LYP sits within $\sim 10\%$ of the experimental value at the high end of the range. The BHandHLYP result may provide the best compromise between the experimental and suggested rate coefficients for this reaction.

Finally, CCSD provides a fairly accurate rate coefficient within a factor of 8 of the suggested value.

Theoretical Case Studies

Case Study 1: $\text{H}_2\text{CN} + \text{H} \longrightarrow \text{HCN} + \text{H}_2$

Tomeczek and Gradoń⁶⁷ used published chemical compositions of the flames of CH_4 and $\text{O}_2 + \text{N}_2$ at 2500 to 1850 K to suggest a temperature-independent rate coefficient for $\text{H}_2\text{CN} + \text{H} \longrightarrow \text{HCN} + \text{H}_2$. They suggest the value $8.3 \times 10^{-11} \text{ cm}^3\text{s}^{-1}$ for this reaction. However, they note that this does not include the effects of an energy barrier. Another way to state this is, they suggest a value for the entropic component of this reaction, but not the energetic component.

We find no previous theoretical reaction rate coefficients for $\text{H}_2\text{CN} + \text{H} \longrightarrow \text{HCN} + \text{H}_2$.

This reaction occurs on the singlet and triplet PES's. There is no energy barrier for this reaction on the singlet PES. Conversely on the triplet PES, where excited ^3HCN is produced, the effects of the energy barrier are significant.

On the singlet surface, we calculate the reaction rate coefficient at the BHandHLYP/aug-cc-pVDZ level of theory to be $1.8 \times 10^{-11} \text{ cm}^3\text{s}^{-1}$. This is less than a factor of 5 larger than the experimental value for the barrierless reaction.

On the triplet surface, the reaction rate coefficient is too small to consider in this study ($k < 10^{-21} \text{ cm}^3\text{s}^{-1}$).

Case Study 2: $2\text{H}_2\text{CN} \longrightarrow \text{HCN} + \text{H}_2\text{CNH}$

Horne and Norrish⁶⁹ calculated the experimental reaction rate coefficient for $2\text{H}_2\text{CN} \longrightarrow \text{HCN} + \text{H}_2\text{CNH}$ at 300 K by monitoring the decay of H_2CN . The assumption they made was that $2\text{H}_2\text{CN} \longrightarrow \text{HCN} + \text{CH}_2\text{NH}$ is the dominant decay pathway of H_2CN . The value they obtained was in the range of $3.3\text{--}8.3 \times 10^{-12} \text{ cm}^3\text{s}^{-1}$.

No theoretical reaction rate coefficients for $2\text{H}_2\text{CN} \longrightarrow \text{HCN} + \text{H}_2\text{CNH}$ have been previously published.

We find a direct reaction pathway on the singlet PES that has no energy barrier. However, the simulations did not converge beyond a N-H bond distance of 1.95 Å and the Gibbs maximum was not found. However, choosing the reaction coordinate at a N-H bond distance of 1.95 Å for the calculation provides us with a lower bound estimate of the rate coefficient, which we calculate to be $3.7 \times 10^{-14} \text{ cm}^3\text{s}^{-1}$. This value is a factor of 89 smaller than the closest experimental value. The discrepancy between the theoretical and experimental values is expected to be due to these convergence issues.

A higher energy reaction pathway involving two ground state H_2CN molecules exists on the triplet sur-

face, however, this reaction produces excited ^3HCN and is likely much less efficient than the singlet case.

Case Study 3: $\text{CH}_4 + \text{N} \longrightarrow \text{products}$

Several experiments have measured the rate coefficient of $\text{CH}_4 + ^2\text{N} \longrightarrow \text{products}$ by monitoring the decay of ^2N in the presence of CH_4 at 295–300 K^{72–75}. The measured values range from $3.0\text{--}5.4 \times 10^{-12} \text{ cm}^3\text{s}^{-1}$. Herron⁷⁶ reviewed these experiments and recommended a value of $k(298) = 4.0 \times 10^{-12} \text{ cm}^3\text{s}^{-1}$. Umemoto et al.³⁹ measured the product yields of H and ^3NH in similar experiments to suggest branching ratios for $\text{CH}_4 + ^2\text{N} \longrightarrow \text{H}_2\text{CNH} + \text{H}$ and $\text{CH}_4 + ^2\text{N} \longrightarrow \text{CH}_3 + ^3\text{NH}$ to be 0.8 ± 0.2 and 0.3 ± 0.1 , respectively. Multiplying with these branching ratios, the experimental rate coefficients for $\text{CH}_4 + ^2\text{N} \longrightarrow \text{H}_2\text{CNH} + \text{H}$ range from $2.4\text{--}4.5 \times 10^{-12} \text{ cm}^3\text{s}^{-1}$ and the experimental rate coefficients for $\text{CH}_4 + ^2\text{N} \longrightarrow \text{CH}_3 + ^3\text{NH}$ range from $0.9\text{--}1.7 \times 10^{-12} \text{ cm}^3\text{s}^{-1}$.

Takayanagi et al.⁷² used CVT at the CASSCF(5,5)/6-311G** level of theory to calculate the rate coefficient of $\text{CH}_4 + \text{N} \longrightarrow \text{products}$ to be $8.5 \times 10^{-14} \text{ cm}^3\text{s}^{-1}$. They note that their disagreement between experimental and theoretical values is due to the CASSCF calculations estimating too large a barrier. Ouk et al.¹⁶⁷ used TST + WTC at the MRCI+P+Q/aug-cc-pVTZ level of theory to calculate the rate coefficient, and obtained a value closer to the experimental values at $6.8 \times 10^{-12} \text{ cm}^3\text{s}^{-1}$. They confirm the results from experiment that suggests a small barrier exists, although no barrier is found using the CCSD(T) and B3LYP levels of theory¹⁶⁸. The experimental barrier has a height of 6.3 kJ mol⁻¹⁷².

In this case study, we analyze the two main branches for the reaction $\text{CH}_4 + ^2\text{N} \longrightarrow \text{products}$. The mechanistic model for these reactions is shown in Figure S3.

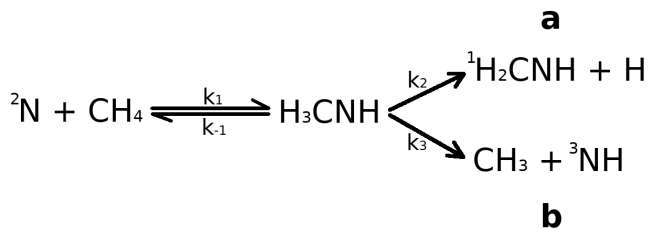


FIG. S3. Mechanistic models for the production of (a) $^1\text{H}_2\text{CNH} + \text{H}$ and (b) $\text{CH}_3 + ^3\text{NH}$ from $^2\text{N} + \text{CH}_4$ on the doublet potential energy surface.

Similar to Balucani et al.¹⁶⁸, we find no barrier for the $\text{CH}_4 + ^2\text{N} \longrightarrow \text{H}_3\text{CNH}$ reaction step. We also run into convergence problems when stretching the C-N bond distance farther than 2.82 Å. Therefore, we are unable to find a Gibbs maximum, and instead choose the reaction coordinate at 2.82 Å for our CVT calculation of k . Past

TABLE S4. Calculated overall rate coefficients for $\text{CH}_4 + {}^2\text{N} \longrightarrow {}^1\text{H}_2\text{CNH} + \text{H}$ and $\text{CH}_4 + {}^2\text{N} \longrightarrow \text{CH}_3 + {}^3\text{NH}$, as well as the intermediate forward and reverse rate coefficients which were used in the calculations. In all simulations, the BHandHLYP method was used with the aug-cc-pVDZ basis set. When using a branching ratio of 0.8 for $\text{CH}_4 + {}^2\text{N} \longrightarrow {}^1\text{H}_2\text{CNH} + \text{H}$ ³⁹, experiments from 295–300 K provide k_a values between 2.4 and $4.5 \times 10^{-12} \text{ cm}^3\text{s}^{-1}$. Similarly when using a branching ratio of 0.3 for $\text{CH}_4 + {}^2\text{N} \longrightarrow \text{CH}_3 + {}^3\text{NH}$, the same experiments provide k_b values between 0.9 – $1.7 \times 10^{-12} \text{ cm}^3\text{s}^{-1}$. First-order rate coefficients have units s^{-1} . Second-order rate coefficients have units cm^3s^{-1} .

Rate coefficient	$k(298)$
k_a	4.7×10^{-11}
k_b	5.8×10^{-29}
k_1	^a 4.7×10^{-11}
k_{-1}	3.0×10^{-66}
k_2	4.9×10^{-13}
k_3	6.0×10^{-31}

^a Simulations did not converge beyond a C-N bond distance of 2.82 \AA ; therefore the rate coefficient is a lower bound.

theoretical works found the transition state to be at a C-N bond distance of 2.26 – 2.45 \AA ^{167–169}.

We find the barrierless reaction rate coefficient of $\text{CH}_4 + {}^2\text{N} \longrightarrow \text{H}_3\text{CNH}$ at the BHandHLYP/aug-cc-pVDZ level of theory to be $6.0 \times 10^{-10} \text{ cm}^3\text{s}^{-1}$, a value two orders of magnitude greater than the closest experimental value. Given that there is likely a small barrier of $\sim 6.3 \text{ kJ mol}^{-1}$ for this reaction, we insert this experimental barrier into the calculation for k , and obtain a value of $4.7 \times 10^{-11} \text{ cm}^3\text{s}^{-1}$. This is only a factor of 9 larger than the nearest experimental value.

There are several decay pathways for the H_3CNH molecule (e.g.¹⁶⁸). Nevertheless, we calculate the upper bound for the rate coefficients of $\text{CH}_4 + {}^2\text{N} \longrightarrow \text{H}_2\text{CNH} + \text{H}$ and $\text{CH}_4 + {}^2\text{N} \longrightarrow \text{CH}_3 + {}^3\text{NH}$ by assuming H_3CNH only decays through these two dominant pathways.

The steady-state solution of the kinetic rate equations for the above mechanistic models lead to the overall rate constants for a) $\text{CH}_4 + {}^2\text{N} \longrightarrow {}^1\text{H}_2\text{CNH} + \text{H}$ and b) $\text{CH}_4 + {}^2\text{N} \longrightarrow \text{CH}_3 + {}^3\text{NH}$ on the doublet PES.

$$k_a = \frac{k_1 k_2}{k_{-1} + k_2 + k_3} \quad (\text{S1})$$

$$k_b = \frac{k_1 k_3}{k_{-1} + k_2 + k_3} \quad (\text{S2})$$

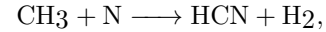
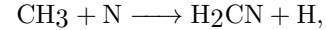
The values of the reaction rate constants at the BHandHLYP/aug-cc-pVDZ level of theory are listed in Table S4.

We calculate the overall rate constant for $\text{CH}_4 + {}^2\text{N} \longrightarrow \text{H}_3\text{CNH} \cdot \longrightarrow {}^1\text{H}_2\text{CNH} + \text{H}$ to be the same

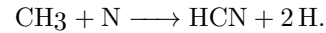
as the rate constant for $\text{CH}_4 + {}^2\text{N} \longrightarrow \text{H}_3\text{CNH}$. This means the first step is the rate-limiting step. We calculate the value for k_a to be $4.7 \times 10^{-11} \text{ cm}^3\text{s}^{-1}$, which is approximately a factor of 10 smaller than the experimental values. We find the overall rate coefficient for $\text{CH}_4 + {}^2\text{N} \longrightarrow \text{H}_3\text{CNH} \cdot \longrightarrow \text{CH}_3 + {}^3\text{NH}$ to be inefficient ($k_b = 5.8 \times 10^{-29} \text{ cm}^3\text{s}^{-1}$). This is several orders of magnitude smaller than the rate coefficients suggested by the experimental branching ratios³⁹. However, some theoretical branching ratios for $\text{CH}_4 + {}^2\text{N} \longrightarrow \text{H}_3\text{CNH} \cdot \longrightarrow \text{CH}_3 + {}^3\text{NH}$ are as low as 0.01 ¹⁶⁷, and in every case, $\text{CH}_4 + {}^2\text{N} \longrightarrow \text{H}_3\text{CNH} \cdot \longrightarrow {}^1\text{H}_2\text{CNH} + \text{H}$ is the dominant product. Considering all this, we do not include the inefficient $\text{CH}_4 + {}^2\text{N} \longrightarrow \text{H}_3\text{CNH} \cdot \longrightarrow \text{CH}_3 + {}^3\text{NH}$ reaction in our network.

Case Study 4: $\text{CH}_3 + \text{N} \longrightarrow \text{products}$

Stief et al.⁶³ experimentally calculated the overall reaction rate constant for $\text{CH}_3 + \text{N} \longrightarrow \text{products}$ at 298 K to be $8.6 \times 10^{-11} \text{ cm}^3\text{s}^{-1}$ by monitoring the decay of reactants CH_3 and N in a volume. Marston et al.²⁸ suggest the three possible branches for the reaction of $\text{CH}_3 + \text{N} \longrightarrow \text{products}$ are:



and



Marston et al.²⁸ monitored the production of H_2 , and H in experiments reacting CH_3 and N , and calculated the above reaction branching ratios to be approximately 0.9, 0.1, and 0 respectively. This suggests a preference for the $\text{CH}_3 + \text{N} \longrightarrow \text{H}_2\text{CN} + \text{H}$ pathway by approximately an order of magnitude over the $\text{CH}_3 + \text{N} \longrightarrow \text{HCN} + \text{H}_2$ pathway. It must be noted that in performing this calculation, Marston et al.²⁸ assumed that H_2 and H were solely generated through the above pathways. They caution the reader that it is also possible that these products formed through the H_2CN intermediate.

Miller and Bowman⁸⁷ suggested the rate coefficient of $\text{CH}_3 + \text{N} \longrightarrow \text{H}_2\text{CN} + \text{H}$ to be $5.0 \times 10^{-11} \text{ cm}^3\text{s}^{-1}$ based on thermodynamic calculations.

There are two main PES's that the $\text{CH}_3 + \text{N}$ reaction evolves on: the triplet and the singlet surfaces. The quintet surface is also possible, however this reaction is much higher in energy and therefore much less likely to occur⁶⁴. Both the ground state nitrogen atom (i.e. ${}^4\text{N}$) and the excited nitrogen atom (i.e. ${}^2\text{N}$) can react with CH_3 on the triplet PES. Only the excited state nitrogen atom can react with CH_3 on the singlet PES.

A computational study of the $\text{CH}_3 + \text{N} \longrightarrow$ products reaction shows a preference for the $\text{CH}_3 + {}^4\text{N} \longrightarrow \text{H}_2\text{CN} + \text{H}$ pathway⁶⁴. This study finds the $\text{CH}_3 + {}^2\text{N} \longrightarrow \text{HCN} + \text{H}_2$ channel to be negligible. Cimas and Largo⁶⁴ suggest that the HCN measured in experiments by Marston et al.²⁸ formed through the H_2CN intermediate, via reaction equations 9–11. Chiba and Yoshida¹⁷⁰ alternatively suggest that $\text{HCN} + \text{H}_2$ may form through the triplet-singlet spin-forbidden process.

Alves et al.¹⁴³ and Cimas and Largo⁶⁴ analyzed $\text{CH}_3 + \text{N} \longrightarrow$ products theoretically using quantum computational simulations at the CCSD(T)/CBS and CCSD(T)/cc-pVTZ levels of theory, and calculated its reaction rate coefficients to be $1.93 \times 10^{-10} \text{ cm}^3\text{s}^{-1}$ and $9.1 \times 10^{-12} \text{ cm}^3\text{s}^{-1}$, respectively.

In this case study, we analyze the three suggested main branches for $\text{CH}_3 + \text{N} \longrightarrow$ products using CVT (see the methods section for full details). Computational studies show that $\text{CH}_3 + {}^4\text{N} \longrightarrow$ products reactions first proceed through a barrierless reaction to H_3CN on the triplet surface^{64,143}. We confirm this barrierless reaction ($\text{CH}_3 + {}^4\text{N} \longrightarrow {}^3\text{H}_3\text{CN}$) and calculate its rate coefficients at the BHandHLYP/aug-cc-pVDZ level of theory to be $3.3 \times 10^{-11} \text{ cm}^3\text{s}^{-1}$. This result is less than a factor of 3 smaller than the experimental result ($8.6 \times 10^{-11} \text{ cm}^3\text{s}^{-1}$ ¹⁶³). Our calculated rate coefficient is also within a factor of 3 of the calculated value by Cimas and Largo⁶⁴ at the CCSD(T)/cc-pVTZ level of theory ($9.1 \times 10^{-12} \text{ cm}^3\text{s}^{-1}$).

We do not find a direct reaction pathway on the singlet or triplet surface to $\text{CH}_3 + \text{N} \longrightarrow \text{HCN} + 2\text{H}$.

We display the mechanistic models for forming $\text{H}_2\text{CN} + \text{H}$, and $\text{HCN} + \text{H}_2$ from $\text{CH}_3 + \text{N}$ in Figure S4. These mechanistic models are similar to that used in Alves et al.¹⁴³. Note we do not analyze spin-forbidden processes in these models.

$\text{H}_2\text{CN} + \text{H}$ can form directly from ${}^3\text{H}_3\text{CN}$, or after isomerization from the intermediate ${}^3\text{H}_2\text{CNH}$. Similarly, $\text{HCN} + \text{H}_2$ can form directly from ${}^1\text{H}_3\text{CN}$, or from the intermediate ${}^1\text{H}_2\text{CNH}$. On the singlet surface, we find $\text{H}_2\text{CN} + \text{H}$ forms from the intermediate ${}^1\text{H}_2\text{CNH}$, however we do not find a pathway from ${}^1\text{H}_3\text{CN}$. We find a smooth decrease in Gibbs free energy along the MEP for the reaction ${}^1\text{H}_3\text{CN} \longrightarrow {}^1\text{H}_2\text{CNH}$, suggesting this reaction has neither an energy barrier nor an entropic barrier. We estimate the rate coefficient for this reaction by choosing the reactant geometry as the transition state. We find the overall rate coefficients for $\text{CH}_3 + \text{N} \longrightarrow \text{H}_2\text{CN} + \text{H}$ and $\text{CH}_3 + \text{N} \longrightarrow \text{H}_2\text{CN} + \text{H}$ to be insensitive to this intermediate rate coefficient by varying the latter's value by over 10 orders of magnitude in both directions. The optimization of ${}^1\text{H}_3\text{CN}$ does not converge, therefore we use a reactant geometry close to ${}^1\text{H}_3\text{CN}$ that has vibrational modes for $\text{HCN} + \text{H}_2$ and ${}^1\text{H}_2\text{CNH}$. In any case, we find the values of k_c and k_d are independent of the ${}^1\text{H}_3\text{CN}$ geometry.

The steady-state solution of the kinetic rate equations

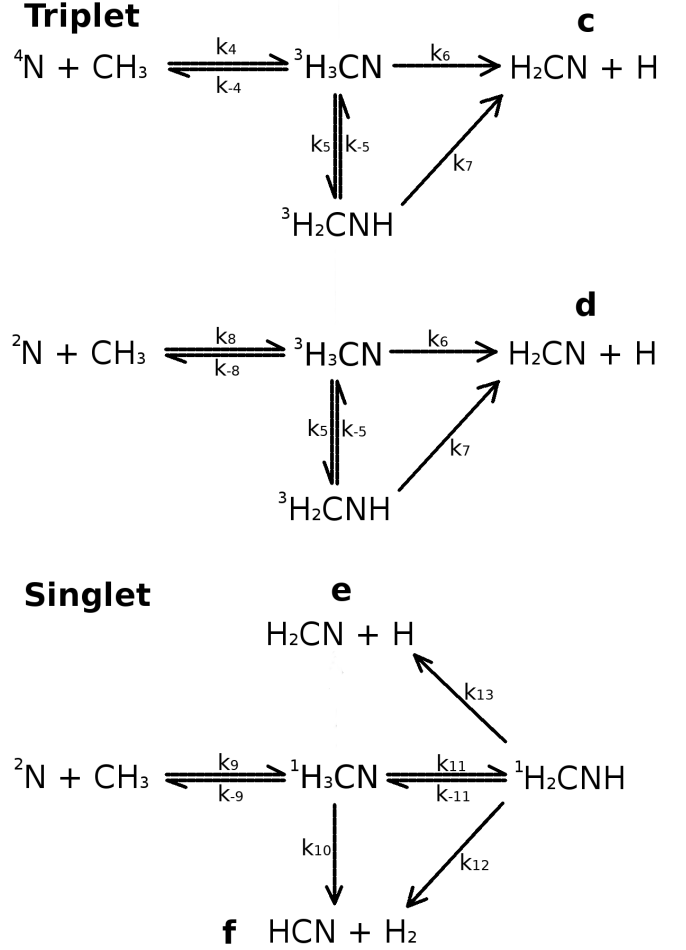


FIG. S4. Mechanistic models for the production of $\text{H}_2\text{CN} + \text{H}$ on the triplet surface from reactants (c) ${}^4\text{N} + \text{CH}_3$ and (d) ${}^2\text{N} + \text{CH}_3$, and production of (e) $\text{H}_2\text{CN} + \text{H}$ and (f) $\text{HCN} + \text{H}_2$ on the singlet surface, from $\text{CH}_3 + {}^2\text{N}$.

for the above mechanistic models give us the overall rate constants for c) $\text{CH}_3 + {}^4\text{N} \longrightarrow \text{H}_2\text{CN} + \text{H}$ and d) $\text{CH}_3 + {}^2\text{N} \longrightarrow \text{H}_2\text{CN} + \text{H}$ on the triplet surface, and e) $\text{CH}_3 + {}^2\text{N} \longrightarrow \text{H}_2\text{CN} + \text{H}$ and f) $\text{CH}_3 + {}^2\text{N} \longrightarrow \text{HCN} + \text{H}_2$ on the singlet surface.

$$k_c = \frac{k_4}{A} \left(k_6 + \frac{k_5 k_7}{k_{-5} + k_7} \right). \quad (\text{S3})$$

$$k_d = \frac{k_8}{B} \left(k_6 + \frac{k_5 k_7}{k_{-5} + k_7} \right). \quad (\text{S4})$$

$$k_e = \frac{k_9}{C} \left(\frac{k_{11} k_{13}}{k_{-11} + k_{12} + k_{13}} \right). \quad (\text{S5})$$

$$k_f = \frac{k_9}{C} \left(k_{10} + \frac{k_{11} k_{12}}{k_{-11} + k_{12} + k_{13}} \right). \quad (\text{S6})$$

$$A = k_{-4} + k_5 + k_6 - \frac{k_{-5}k_5}{k_{-5} + k_7}. \quad (\text{S7})$$

$$B = k_{-8} + k_5 + k_6 - \frac{k_{-5}k_5}{k_{-5} + k_7}. \quad (\text{S8})$$

$$C = k_{-9} + k_{10} + k_{11} - \frac{k_{-11}k_{11}}{k_{-11} + k_{12} + k_{13}}. \quad (\text{S9})$$

The values of the reaction rate constants using the BHandHLYP method and aug-cc-pVDZ basis set are listed in Table S5.

The rate coefficients of k_c , k_d , and k_e are equivalent to those of k_4 , k_8 , and k_9 , respectively. Thus the rate-limiting steps for these reactions are the first steps, i.e. $\text{CH}_3 + \text{N} \longrightarrow \text{H}_3\text{CN}$.

On the triplet surface, or theoretical value of k_c at the BHandHLYP/aug-cc-pVDZ level of theory is a factor of 1.5–2.5 smaller than the values calculated in experiments and suggested by thermodynamics^{28,63,87}.

On the singlet surface, there is a strong preference to produce $\text{H}_2\text{CN} + \text{H}$ over HCN . The rate coefficient of $\text{CH}_3 + {}^2\text{N} \longrightarrow \text{HCN} + \text{H}_2$ is less than $10^{-21} \text{ cm}^3\text{s}^{-1}$, therefore we do not include this reaction in our network.

Case Study 5: $\text{CH}_2 + \text{H} \longleftrightarrow \text{CH}_3 \cdot \longleftrightarrow \text{CH} + \text{H}_2$

There are three spin configurations for this reaction. ${}^3\text{CH}_2 + \text{H} \longrightarrow \text{CH}_3 \cdot \longrightarrow \text{CH} + \text{H}_2$ and ${}^1\text{CH}_2 + \text{H} \longrightarrow \text{CH}_3 \cdot \longrightarrow \text{CH} + \text{H}_2$ occur on the doublet PES, and ${}^3\text{CH}_2 + \text{H} \longrightarrow {}^4\text{CH} + \text{H}_2$ occurs on the quartet PES.

Several experiments have calculated the reaction rate coefficient for ${}^3\text{CH}_2 + \text{H} \longrightarrow \text{CH} + \text{H}_2$ at 285–300 K^{29–34}. Although methodology differs between experiments, they generally involve monitoring the decay of ${}^3\text{CH}_2$. The experimental values are as low as $8.3 \times 10^{-11} \text{ cm}^3\text{s}^{-1}$ and as high as $2.7 \times 10^{-10} \text{ cm}^3\text{s}^{-1}$. Two studies have reviewed a variety of experiments at a range of temperatures and suggested values of $2.7 \times 10^{-10} \text{ cm}^3\text{s}^{-1}$ ⁸⁶ and $2.0 \times 10^{-10} \text{ cm}^3\text{s}^{-1}$ ⁶².

Although no experiments have been performed for the reaction of ${}^1\text{CH}_2 + \text{H} \longrightarrow \text{CH} + \text{H}_2$, Tsang and Hampson⁸⁶ suggest the value should be near $5.0 \times 10^{-11} \text{ cm}^3\text{s}^{-1}$ based on thermodynamics.

To date there have been no published theoretical reaction rate coefficients for any spin configuration of this reaction.

On the quartet PES, we find the reaction proceeds directly ${}^3\text{CH}_2 + \text{H} \longrightarrow {}^4\text{CH} + \text{H}_2$. We calculate the rate coefficient for this reaction at the BHandHLYP/aug-cc-pVDZ level of theory to be $\sim 10^{-25} \text{ cm}^3\text{s}^{-1}$, which is too inefficient to consider in this network.

TABLE S5. Calculated overall rate coefficients for $\text{CH}_3 + {}^4\text{N} \longrightarrow \text{H}_2\text{CN} + \text{H}$ and $\text{CH}_3 + {}^2\text{N} \longrightarrow \text{H}_2\text{CN} + \text{H}$ on the triplet surface, and $\text{CH}_3 + {}^2\text{N} \longrightarrow \text{H}_2\text{CN} + \text{H}$ and $\text{CH}_3 + {}^2\text{N} \longrightarrow \text{HCN} + \text{H}_2$ on the singlet surface, as well as the intermediate forward and reverse rate coefficients which were used in the calculations. In all simulations, the BHandHLYP method was used with the aug-cc-pVDZ basis set. To reduce computational time, forward and reverse rate coefficients for k_5 , k_7 , and k_{12} were calculated with the transition state at the classical location (the saddle point) instead of the variational location. We find the overall rate coefficients k_c , k_d and k_e to be insensitive to changes in these intermediate coefficients of over 10 orders of magnitude. k_f is also insensitive to increases in k_{12} by over 10 orders of magnitude, however, decreasing k_{12} directly decreases k_f . Because we do not consider reactions with rate coefficients lower than $10^{-21} \text{ cm}^3\text{s}^{-1}$, we make no attempt to increase the accuracy of k_f . Experiments at 298 K provide a k_c value of 7.7×10^{-11} and a k_d value of $8.6 \times 10^{-12} \text{ cm}^3\text{s}^{-1}$ ^{28,63}. First-order rate coefficients have units s^{-1} . Second-order rate coefficients have units cm^3s^{-1} .

Rate coefficient	k(298)
k_c	3.3×10^{-11}
k_d	1.0×10^{-10}
k_e	3.1×10^{-11}
k_f	2.3×10^{-28}
k_4	3.3×10^{-11}
k_{-4}	1.3×10^{-32}
k_5	1.1×10^{-19}
k_{-5}	8.2×10^{-11}
k_6	3.0×10^{-12}
k_7	5.6×10^{-7}
k_8	1.0×10^{-10}
k_{-8}	3.0×10^{-51}
k_9	3.1×10^{-11}
k_{-9}	6.3×10^{-41}
k_{10}	1.5×10^{-14}
${}^a k_{11}$	1.9×10^{13}
k_{-11}	3.9×10^{-57}
k_{12}	2.0×10^{-56}
k_{13}	2.9×10^{-39}

^a No energy or entropic barrier. Transition state chosen at reactant geometry (${}^1\text{H}_3\text{CN}$).

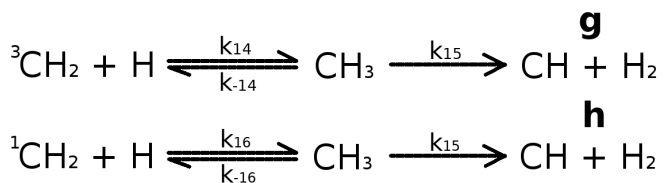


FIG. S5. Mechanistic models for the production of $\text{CH} + \text{H}_2$ from ${}^3\text{CH}_2 + \text{H}$ and ${}^1\text{CH}_2 + \text{H}$.

The doublet PES reactions proceed through the CH_3 intermediate. The mechanistic model for these reactions is shown in Figure S5.

Although there are many reaction pathways for the

TABLE S6. Calculated overall rate coefficient for ${}^3\text{CH}_2 + \text{H} \longrightarrow \text{CH} + \text{H}_2$, and ${}^1\text{CH}_2 + \text{H} \longrightarrow \text{CH} + \text{H}_2$, as well as the intermediate forward and reverse rate coefficients which were used in the calculations. In all simulations, the BHandHLYP method was used with the aug-cc-pVDZ basis set. Experiments at 298 K provide k_g values between 8.3×10^{-11} and $2.7 \times 10^{-10} \text{ cm}^3 \text{s}^{-1}$ ²⁹⁻³⁴. A value of $5.0 \times 10^{-11} \text{ s}^{-1}$ is suggested for k_h ⁸⁶. First-order rate coefficients have units s^{-1} . Second-order rate coefficients have units $\text{cm}^3 \text{s}^{-1}$.

Rate coefficient	$k(298)$
k_g	4.3×10^{-10}
k_h	8.4×10^{-11}
k_{14}	5.6×10^{-10}
k_{-14}	3.7×10^{-58}
k_{15}	1.2×10^{-57}
k_{16}	8.4×10^{-11}
k_{-16}	9.5×10^{-68}

CH_3 molecule, we calculate the upper bound for the rate constants of ${}^3\text{CH}_2 + \text{H} \longrightarrow \text{CH}_3 \cdot \longrightarrow \text{CH} + \text{H}_2$ and ${}^1\text{CH}_2 + \text{H} \longrightarrow \text{CH}_3 \cdot \longrightarrow \text{CH} + \text{H}_2$ by assuming all CH_3 reacts to form $\text{CH} + \text{H}_2$.

The steady-state solutions of the kinetic rate equations for these mechanistic models give us the overall rate constants for ${}^3\text{CH}_2 + \text{H} \longrightarrow \text{CH} + \text{H}_2$ and ${}^1\text{CH}_2 + \text{H} \longrightarrow \text{CH} + \text{H}_2$.

$$k_g = \frac{k_{15}k_{14}}{k_{-14} + k_{15}} \quad (\text{S10})$$

$$k_h = \frac{k_{15}k_{16}}{k_{-16} + k_{15}} \quad (\text{S11})$$

The values of the reaction rate constants using the BHandHLYP method and aug-cc-pVDZ basis set are listed in Table S6.

The theoretical value of k_h is equal to the value of k_{16} . Thus the first step is the rate-limiting step. The theoretical value of k_g is nearly the same as the value of k_{14} , however because the reverse rate coefficient (k_{-14}) is comparable to the rate coefficient of the second step (k_{15}), the value of k_g is slightly smaller than that of k_{11} . We calculate k_g to be $4.3 \times 10^{-10} \text{ cm}^3 \text{s}^{-1}$, which is within the range of experimental values for ${}^3\text{CH}_2 + \text{H} \longrightarrow \text{CH} + \text{H}_2$. We calculate k_h to be $8.4 \times 10^{-11} \text{ cm}^3 \text{s}^{-1}$, which is less than a factor of 2 larger than the suggested value by Tsang and Hampson⁸⁶. Our calculations show $\text{CH}_3 \longrightarrow \text{CH} + \text{H}_2$ is inefficient ($k_{15} = \sim 10^{-57} \text{ s}^{-1}$), therefore we do not consider the second step of this reaction in our study.

The same mechanistic approach can be used for the reverse reaction $\text{CH} + \text{H}_2 \longrightarrow \text{CH}_3 \cdot \longrightarrow {}^3\text{CH}_2 + \text{H}$. This reaction could produce ${}^1\text{CH}_2 + \text{H}$ as well, however

k_{-14} is ~ 10 orders of magnitude larger than k_{-16} , suggesting the dominant pathway would be to produce ${}^3\text{CH}_2 + \text{H}$.

Several experiments have calculated the rate coefficient of $\text{CH} + \text{H}_2 \longrightarrow \text{products}$ by monitoring the decay of CH in the presence of H_2 ^{32,35,105-107,109-111}. Becker et al.³⁵ find that 300 K is the threshold temperature, below which the CH_3 product is mainly formed, and above which the ${}^3\text{CH}_2 + \text{H}$ products are mainly formed. Zabarnick et al.³² also suggest CH_3 is the main product below temperatures of 300 K, and recommend a temperature of > 400 K for the formation of $\text{CH}_2 + \text{H}$.

Rate coefficients for the reaction of $\text{CH} + \text{H}_2 \longrightarrow \text{CH}_3$ range from 1.0×10^{-12} to $1.6 \times 10^{-10} \text{ cm}^3 \text{s}^{-1}$.

Mayneris et al.¹⁶⁰ used the quasiclassical trajectory method to calculate the theoretical rate coefficient of $\text{CH} + \text{H}_2 \longrightarrow \text{CH}_3 \cdot \longrightarrow {}^3\text{CH}_2 + \text{H}$. They calculated a value of $3.5 \times 10^{-11} \text{ cm}^3 \text{s}^{-1}$.

We find the first step of the reverse reaction to be the rate-limiting step, i.e. $\text{CH} + \text{H}_2 \longrightarrow \text{CH}_3$. We calculate the rate coefficient of the reverse reaction to be $7.9 \times 10^{-11} \text{ cm}^3 \text{s}^{-1}$. This is within the range of experimental values.

We find the second step of the reverse reaction ($\text{CH}_3 \longrightarrow \text{CH}_2 + \text{H}$) to be too inefficient to consider in this network (i.e. $k < 10^{-21} \text{ s}^{-1}$).

Case Study 6: $\text{CH}_2 + \text{H}_2 \longrightarrow \text{CH}_3 + \text{H}$

This reaction occurs on the singlet and triplet surfaces, as ${}^1\text{CH}_2 + \text{H}_2 \longrightarrow \text{CH}_4 \cdot \longrightarrow \text{CH}_3 + \text{H}$ and ${}^3\text{CH}_2 + \text{H}_2 \longrightarrow \text{CH}_3 + \text{H}$, respectively.

Experiments have measured the rate of ${}^1\text{CH}_2$ decay or CH_3 production to calculate the rate coefficient of ${}^1\text{CH}_2 + \text{H}_2 \longrightarrow \text{CH}_4 \cdot \longrightarrow \text{CH}_3 + \text{H}$ at 295-298 K³⁶⁻³⁸. These values range from 7.0×10^{-12} to $1.3 \times 10^{-10} \text{ cm}^3 \text{s}^{-1}$. Studies reviewing these experiments suggest a rate coefficient of $1.2 \times 10^{-10} \text{ cm}^3 \text{s}^{-1}$ ^{162,86}.

We find no theoretical rate coefficients for the ${}^1\text{CH}_2 + \text{H}_2 \longrightarrow \text{CH}_4 \cdot \longrightarrow \text{CH}_3 + \text{H}$ reaction.

We find the first step to be the rate-limiting step in the reaction ${}^1\text{CH}_2 + \text{H}_2 \longrightarrow \text{CH}_4 \cdot \longrightarrow \text{CH}_3 + \text{H}$. We calculate the rate coefficient to be $1.0 \times 10^{-11} \text{ cm}^3 \text{s}^{-1}$, which is within the range of experimental values. Because CH_4 is a stable product in our reaction network, we only include the first step of this reaction in our network. The second step, $\text{CH}_4 \longrightarrow \text{CH}_3 + \text{H}$, is very inefficient ($k \sim 10^{-60} \text{ s}^{-1}$) and we do not include it in our network.

Although no experiments have directly measured the rate coefficient of ${}^3\text{CH}_2 + \text{H}_2 \longrightarrow \text{CH}_3 + \text{H}$, a few models have placed an upper bound on its value by considering the affect of various gases on the ${}^3\text{CH}_2$ molecule. These upper bounds range from 5.0×10^{-15} to $5.0 \times 10^{-14} \text{ cm}^3 \text{s}^{-1}$.

Lu et al.¹⁵⁸ calculated the theoretical rate coefficient of ${}^3\text{CH}_2 + \text{H}_2 \longrightarrow \text{CH}_3 + \text{H}$ using transition state theory.

TABLE S7. Calculated rate coefficients for $\text{CH}_2 + \text{N} \longrightarrow \text{H}_2\text{CN}$, and $\text{H}_2\text{CN} \longrightarrow \text{HCN} + \text{H}$ on the doublet and quartet potential energy surfaces. In all simulations, the BHandHLYP method was used with the aug-cc-pVDZ basis set. First-order rate coefficients have units s^{-1} . Second-order rate coefficients have units cm^3s^{-1} .

Reaction	k(298) doublet	k(298) quartet
$^1\text{CH}_2 + ^2\text{N} \longrightarrow \text{H}_2\text{CN}$	1.5×10^{-10}	
$^1\text{CH}_2 + ^4\text{N} \longrightarrow \text{H}_2\text{CN}$		1.1×10^{-10}
$^3\text{CH}_2 + ^4\text{N} \longrightarrow \text{H}_2\text{CN}$	1.3×10^{-10}	
$^3\text{CH}_2 + ^2\text{N} \longrightarrow \text{H}_2\text{CN}$	2.7×10^{-10}	4.3×10^{-10}
$\text{H}_2\text{CN} \longrightarrow \text{HCN} + \text{H}$	1.6×10^{-11}	4.6×10^{-24}

They employed the G2M(RCC2) computational method with B3LYP optimized geometries and obtained a value of $1.5 \times 10^{-18} \text{cm}^3\text{s}^{-1}$.

We calculate the rate coefficient of $^3\text{CH}_2 + \text{H}_2 \longrightarrow \text{CH}_3 + \text{H}$ to be $2.5 \times 10^{-16} \text{cm}^3\text{s}^{-1}$. This value agrees with the upper bounds for the rate coefficient from experiments.

We find the reverse rate coefficient, $\text{CH}_3 + \text{H} \longrightarrow ^3\text{CH}_2 + \text{H}_2$ to have a value of $1.4 \times 10^{-20} \text{cm}^3\text{s}^{-1}$. We include this reverse reaction in our network as its rate coefficient is within the threshold of what we define to be a fast reaction (i.e. $k > 10^{-21} \text{cm}^3\text{s}^{-1}$).

Case Study 7: $\text{CH}_2 + \text{N} \longrightarrow \text{HCN} + \text{H}$

Catling and Kasting⁷ suggest $\text{CH}_2 + \text{N} \longrightarrow \text{HCN} + \text{H}$ is one of the main pathways forming HCN in the early atmosphere. They note however that the rate constant for this reaction has not yet been studied experimentally.

Herbst et al.¹⁵⁹ performed quantum dynamics simulations to calculate the rate coefficient of $^3\text{CH}_2 + ^4\text{N} \longrightarrow \text{H}_2\text{CN} \cdot \longrightarrow \text{HCN} + \text{H}$. They calculated a value of $7.9 \times 10^{-11} \text{cm}^3\text{s}^{-1}$.

We find no direct reaction pathway for $\text{CH}_2 + \text{N} \longrightarrow \text{HCN} + \text{H}$ on the doublet, quartet, or sextet PES's. We do however find two-step reactions $\text{CH}_2 + \text{N} \longrightarrow \text{H}_2\text{CN}$ and $\text{H}_2\text{CN} \longrightarrow \text{HCN} + \text{H}$ on the doublet and quartet surfaces.

We list the calculated reaction rate coefficients on the doublet and quartet energy surfaces in Table S7.

All spin configurations of $\text{CH}_2 + \text{N} \longrightarrow \text{H}_2\text{CN}$ are barrierless and have efficient reaction rate coefficients. $\text{H}_2\text{CN} \longrightarrow \text{HCN} + \text{H}$, however, is only efficient on the doublet surface. We distinguish between the quartet and doublet H_2CN molecules in our network, as the deexcitation of $^4\text{H}_2\text{CN}$ to $^2\text{H}_2\text{CN}$ is spin-forbidden, and we can't assume $^4\text{H}_2\text{CN}$ will efficiently decay into its ground state in an atmosphere.

Our calculated rate coefficient for $^3\text{CH}_2 + ^4\text{N} \longrightarrow \text{H}_2\text{CN}$ is approximately a factor of 1.5 greater than the

previous theoretical value¹⁵⁹.

We include all five $\text{CH}_2 + \text{N} \longrightarrow \text{H}_2\text{CN}$ reaction spin configurations as well as the efficient doublet $\text{H}_2\text{CN} \longrightarrow \text{HCN} + \text{H}$ reaction in our network.

Case Study 8: $2\text{CH}_2 \longrightarrow \text{C}_2\text{H}_4 \cdot \longrightarrow \text{products}$

There are three spin configurations for this reaction on a total of two PES's. On the singlet surface, there is $^3\text{CH}_2 + ^3\text{CH}_2 \longrightarrow ^1\text{C}_2\text{H}_4 \cdot \longrightarrow \text{C}_2\text{H}_3 \cdot + \text{H} \cdot \longrightarrow \text{C}_2\text{H}_2 + 2\text{H}$ and $^1\text{CH}_2 + ^1\text{CH}_2 \longrightarrow ^1\text{C}_2\text{H}_4 \cdot \longrightarrow \text{products}$, and on the triplet PES there is $^3\text{CH}_2 + ^1\text{CH}_2 \longrightarrow ^3\text{C}_2\text{H}_4 \cdot \longrightarrow \text{products}$.

Braun et al.³⁶ monitored the decay of $^3\text{CH}_2$ and the production of C_2H_2 in experiments to measure the rate coefficient of $^3\text{CH}_2 + ^3\text{CH}_2 \longrightarrow \text{C}_2\text{H}_2 + \text{product}$ at 298 K. This measurement was $5.3 \times 10^{-11} \text{cm}^3\text{s}^{-1}$. Braun et al.³⁶ assumed that molecular hydrogen was produced along with C_2H_2 in this reaction, however Becerra et al.¹⁷¹ modeled the reaction network starting from the decomposition of ketene and found that $^3\text{CH}_2 + ^3\text{CH}_2 \longrightarrow \text{C}_2\text{H}_2 + 2\text{H}$ was more likely. Becerra et al.¹⁷¹ found that $^3\text{CH}_2 + \text{H} \longrightarrow \text{CH} + \text{H}_2$ can account for the molecular hydrogen observed in reactions of this kind.

Braun et al.³⁶ suggest that the reaction of $^3\text{CH}_2$ with $^3\text{CH}_2$ passes through the C_2H_4 intermediate.

Jasper et al.⁵⁹ calculate the theoretical rate coefficient for $^3\text{CH}_2 + ^3\text{CH}_2 \longrightarrow \text{C}_2\text{H}_4 \cdot \longrightarrow \text{C}_2\text{H}_2 + 2\text{H}$ using variable reaction coordinate transition state theory. Their value is $1.5 \times 10^{-10} \text{cm}^3\text{s}^{-1}$.

There is no experimental data for $^1\text{CH}_2 + ^1\text{CH}_2 \longrightarrow \text{C}_2\text{H}_4 \cdot \longrightarrow \text{products}$, however it is expected to proceed rapidly, and yield the same products as $^3\text{CH}_2 + ^3\text{CH}_2 \longrightarrow \text{C}_2\text{H}_4 \cdot \longrightarrow \text{C}_2\text{H}_2 + 2\text{H}$ ⁸⁶. Tsang and Hampson⁸⁶ recommend a value of $5.0 \times 10^{-11} \text{cm}^3\text{s}^{-1}$ for this reactions.

Similarly, there is no experimental data for $^3\text{CH}_2 + ^1\text{CH}_2 \longrightarrow ^3\text{C}_2\text{H}_4 \cdot \longrightarrow \text{products}$, however it is also expected to be rapid. Conversely, it is suggested that the preferred products for this reaction are $^3\text{CH}_2 + ^1\text{CH}_2 \longrightarrow ^3\text{C}_2\text{H}_4 \cdot \longrightarrow ^3\text{C}_2\text{H}_2 + \text{H}_2$. Tsang and Hampson⁸⁶ suggest a value of $3.0 \times 10^{-11} \text{cm}^3\text{s}^{-1}$ for this reaction.

To our knowledge there have been no theoretical reaction rate coefficients for $^1\text{CH}_2 + ^1\text{CH}_2 \longrightarrow \text{C}_2\text{H}_2 + 2\text{H}$, or $^1\text{CH}_2 + ^3\text{CH}_2 \longrightarrow ^3\text{C}_2\text{H}_2 + \text{H}_2$ published to date.

Because in some of the other reactions in our network, C_2H_4 is a stable product, i.e. $\text{CH} + \text{CH}_4 \longrightarrow \text{C}_2\text{H}_5 \cdot \longrightarrow \text{C}_2\text{H}_4 + \text{H}$, $\text{CH}_2 + \text{CH}_3 \longrightarrow \text{C}_2\text{H}_5 \cdot \longrightarrow \text{C}_2\text{H}_4 + \text{H}$, we only include the first steps of these reactions in our network (i.e. $2\text{CH}_2 \longrightarrow \text{C}_2\text{H}_4$). We find the first steps of reactions $^3\text{CH}_2 + ^3\text{CH}_2 \longrightarrow \text{C}_2\text{H}_4 \cdot \longrightarrow \text{C}_2\text{H}_2 + 2\text{H}$ and $^1\text{CH}_2 + ^1\text{CH}_2 \longrightarrow \text{C}_2\text{H}_4 \cdot \longrightarrow \text{C}_2\text{H}_2 + 2\text{H}$ to be the rate-limiting

TABLE S8. Calculated rate coefficients for $2\text{CH}_2 \rightarrow \text{C}_2\text{H}_4$ on the singlet and triplet potential energy surfaces. These rate coefficients are compared with the experimental rate coefficient of the multi-step reaction ${}^3\text{CH}_2 + {}^3\text{CH}_2 \rightarrow \text{C}_2\text{H}_4 \cdot \rightarrow \text{C}_2\text{H}_2 + 2\text{H}$ as well as the suggested rate coefficients for ${}^1\text{CH}_2 + {}^1\text{CH}_2 \rightarrow \text{C}_2\text{H}_4 \cdot \rightarrow \text{C}_2\text{H}_2 + 2\text{H}$, and ${}^1\text{CH}_2 + {}^3\text{CH}_2 \rightarrow {}^3\text{C}_2\text{H}_4 \cdot \rightarrow \text{products}$ in the literature. We find the first steps of the reactions of ${}^3, {}^1\text{CH}_2 + {}^3, {}^1\text{CH}_2 \rightarrow \text{C}_2\text{H}_4 \cdot \rightarrow \text{C}_2\text{H}_2 + 2\text{H}$ to be the rate-limiting steps and assume the same for ${}^1\text{CH}_2 + {}^3\text{CH}_2 \rightarrow {}^3\text{C}_2\text{H}_4 \cdot \rightarrow \text{products}$. In all simulations, the BHandHLYP method was used with the aug-cc-pVDZ basis set. Rate coefficients have units cm^3s^{-1} .

	${}^3\text{CH}_2 + {}^3\text{CH}_2$	${}^1\text{CH}_2 + {}^1\text{CH}_2$	${}^1\text{CH}_2 + {}^3\text{CH}_2$
$k_{\text{calc}}(298)$	4.2×10^{-11}	9.9×10^{-12}	${}^a 3.5 \times 10^{-11}$
$k_{\text{lit}}(298)$	5.3×10^{-11}	5.0×10^{-11}	3.0×10^{-11}

^a Simulations did not converge beyond a C-C bond distance of 3.52 Å. Therefore the calculated rate coefficient is a lower bound.

steps, and assume the same for ${}^1\text{CH}_2 + {}^3\text{CH}_2 \rightarrow {}^3\text{C}_2\text{H}_4 \rightarrow \text{products}$.

We list the calculated reaction rate coefficients on the singlet and triplet energy surfaces in Table S8.

Our calculated $k(298)$ value for ${}^3\text{CH}_2 + {}^3\text{CH}_2 \rightarrow \text{C}_2\text{H}_4$ is within 30% of the experimental value for ${}^3\text{CH}_2 + {}^3\text{CH}_2 \rightarrow \text{C}_2\text{H}_2 + 2\text{H}$. The $k(298)$ value for ${}^1\text{CH}_2 + {}^1\text{CH}_2 \rightarrow \text{C}_2\text{H}_4$ is a factor of 5 smaller than the suggested value. Simulations did not converge for ${}^1\text{CH}_2 + {}^3\text{CH}_2 \rightarrow {}^3\text{C}_2\text{H}_4$ beyond a C-C reaction coordinate of 3.52 Å, however using this location for the variational transition state leads to a calculated rate coefficient that is within 20% of the suggested value.

Case Study 9: $\text{CH}_2 + \text{CH}_3 \rightarrow \text{C}_2\text{H}_5 \cdot \rightarrow \text{C}_2\text{H}_4 + \text{H}$

This is a two step reaction, passing through the C_2H_5 intermediate^{86,102,103}. On the doublet surface, both ${}^3\text{CH}_2$ and ${}^1\text{CH}_2$ can react with CH_3 to produce the C_2H_5 intermediate. On the quartet surface, ${}^3\text{CH}_2$ reacts with CH_3 to produce excited ${}^4\text{C}_2\text{H}_5$. However this reaction is higher in energy than the doublet reactions, and has a very slow rate coefficient ($\sim 10^{-57} \text{ cm}^3\text{s}^{-1}$).

Pilling and Robertson¹⁰³ and Laufer and Bass¹⁰² experimentally measured the production of various products (e.g. C_2H_2 , C_2H_4 , C_2H_6) to model the reaction network spanned by reactions between ${}^3\text{CH}_2$ and CH_3 . Their models led to reaction rate coefficients of 5.0×10^{-11} and $1.0 \times 10^{-10} \text{ cm}^3\text{s}^{-1}$, respectively. Wang and Fockenberg⁹⁶ performed similar experiments but used the ${}^3\text{CH}_2$ decay profile for their calculation, and obtained a rate of $2.1 \times 10^{-10} \text{ cm}^3\text{s}^{-1}$ at 300 K. Deters et al.¹⁰¹ measured the decay of both ${}^3\text{CH}_2$ and CH_3 in a similar experiment to obtain a rate coefficient

of $1.1 \times 10^{-10} \text{ cm}^3\text{s}^{-1}$ at 298 K. Baulch et al.⁶² and Tsang and Hampson⁸⁶ reviewed various experiments and suggest a value of $7.0 \times 10^{-11} \text{ cm}^3\text{s}^{-1}$ for the ${}^3\text{CH}_2 + \text{CH}_3 \rightarrow \text{C}_2\text{H}_5 \cdot \rightarrow \text{C}_2\text{H}_4 + \text{H}$ rate coefficient.

Conversely, there is no experimental data for ${}^1\text{CH}_2 + \text{CH}_3 \rightarrow \text{C}_2\text{H}_5 \cdot \rightarrow \text{C}_2\text{H}_4 + \text{H}$, however the reaction is thought to proceed rapidly and suggested to have a rate coefficient near $3.0 \times 10^{-11} \text{ cm}^3\text{s}^{-1}$ ⁸⁶.

There have been no published theoretical reaction rate coefficients for $\text{CH}_2 + \text{CH}_3 \rightarrow \text{C}_2\text{H}_4 + \text{H}$.

We find the first steps of these reactions, ${}^3\text{CH}_2 + \text{CH}_3 \rightarrow \text{C}_2\text{H}_5$ and ${}^1\text{CH}_2 + \text{CH}_3 \rightarrow \text{C}_2\text{H}_5$, do not have barriers. The second step however ($\text{C}_2\text{H}_5 \rightarrow \text{C}_2\text{H}_4 + \text{H}$), has a barrier. The mechanistic model for the reaction, involving the triplet and singlet CH_2 molecule, is shown in Figure S6.

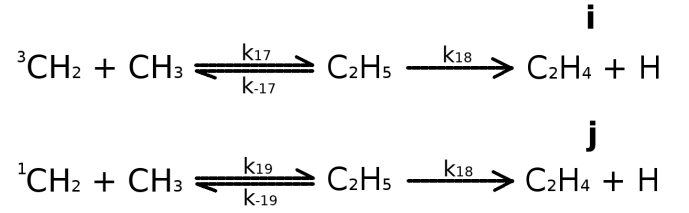


FIG. S6. Mechanistic model for the production of $\text{C}_2\text{H}_4 + \text{H}$ from i) ${}^3\text{CH}_2 + \text{CH}_3$ and j) ${}^1\text{CH}_2 + \text{CH}_3$ on the doublet surface.

We calculate the upper bounds for the rate constants by assuming all C_2H_5 reacts to form $\text{C}_2\text{H}_4 + \text{H}$.

The steady-state solutions of the kinetic rate equations for this mechanistic model gives us the overall rate constant for $\text{CH}_2 + \text{CH}_3 \rightarrow \text{C}_2\text{H}_4 + \text{H}$.

$$k_i = \frac{k_{18}k_{17}}{k_{-17} + k_{18}} \quad (\text{S12})$$

$$k_j = \frac{k_{18}k_{19}}{k_{-19} + k_{18}} \quad (\text{S13})$$

We list the calculated reaction rate coefficients for this mechanistic model in Table S9.

The theoretical values of k_i and k_j are equal to the values of k_{17} and k_{19} , respectively. Thus the first steps of these reactions are the rate-limiting steps. At the BHandHLYP/aug-cc-pVDZ level of theory, we calculate k_i to be $8.8 \times 10^{-12} \text{ cm}^3\text{s}^{-1}$. This value is approximately a factor of 6 slower than the slowest experimental value. Similarly, we calculate k_j to be $2.3 \times 10^{-11} \text{ cm}^3\text{s}^{-1}$, which is within order unity of the suggested value.

Case Study 10: $\text{CH}_2 + \text{CH}_4 \rightarrow 2\text{CH}_3$

This reaction occurs on the singlet PES as ${}^1\text{CH}_2 + \text{CH}_4 \rightarrow \text{C}_2\text{H}_6 \cdot \rightarrow 2\text{CH}_3$. and on the triplet PES

TABLE S9. Calculated overall rate coefficient for ${}^3\text{CH}_2 + \text{CH}_3 \longrightarrow \text{C}_2\text{H}_4 + \text{H}$ and ${}^1\text{CH}_2 + \text{CH}_3 \longrightarrow \text{C}_2\text{H}_4 + \text{H}$, as well as the intermediate forward and reverse rate coefficients which were used in the calculation. In all simulations, the BHandHLYP method was used with the aug-cc-pVDZ basis set. Experiments at 298 K provide a k_i value in the range of 5.0×10^{-11} to $2.1 \times 10^{-10} \text{ cm}^3 \text{ s}^{-196,102,103}$. k_j is suggested to have a rate coefficient near $3.0 \times 10^{-11} \text{ cm}^3 \text{ s}^{-186}$. First-order rate coefficients have units s^{-1} . Second-order rate coefficients have units $\text{cm}^3 \text{ s}^{-1}$.

Rate coefficient	$k(298)$
k_i	8.8×10^{-12}
k_j	2.3×10^{-11}
k_{17}	8.8×10^{-12}
k_{-17}	1.4×10^{-48}
k_{18}	4.0×10^{-15}
k_{19}	2.3×10^{-11}
k_{-19}	3.0×10^{-57}

as ${}^3\text{CH}_2 + \text{CH}_4 \longrightarrow 2 \text{CH}_3$.

Experimentalists have measured the rate coefficient of ${}^1\text{CH}_2 + \text{CH}_4 \longrightarrow \text{C}_2\text{H}_6 \cdot \longrightarrow 2 \text{CH}_3$ at 295–298 K by measuring the decay of ${}^1\text{CH}_2$ or the production of CH_3 . These values range from 1.9×10^{-12} to $7.3 \times 10^{-11} \text{ cm}^3 \text{ s}^{-136-38}$. Tsang and Hampson⁸⁶ reviewed these experiments and suggested a value of $7.1 \times 10^{-11} \text{ cm}^3 \text{ s}^{-1}$. We find no published theoretical rate coefficients for this reaction.

We find the reaction on the singlet PES proceeds through the C_2H_6 intermediate and that the first step of this reaction is the rate-limiting step. We calculate its rate coefficient to be $6.1 \times 10^{-13} \text{ cm}^3 \text{ s}^{-1}$, which is a factor of 3 smaller than the closest experimental value. Because C_2H_6 is a stable product in other reactions in our network (e.g. $2 \text{CH}_3 \longrightarrow \text{C}_2\text{H}_6$), we only consider the first step of this reaction in our network. The second step of this reaction $\text{C}_2\text{H}_6 \longrightarrow 2 \text{CH}_3$ is too slow to consider in this network ($k \sim 10^{-55} \text{ s}^{-1}$).

Böhland et al.¹⁰⁴ performed experiments on the reaction of ${}^3\text{CH}_2$ with n-hexane at $T = 413\text{--}707 \text{ K}$ to estimate the rate coefficient for ${}^3\text{CH}_2 + \text{CH}_4 \longrightarrow 2 \text{CH}_3$ at 298 K. They calculated a value of $3.1 \times 10^{-19} \text{ cm}^3 \text{ s}^{-1}$. Braun et al.³⁶ placed an upper bound on the rate coefficient by considering the affect of various gases on the ${}^3\text{CH}_2$ molecule. They estimate a value of $< 3.1 \times 10^{-14} \text{ cm}^3 \text{ s}^{-1}$. Tsang and Hampson⁸⁶ suggest an upper bound of $3.0 \times 10^{-19} \text{ cm}^3 \text{ s}^{-1}$ based on the results of a photolysis study of the $\text{CH}_2\text{CO-CH}_4$ system. We find no theoretical rate coefficients for the ${}^3\text{CH}_2 + \text{CH}_4 \longrightarrow 2 \text{CH}_3$ reaction.

We calculate ${}^3\text{CH}_2 + \text{CH}_4 \longrightarrow 2 \text{CH}_3$ to have a rate coefficient of $1.4 \times 10^{-16} \text{ cm}^3 \text{ s}^{-1}$. This value agrees with the upper bound from Braun et al.³⁶, and is a couple orders of magnitude higher than the experimental value from Böhland et al.¹⁰⁴.

Case Study 11: $\text{CH} + \text{N} \longrightarrow \text{HCN} \longrightarrow \text{CN} + \text{H}$

There are two spin configurations for this reaction on the triplet surface, which pass through the excited ${}^3\text{HCN}$ intermediate: $\text{CH} + {}^4\text{N} \longrightarrow {}^3\text{HCN} \longrightarrow \text{CN} + \text{H}$ and $\text{CH} + {}^2\text{N} \longrightarrow {}^3\text{HCN} \longrightarrow \text{CN} + \text{H}$. There is also potentially a reaction of $\text{CH} + {}^2\text{N}$ on the singlet surface to produce ground state HCN, however we were unable to obtain a convergent solution for such a reaction. Moreover, there is no experimental or past theoretical work for a singlet surface reaction of $\text{CH} + {}^2\text{N}$ to suggest it occurs efficiently. For these reasons, we only consider the two spin configurations on the triplet surface in this network.

A few experiments have measured the rate coefficient of $\text{CH} + {}^4\text{N} \longrightarrow \text{CN} + \text{H}$ at 296–298 K by monitoring the decay of CH and/or the production of CN^{60,112,113}. The experimental values of the rate coefficient range from 2.1×10^{-11} to $1.6 \times 10^{-10} \text{ cm}^3 \text{ s}^{-1}$.

Daranlot et al.⁶⁰ performed quantum dynamics calculations to obtain a theoretical rate coefficient for $\text{CH} + {}^4\text{N} \longrightarrow {}^3\text{HCN} \longrightarrow \text{CN} + \text{H}$. They calculate a value of $k(298) = 1.2 \times 10^{-10} \text{ cm}^3 \text{ s}^{-1}$.

We find no experimental or theoretical rate coefficients for $\text{CH} + {}^2\text{N} \longrightarrow {}^3\text{HCN} \longrightarrow \text{CN} + \text{H}$.

Our theoretical calculations show both $\text{CH} + {}^4\text{N}$ and $\text{CH} + {}^2\text{N}$ react without a barrier to form the ${}^3\text{HCN}$ intermediate. We find the first step for both of these reactions to be the rate-limiting steps. The second step of this reaction, i.e., the decay of ${}^3\text{HCN}$ into $\text{CN} + \text{H}$, is extremely efficient ($k = 3.6 \times 10^9 \text{ s}^{-1}$).

We calculate the rate coefficient for $\text{CH} + {}^4\text{N} \longrightarrow {}^3\text{HCN} \longrightarrow \text{CN} + \text{H}$ to be $1.1 \times 10^{-10} \text{ cm}^3 \text{ s}^{-1}$. This value is within the range of experimental values, and agrees well with the previous calculated theoretical value⁶⁰.

We calculate the rate coefficient for $\text{CH} + {}^2\text{N} \longrightarrow {}^3\text{HCN} \longrightarrow \text{CN} + \text{H}$ to be $2.7 \times 10^{-10} \text{ cm}^3 \text{ s}^{-1}$.

Case Study 12: $\text{CH} + \text{CH}_4 \longrightarrow \text{C}_2\text{H}_5 \cdot \longrightarrow \text{C}_2\text{H}_4 + \text{H}$

This reaction occurs on the doublet surface. Several experiments have calculated the rate coefficient for this reaction at 295–298 K by monitoring the production of C_2H_4 or the decay of CH^{109–111,114–119}. The experimental rate coefficient ranges from 2.0×10^{-12} to $3.0 \times 10^{-10} \text{ cm}^3 \text{ s}^{-1}$.

A pair of theoretical studies have been performed on this reaction, however theoretical rate coefficients were not calculated^{172,173}.

At the BHandHLYP/aug-cc-pVDZ level of theory, we find this reaction to have a small barrier ($E_0 = 11.5 \text{ kJ mol}^{-1}$). This is smaller than the barrier predicted by Yu et al.¹⁷² ($E_0 = 57.3 \text{ kJ mol}^{-1}$), who used the Moller-Plesset perturbation theory (MP) method with geometries optimized using the Hartree-Fock method. However, Wang et al.¹⁷³ calculated the reaction to be barri-

erless (-1.3 kJ mol^{-1}) using the MP method with MP optimized geometries. Experiments suggests the reaction is barrierless, with an activation energy of -1.7 kJ mol^{-1} ¹¹⁶. At the B3LYP/aug-cc-pVDZ level of theory, we find this reaction to be barrierless, with an activation energy of $-18.2 \text{ kJ mol}^{-1}$. Because experiment predicts this reaction to be barrierless^{116,117,119}, and the existence of the theoretical barrier is dependent on the computational method, we artificially remove the barrier from our calculation of the rate coefficient at the BHandHLYP/aug-cc-pVDZ level of theory.

We find the first step of this reaction $\text{CH} + \text{CH}_4 \longrightarrow \text{C}_2\text{H}_5$ to be the rate-limiting step, with a barrierless rate coefficient of $3.8 \times 10^{-13} \text{ cm}^3\text{s}^{-1}$. This is a factor of 5 slower than the nearest experimental value. We calculate the rate coefficient of second step of this reaction $\text{C}_2\text{H}_5 \longrightarrow \text{C}_2\text{H}_4 + \text{H}$ to be $1.8 \times 10^{-11} \text{ s}^{-1}$, suggesting the C_2H_5 intermediate is fairly unstable. Thus we include this two-step reaction in our network as a single step $\text{CH} + \text{CH}_4 \longrightarrow \text{C}_2\text{H}_4 + \text{H}$.

Case Study 13: $\text{NH} + \text{H} \longleftrightarrow \text{N} + \text{H}_2$

This reaction has two spin configurations on the doublet PES, $^1\text{NH} + \text{H} \longrightarrow ^2\text{N} + \text{H}_2$ and $^3\text{NH} + \text{H} \longrightarrow ^2\text{N} + \text{H}_2$, and one spin configuration on the quartet PES, $^3\text{NH} + \text{H} \longrightarrow ^4\text{N} + \text{H}_2$.

Adam et al.¹²⁰ calculated the experimental rate coefficient of $^3\text{NH} + \text{H} \longrightarrow ^4\text{N} + \text{H}_2$ at 298 K by monitoring the decay of ^3NH . They found the rate coefficient to have a value of $3.2 \times 10^{-12} \text{ cm}^3\text{s}^{-1}$.

Adam et al.¹²⁰ also used the classical trajectory method to calculate the theoretical rate coefficient for $^3\text{NH} + \text{H} \longrightarrow ^4\text{N} + \text{H}_2$ at the MRCI/aug-cc-pVQZ level of theory. They found this reaction proceeds directly, rather than through the NH_3 intermediate. They calculated the rate coefficient to be $1.5 \times 10^{-12} \text{ cm}^3\text{s}^{-1}$. Other theoretical works calculated the rate coefficient with CVT and QCT to range from 2.0×10^{-13} to $5.2 \times 10^{-12} \text{ cm}^3\text{s}^{-1}$ ^{1162,163}.

We find no published experimental or theoretical rate coefficients for the two spin configurations on the doublet PES.

On the quartet surface, we calculate the $^3\text{NH} + \text{H} \longrightarrow \text{H}_2 + ^4\text{N}$ configuration to be $1.4 \times 10^{-11} \text{ cm}^3\text{s}^{-1}$. This is a factor of 4 greater than the experimental value reported by Adam et al.¹²⁰.

On the doublet surface, we do not calculate the $^1\text{NH} + \text{H} \longrightarrow \text{H}_2 + ^2\text{N}$ configuration as ^1NH is not efficiently produced in this reaction network.

We find the $^3\text{NH} + \text{H} \longrightarrow \text{H}_2 + ^2\text{N}$ configuration to proceed through the NH_2 intermediate. This is consistent with theoretical studies of the reverse reaction^{165,166}. We find the total forward rate coefficient to be too slow to consider in this study ($\sim 10^{-80} \text{ cm}^3\text{s}^{-1}$).

Regarding the reverse reaction, various experiments have been performed on the deactivation of ^2N by H_2 at 295–300 K^{73,75,123–129}. The rate coefficients have been measured by monitoring the decay of ^2N and range from $1.7\text{--}5.0 \times 10^{-12} \text{ cm}^3\text{s}^{-1}$. Donovan and Husain¹⁷⁴ indicate that $^2\text{N} + \text{H}_2$ should readily undergo chemical reaction into $^3\text{NH} + \text{H}$ via a direct path on the doublet PES. However, theoretical works suggest this reaction will proceed through the NH_2 intermediate^{165,166}. Herron⁷⁶ reviewed the deactivation experiments and suggested a rate coefficient of $2.2 \times 10^{-12} \text{ cm}^3\text{s}^{-1}$ for $^2\text{N} + \text{H}_2 \longrightarrow ^3\text{NH} + \text{H}$.

Theoretical rate coefficient calculations of the reaction $^2\text{N} + \text{H}_2 \longrightarrow ^3\text{NH} + \text{H}$ have been performed using QCT^{164–166}, quantum dynamics¹⁶⁴, and CVT¹⁶⁵ with the CASSCF and MRCI computational methods. Kobayashi et al.¹⁶⁵ and Pederson et al.¹⁶⁶ suggest this reaction proceeds through the NH_2 intermediate. Pederson et al.¹⁶⁶ find the H_2 molecule approaches the N atom perpendicularly, and that there is no collinear reaction path. The calculated theoretical rate coefficients range from 8.9×10^{-13} – $3.3 \times 10^{-12} \text{ cm}^3\text{s}^{-1}$.

Experimental and theoretical studies both suggest $^2\text{N} + \text{H}_2 \longrightarrow ^3\text{NH} + \text{H}$ has a small energy barrier. The experimental value is 7.3 kJ mol^{-1} ¹²⁴.

We find no published experimental or theoretical rate coefficients for the two other reverse reaction spin configurations ($^2\text{N} + \text{H}_2 \longrightarrow ^1\text{NH} + \text{H}$ and $^4\text{N} + \text{H}_2 \longrightarrow ^3\text{NH} + \text{H}$).

At the BHandHLYP/aug-cc-pVDZ level of theory, we find the first step of the reverse reaction, $\text{H}_2 + ^2\text{N} \longrightarrow \text{NH}_2$, to be barrierless. This step is also the rate-limiting step. Similarly to Pederson et al.¹⁶⁶, we find the H_2 molecule approaches the N atom perpendicularly. The second step, $\text{NH}_2 \longrightarrow ^3\text{NH} + \text{H}$, proceeds through a barrier. We calculate the overall barrierless rate coefficient to be $9.7 \times 10^{-10} \text{ cm}^3\text{s}^{-1}$. This value is over 2 orders of magnitude larger than the experimental values. This disagreement with experiment is due to the lack of a barrier calculated when using the BHandHLYP method. For this reason, we introduce the experimental barrier of 7.3 kJ mol^{-1} ¹²⁴ to our calculation to obtain an overall rate coefficient of $5.1 \times 10^{-10} \text{ cm}^3\text{s}^{-1}$. This value is only 1 order of magnitude larger than the experimental value.

We expect the remaining discrepancy to be a result of our chosen computational method, as our reaction geometry is the same as other theoretical works^{165,166}.

We find the other two reverse rate coefficients ($^2\text{N} + \text{H}_2 \longrightarrow ^1\text{NH} + \text{H}$ and $^4\text{N} + \text{H}_2 \longrightarrow ^3\text{NH} + \text{H}$) to be too inefficient to consider in this study ($k < 10^{-21} \text{ cm}^3\text{s}^{-1}$).

Case Study 14: $\text{NH} + \text{N} \longrightarrow \text{N}_2\text{H} \longrightarrow \text{N}_2 + \text{H}$

This reaction occurs on the doublet PES. There are three possible spin configurations: $^3\text{NH} + ^4\text{N} \longrightarrow$

$\text{N}_2\text{H}\cdot \longrightarrow \text{N}_2 + \text{H}$, ${}^3\text{NH} + {}^2\text{N} \longrightarrow \text{N}_2\text{H}\cdot \longrightarrow \text{N}_2 + \text{H}$, and ${}^1\text{NH} + {}^2\text{N} \longrightarrow \text{N}_2\text{H}\cdot \longrightarrow \text{N}_2 + \text{H}$. Because ${}^1\text{NH}$ is not produced efficiently by any reaction in this study, we only analyze the two spin configurations involving ${}^3\text{NH}$.

Hack et al.¹²¹ experimentally measured the rate coefficient of ${}^3\text{NH} + \text{N} \longrightarrow \text{products}$ at 298 K by monitoring the decay profile of ${}^3\text{NH}$. They measured the value to be $2.5 \times 10^{-11} \text{ cm}^3\text{s}^{-1}$.

Konnov and De Ruyck¹²² used the experimental value from Hack et al.¹²¹, as well as a suggested $T^{0.5}$ dependence to estimate a value of $2.6 \times 10^{-11} \text{ cm}^3\text{s}^{-1}$.

Caridade et al.¹⁶¹ calculated the theoretical rate coefficient of ${}^3\text{NH} + {}^4\text{N} \longrightarrow \text{N}_2\text{H}\cdot \longrightarrow \text{N}_2 + \text{H}$ to be $1.9 \times 10^{-11} \text{ cm}^3\text{s}^{-1}$ using quasi-classical trajectory theory at the MRCI/aug-cc-pVQZ level of theory.

We find no published experimental or theoretical rate coefficients for ${}^3\text{NH} + {}^2\text{N} \longrightarrow \text{N}_2\text{H}\cdot \longrightarrow \text{N}_2 + \text{H}$.

Consistent with a previous theoretical study, we find the ${}^3\text{NH} + {}^2\text{N}$ reaction proceeds through the N_2H intermediate. We find the rate-limiting step to be ${}^3\text{NH} + {}^4\text{N} \longrightarrow \text{N}_2\text{H}$, with a rate coefficient of 4.0×10^{-11}

cm^3s^{-1} . This value is only a factor of 1.5 larger than the experimental value, and a factor of 2 larger than the theoretical value.

Reaction Path Symmetry Numbers

The reaction path symmetry number, or reaction path multiplicity, can be calculated with the following equation.

$$\sigma = \frac{\prod_{i=1}^N \sigma_i}{\sigma^\ddagger} \quad (\text{S14})$$

where σ is the reaction path symmetry number, σ_i is the rotational symmetry number of reactant i , and σ^\ddagger is the rotational symmetry number of the transition state.

In Table S10 we list the reaction path symmetry numbers for all the reactions in our network, as well as the rotational symmetry numbers of the reactants and products used in the calculation.

TABLE S10. Reaction path symmetry numbers for each reaction (σ), as well as the rotational symmetry numbers of the reactants (σ_i) and transition states (σ^\ddagger) used in the calculation. All steps in multi-step reactions are included. Spins are labeled only if reaction spin configurations have different reaction path symmetry numbers. $\sigma = \frac{\prod_{i=1}^N \sigma_i}{\sigma^\ddagger}$.

Reaction Equation	σ_1	σ_2	σ^\ddagger	σ
$\text{H}_2\text{CN} \longrightarrow \text{HCN} + \text{H}$	2		1	2
$\text{HCN} + \text{H} \longrightarrow \text{H}_2\text{CN}$	1	1	1	1
$\text{H}_2\text{CN} + \text{H} \longrightarrow \text{HCN} + \text{H}_2$	2	1	1	2
$\text{H}_2\text{CN} + \text{N} \longrightarrow \text{HCN} + \text{NH}$	2	1	1	2
$2\text{H}_2\text{CN} \longrightarrow \text{HCN} + \text{H}_2\text{CNH}$	2	2	1	4
$\text{CH}_4 + \text{H} \longrightarrow \text{CH}_3 + \text{H}_2$	12	1	3	4
$\text{CH}_4 + \text{N} \longrightarrow \text{H}_3\text{CNH}$	12	1	1	12
$\text{H}_3\text{CNH} \longrightarrow \text{H}_2\text{CNH} + \text{H}$	1	1	1	1
$\text{CH}_3 + \text{H} \longrightarrow \text{CH}_4$	6	1	3	2
$\text{CH}_3 + \text{H}_2 \longrightarrow \text{CH}_4 + \text{H}$	6	2	3	4
$\text{CH}_3 + \text{N} \longrightarrow \text{H}_3\text{CN}$	6	1	3	2
$\text{H}_3\text{CN} \longrightarrow \text{H}_2\text{CN} + \text{H}$	3		1	3
$\text{H}_3\text{CN} \longrightarrow \text{H}_2\text{CNH}$	3		1	3
$\text{H}_2\text{CNH} \longrightarrow \text{H}_2\text{CN} + \text{H}$	1		1	1
$2\text{CH}_3 \longrightarrow \text{C}_2\text{H}_6$	6	6	6	6
$2\text{CH}_3 \longrightarrow \text{CH}_2 + \text{CH}_4$	6	6	1	36
$\text{CH}_2 + \text{H} \longrightarrow \text{CH}_3$	2	1	1	2
$\text{CH}_2 + \text{H}_2 \longrightarrow \text{CH}_4$	2	2	1	4
$\text{CH}_2 + \text{H}_2 \longrightarrow \text{CH}_3 + \text{H}$	2	2	2	2
$\text{CH}_2 + \text{N} \longrightarrow \text{H}_2\text{CN}$	2	1	1	2
$^1\text{CH}_2 + ^1\text{CH}_2 \longrightarrow \text{C}_2\text{H}_4$	2	2	1	4
$^1\text{CH}_2 + ^3\text{CH}_2 \longrightarrow \text{C}_2\text{H}_4$	2	2	1	4
$^3\text{CH}_2 + ^3\text{CH}_2 \longrightarrow \text{C}_2\text{H}_4$	2	2	2	2
$\text{CH}_2 + \text{CH}_3 \longrightarrow \text{C}_2\text{H}_5$	2	6	1	12
$\text{C}_2\text{H}_5 \longrightarrow \text{C}_2\text{H}_4 + \text{H}$	1		1	1
$\text{CH}_2 + \text{CH}_4 \longrightarrow \text{C}_2\text{H}_6$	2	12	1	24
$\text{CH}_2 + \text{CH}_4 \longrightarrow 2\text{CH}_3$	2	12	1	24
$\text{CH} + \text{H}_2 \longrightarrow \text{CH}_3$	1	2	1	2
$\text{CH} + \text{N} \longrightarrow \text{HCN}$	1	1	1	1
$\text{HCN} \longrightarrow \text{CN} + \text{H}$	1		1	1
$2\text{CH} \longrightarrow \text{C}_2\text{H}_2$	1	1	1	1
$\text{CH} + \text{CH}_4 \longrightarrow \text{C}_2\text{H}_5$	1	12	1	12
$\text{NH} + \text{H} \longrightarrow \text{H}_2 + \text{N}$	1	1	1	1
$\text{N} + \text{H}_2 \longrightarrow \text{NH}_2$	1	2	2	1
$\text{NH}_2 \longrightarrow \text{NH} + \text{H}$	2		1	2
$\text{NH} + \text{N} \longrightarrow \text{N}_2\text{H}$	1	1	1	1
$\text{N}_2\text{H} \longrightarrow \text{N}_2 + \text{H}$	1		1	1